

# ScholarWorks@GSU

## Study of PepT1 and SPAK on Intestinal Homeostasis and Intestinal Inflammation

Authors	Zhang, Yuchen
Citation	Zhang, Yuchen. 2016. "Study of PepT1 and SPAK on Intestinal Homeostasis and Intestinal Inflammation." Georgia State University. <a href="https://doi.org/10.57709/9399989">https://doi.org/10.57709/9399989</a>
DOI	<a href="https://doi.org/10.57709/9399989">https://doi.org/10.57709/9399989</a>
Download date	2026-05-13 16:32:51
Link to Item	<a href="https://hdl.handle.net/20.500.14694/1976">https://hdl.handle.net/20.500.14694/1976</a>

STUDY OF PEPT1 AND SPAK ON INTESTINAL HOMEOSTASIS AND INTESTINAL  
INFLAMMATION

by

YUCHEN ZHANG

Under the Direction of Didier Merlin, PhD

ABSTRACT

Inflammatory bowel disease (IBD), mainly including ulcerative colitis (UC) and Crohn's disease (CD), has become a serious clinical problem in the developed countries. IBD is characterized by epithelial barrier disruption and alterations in immune regulation with symptoms of passive leaky diarrhea, fever, fatigue and abdominal pain. For the past few decades, significant numbers of investigations have been performed on IBD. However, there are still critical problems remain to be resolved. In our laboratory, we are interested in studying di-/tri- peptide transporter PepT1 and Ste20-like proline/alanine-rich kinase (SPAK). PepT1 and SPAK are believed to be highly involved in intestinal homeostasis and

IBD. Insights into the function of PepT1 and SPAK are expected to facilitate a better understanding of gastrointestinal tract and IBD.

PepT1, a di/tri peptide transporter, is primarily expressed in the small intestine of healthy individuals. In the jejunum, PepT1 is particularly enriched in the well-differentiated absorptive epithelial cells in the villi. Studies of expression and function of PepT1 along the crypt-villus axis demonstrated that this protein is crucial to the process of di/tripeptide absorption. We recently exhibited that PepT1 plays an important role in multiple biological functions, including the ability to regulate the expression/secretion of specific microRNAs (miRNAs) and the expression levels of multiple proteins. Our results suggest that PepT1 contributes to maintain balance of homeostasis and proper functions in the small intestine, and dysregulated miRNAs and proteins along the crypt-villus axis are highly related to this process.

Furthermore, Ste20-like proline/alanine-rich kinase (SPAK) also plays a role in intestinal inflammation. My study has revealed that SPAK knockout (KO) significantly increases the intestinal trans-epithelial resistance and the expression of junction proteins as claudin-2 or E-cadherin. In murine models of colitis induced by dextran sulfate sodium and trinitrobenzene sulfuric acid, KO mice were more tolerant than WT mice. In conclusion, SPAK deficiency increases intestinal innate immune homeostasis, which is important for control or attenuation of pathological responses in inflammatory bowel diseases.

Collectively, PepT1 and SPAK both play significant role in maintaining intestinal homeostasis. With further investigation, they could be good target in study of new therapies on IBD.

INDEX WORDS: IBD, PepT1, SPAK, crypt-villus axis, intestinal homeostasis, epithelial permeability

STUDY OF PEPT1 AND SPAK ON INTESTINAL HOMEOSTASIS AND INTESTINAL  
INFLAMMATION

by

YUCHEN ZHANG

A Dissertation Submitted in Partial Fulfillment of the Requirements for the Degree of

Doctor of Philosophy

in the College of Arts and Sciences

Georgia State University

2016

Copyright by

Yuchen Zhang

2016

STUDY OF PEPT1 AND SPAK ON INTESTINAL HOMEOSTASIS AND INTESTINAL  
INFLAMMATION

by

YUCHEN ZHANG

Committee Chair: Didier Merlin

Committee: Andrew Gewirtz

Zhi-Ren Liu

Electronic Version Approved:

Office of Graduate Studies

College of Arts and Sciences

Georgia State University

December 2016

## DEDICATION

To my parents, Qinghua Zhang and Fuqin Zhang, who taught me the morals of being a man.

To my wife, Jiawei Liu, who provided me solid support and encouragement during this long journey.

To my aunt Ying Zhang and my cousin Oliver, who made a foreign town feels like home.

## ACKNOWLEDGEMENTS

“Happiness only real when shared”

It has been a long journey. Fortunately, there are always great people helping me.

My deepest gratitude to Dr. Didier Merlin for not only being my advisor in science but also being my mentor for life. Thank you for the guidance when I lose direction. Thank you for the tolerance when I made mistake. Thank you for the encouragement when I drop confidence. Thank you for everything. I did learn a lot.

Thank you to my dissertation committee: Dr. Andrew Gewirtz and Dr. Zhi-Ren Liu for all your dedication and continuous support.

Thank you Dr. Yutao Yan, Dr. Pallavi Garg, Dr. Yuan Liu and Dr. Hamed Laroui for your guidance and help.

I also wish to thank everyone in Dr. Merlin’s lab for adding so much fun to my life: “Almost-Dr.” Lewins Walter, Dr. Emilie Viennois, Dr. Bo Xiao, Dr. Mingzhen Zhang, Adani Pujada, Mark Baker, Lixin Wang, and Moon Han.

Special thanks to all my friends who have supported me along the way: Jun Xia, Xiaolei Zhang, Yanan Yin, Chenxue Li, Siyu Tian, Xiaolin Li, Zhujun Li, Hesong Han.

Finally, I would like to thank my family: mom, dad, my grandparents, my wife, my aunt, my uncle and cousin. Thank you for everything you have done for me.

It has been a long journey. Fortunately, I have you by my side.

Thank you

## TABLE OF CONTENTS

<b>ACKNOWLEDGEMENTS</b> .....	v
<b>LIST OF FIGURES</b> .....	ix
<b>LIST OF TABLES</b> .....	xi
<b>LIST OF SUPPLEMENTAL FIGURES</b> .....	xii
<b>LIST OF ABBREVIATIONS</b> .....	xiii
<b>1 SPECIFIC AIMS AND HYPOTHESIS</b> .....	1
<b>2 GENERAL BACKGROUND</b> .....	3
<b>2.1 Inflammatory Bowel Disease</b> .....	3
<i>2.1.1 Overview of Inflammatory Bowel Disease</i> .....	3
2.1.2 Pathogenesis of IBD .....	4
<i>2.1.3 Genetics of IBD</i> .....	5
<i>2.1.4 Barrier Function and IBD</i> .....	6
<i>2.1.5 microRNA and IBD</i> .....	8
<i>2.1.6 Structure of Intestine and Crypt-Villus Axis</i> .....	10
<b>2.2 Intestinal H<sup>+</sup>-Coupled Oligo-Nucleotide Transporter PepT1</b> .....	11
<i>2.2.1 Function and Expression of PepT1</i> .....	11
<i>2.2.2 PepT1 Transport Bacterial Di/Tri-Peptide</i> .....	13
<i>2.2.3 PepT1 and The Structure of Small Intestine and Colon</i> .....	15

2.2.4	<i>Colonic Epithelial PepT1 Expression Modifies Colonic microRNA Expression</i> ....	15
2.2.5	<i>Abnormal Expression of PepT1 Regulates Intestinal Inflammation</i> .....	17
<b>2.3</b>	<b>Ste20 Like Proline/Alanine Rich-Kinase SPAK</b> .....	18
2.3.1	<i>Overview of SPAK</i> .....	18
2.3.2	<i>SPAK and IBD</i> .....	19
<b>2.4</b>	<b>Mice Model Of Inflammatory Bowel Disease</b> .....	19
2.4.1	<i>Dextran Sulfate Sodium (DSS)-Induced Colitis Model</i> .....	20
2.4.2	<i>TNBS-Induced Colitis Model</i> .....	20
2.4.2	<i>Indomethacin-Induced Colitis Model</i> .....	21
<b>3</b>	<b>Experiment</b> .....	21
<b>3.1</b>	<b>Animals</b> .....	21
3.1.1	<i>C57BL/6 Mice</i> .....	21
3.1.2	<i>SPAK KO Mice</i> .....	22
3.1.3	<i>Pept1 KO Mice</i> .....	22
<b>4</b>	<b>RESULT 1: Knockout Of Ste20-Like Proline/Alanine-Rich Kinase (SPAK) Attenuates Intestinal Inflammation In Mice</b> .....	24
<b>4.1</b>	<b>Abstract</b> .....	24
<b>4.2</b>	<b>Introduction</b> .....	25
<b>4.3</b>	<b>Results</b> .....	27

<b>4.4 Discussion</b> .....	33
<b>4.5 Materials And Methods</b> .....	38
<b>4.6 Acknowledgments</b> .....	44
<b>5 RESULT 2: Pept1 Expression Helps Maintain Intestinal Homeostasis By Mediating The Differential Expression Of Mirnas Along The Crypt-Villus Axis</b> .....	60
<b>5.1 Abstract</b> .....	60
<b>5.2 Introduction</b> .....	61
<b>5.3 Results</b> .....	64
<b>5.4 Discussion</b> .....	75
<b>5.5 Methods</b> .....	80
<b>5.6 Acknowledgments</b> .....	88
<b>5.7 Author Contributions</b> .....	89
<b>5.8 Competing Financial Interests</b> .....	89
<b>REFERENCE</b> .....	130
<b>APPENDICES: PUBLICATIONS</b> .....	155

## LIST OF FIGURES

Figure 4.1 SPAK is involved in the regulation of barrier function of IECs in vivo. ....	47
Figure 4.2 SPAK is involved in expression modulation of junction proteins. ....	49
Figure 4.3 Deficiency of SPAK regulates WNK function.....	50
Figure 4.4 SPAK KO mice exhibit attenuated inflammation. ....	51
Figure 4.5 SPAK deficiency decreased and delayed the enhancement of inflammatory cytokine production induced by DSS. ....	53
Figure 4.6 Deficiency of SPAK decreases the luminal bacteria burden and translocation. ....	56
Figure 5.1 PepT1 knockout reduces mouse body weight and the size of intestinal microvilli. .....	91
Figure 5.2 Flow diagram of the low-temperature method used to obtain villi and crypts from intestinal epithelial cells at 4°C.....	93
Figure 5.3 Isolation of villi and crypt epithelial cells of the jejunum from BL-6 WT and PepT1 KO mice.....	95
Figure 5.4 Expression levels of miRNAs in crypt and villus epithelial cells from BL-6 WT and PepT1 KO mice.....	97
Figure 5.5 Overall distribution of miRNAs in crypt and villus cells from PepT1 KO and BL-6 WT mice.....	98
Figure 5.6 Differential expression of proteins along the crypt-villus axis. ....	99
Figure 5.7 2D-DIGE-based assessment of differential protein expression.....	101
Figure 5.8 The protein expression gradient differs along the crypt-villus axis of PepT1 KO and BL-6 WT mice. ....	103

Figure 5.9 PepT1 KO alters the protein expression levels of Rab21 and Fabp1. ....	105
Figure 5.10 PepT1 KO alters the profiles of specific proteins along the crypt-villus axis....	108
Figure 5.11 PepT1 KO modulates the expression levels of certain miRNAs, thereby altering the expression levels of their target proteins.....	110
Figure 5.12 PepT1 KO increases small intestinal epithelial cell proliferation and apoptosis. .....	112

**LIST OF TABLES**

Table 4.1 Primers Used for the Quantification of Inflammatory Mediators.....	45
Table 5.1 Identification of picked proteins differentially expressed between WT villus and WT crypt.....	113
Table 5.2 Identification of picked proteins differentially expressed between KO villus and KO crypt.....	114
Table 5.3 Identification of picked proteins differentially expressed between WT villus and KO villus.....	115
Table 5.4 Identification of picked proteins differentially expressed between WT crypt and KO crypt .....	116
Table 5.5 Expression of the miRNA and its corresponding protein target .....	117

**LIST OF SUPPLEMENTAL FIGURES**

Supplemental Figure 4.1 Body weight measurements.....	57
Supplemental Figure 4.2 An IEC ultrastructure examination reveals abnormal morphological characteristics in enterocytes in KO compared with WT littermates. ....	58
Supplemental Figure 5.1 Expression of PepT1 and Lgr5 in isolated epithelial cells of the jejunum from BL-6 WT mice. ....	118
Supplemental Figure 5.2 Expression of Muc2, Lgr5, and mPepT1 in WT and KO mice. ....	120
Supplemental Figure 5.3 Clustering graph of selected miRNAs.....	122
Supplemental Figure 5.4 Expression levels of selected miRNAs in crypt and villus epithelial cells from BL-6 WT and PepT1 KO mice. ....	123
Supplemental Figure 5.5 PepT1 expression disturbs normal differential protein expression along the crypt-villus axis.....	126
Supplemental Figure 5.6 PepT1 expression altered the normal protein profile in villus and crypt, respectively. ....	128

**LIST OF ABBREVIATIONS**

2D-DIGE two-dimensional difference gel electrophoresis

Acadvl acyl-CoA dehydrogenase, mitochondrial

Acta1 skeletal muscle alpha-actin mRNA

Aldob fructose-bisphosphate aldolase

ASCA anti-Saccharomyces cerevisiae antibodies

Atp5b ATP synthase subunit beta, mitochondrial

Capza1 capping protein muscle Z-line, alpha 1

CARD15 caspase recruitment domain family member 15

CD Crohn's disease

CFU colony-forming units

Cndp2 cytosolic non-specific di-peptidase

Dhrs11 dehydrogenase

DSS dextran sulfate sodium

Eif4a1 eukaryotic translation initiation factor 4Aa1

ErK extracellular signal-regulated kinase

Fabp1 fatty acid-binding protein

Fabp6 gastrotropin

fMLP formyl-methionyl-leucyl-phenylalanine

GCK germinal center kinase

GCK VI subfamily VI of germinal center kinase

GI gastrointestinal

Gstm1 glutathione S-transferase Mu1

Gyk glycerol kinase

hPepT1 human PepT1

IBD inflammatory bowel disease

IEC intestinal epithelial cells

IFN- $\gamma$  interferon-gamma

IL interleukin

INN indomethacin

ITSN intersectin

LOK lymphocyte-oriented kinase

MAP4K mitogen-activated protein kinase kinase kinase kinase

MAPK mitogens activated protein kinases

MDCK madin-darby canine kidney

MDP muramyl dipeptide

MHC II Class II major histocompatibility complex

MPO myeloperoxidase

NOD2 nucleotide-binding oligomerization domain containing 2

OmpC Escherichia coli outer membrane protein C

PAK p21-activated kinase

PAPA box proline/alanine repeats

Pcna proliferating cell nuclear antigen

PepT1 H<sup>+</sup>-coupled oligo-nucleotide transporter

PI isoelectric point

POT H<sup>+</sup>-coupled oligopeptide transporter

Prss1 trypsin 1

Psmc3 26S protease regulatory subunit 6A

Rab-21 ras-related protein Rab-21

RISC-miRNP RNA-induced silencing complex micro-ribonucleoprotein

ROMK1 renal outer medullar potassium

Rplp0 60S acidic ribosomal protein P0

Rpsa laminin receptor

Serpinb1a leukocyte elastase inhibitor A

SLC solute carrier family

SLK ste20 like kinase

SPAK ste20-like proline/alanine-rich kinase

TG transgenic

TLR toll-like receptor

TLR4 toll-like receptor 4

TNBS trinitrobenzene sulfonic acid

TNF- $\alpha$  tumor necrosis factor-alpha

Tri-DAP L-Ala- $\gamma$ -D-Glu-meso-DAP

Tuba1c tubulin alpha-1C chain

UC ulcerative colitis

UTRs untranslated regions

WT wild type

## **1 SPECIFIC AIMS AND HYPOTHESIS**

Inflammatory bowel disease (IBD) is a critical chronic intestinal inflammatory condition. It is characterized by epithelial barrier disruption and alterations in immune regulation with symptoms of passive leaky diarrhea, and abdominal pain (Abraham and Cho, 2009). IBD, which mainly includes ulcerative colitis (UC) and Crohn's disease (CD), affects approximately 1 to 4 million individuals in the United States and about 2.2 million in Europe every year. Currently, there is no effective clinical therapy or treatments for IBD and IBD patients generally need a lifetime of care (Baumgart and Carding, 2007; Baumgart and Sandborn, 2007; Xavier and Podolsky, 2007).

Although the understanding of IBD has been significantly improved over the last century, there are still critical problems remain to be resolved. The key to resolve these problems and to better understand IBD is to investigate the major proteins and kinase that play important roles in inflammation. Thus, I proposed studies to address three specific aims.

*Specific Aim 1: Effect of Ste20-like proline/alanine-rich kinase (SPAK) expression on pathogenesis of IBD*

Ste20 like proline/alanine rich-kinase (SPAK), one of two forms of subfamily VI of germinal center kinase (GCK VI), plays important roles in multiple physiological processes including cell differentiation (Johnston et al., 2000), cell transformation and proliferation (Li et al., 2004), and regulation of chloride transport (Piechotta et al., 2002). Our previous data showed that SPAK expression is increased in colonic mucosa from CD (Yan et al., 2009) and UC (Yan et al., 2008) patients, and from DSS-colitis (Yan et al., 2007), as well as in pro-inflammatory signal TNF- $\alpha$  (Yan et al., 2008) and hyperosmotic medium (Yan et al.,

2009) treated intestinal epithelial cells (IEC), but the underlying mechanisms are yet to be defined.

In the present study, I propose to investigate the effect of knocking down SPAK on the pathogenesis of IBD.

*Specific Aim 2: Effect of intestinal H<sup>+</sup>-coupled oligo-nucleotide transporter (PepT1) expression on intestinal homeostasis*

One of the most significant function of small intestine is the absorption of nutrients including di/tri-peptides from the diet. This process is mediated by peptide transport activity (Adibi, 2003; Mathews and Adibi, 1976). The trans-membrane protein, intestinal H<sup>+</sup>-coupled oligo-nucleotide transporter (PepT1), which is a member of the SLC15 family of proton-oligopeptide cotransporters, has been found to mediate this activity. PepT1 assists the transportation of di/tri-peptides (but not free amino acids or peptides with more than three amino residues) from the intestinal lumen into epithelial cells (Fei et al., 1994; Liang et al., 1995). Moreover, it was recently shown that PepT1 also transport anti-inflammatory tri-peptides (e.g., KPV and VPY) (Dalmaso et al., 2008; Kovacs-Nolan et al., 2012), peptidomimetic drugs (e.g.,  $\beta$ -lactam antibiotics, antiviral drugs and antineoplastic agents (Boggavarapu et al., 2015; Bretschneider et al., 1999; Brodin et al., 2002; de Vruet et al., 1998; Friedman and Amidon, 1989; Kramer et al., 1990), and bacterial pro-inflammatory peptides (e.g., muramyl dipeptide (MDP), formyl-methionyl-leucyl-phenylalanine (fMLP), and L-Ala- $\gamma$ -D-Glu-meso-DAP (Tri-DAP)) (Charrier et al., 2006; Dalmaso et al., 2010a; Merlin et al., 1998; Vavricka et al., 2004). The absorption of bacterial oligopeptides was found to further trigger NF- $\kappa$ B signaling and induce inflammation (Dai et al., 2015;

Dalmaso et al., 2010a; Dalmaso et al., 2011; Ingersoll et al., 2012; Ma et al., 2015). These results indicate that PepT1, through its transporter activity, plays an important role in the intestine under physiological and pathological conditions, and this protein may thus be a candidate target for therapeutic applications.

Therefore, I propose to investigate the effect of PepT1 expression on intestinal homeostasis.

## **2 GENERAL BACKGROUND**

### **2.1 Inflammatory Bowel Disease**

#### *2.1.1 Overview of Inflammatory Bowel Disease*

Inflammatory bowel diseases (IBDs), principally Crohn's disease (CD) and ulcerative colitis (UC), is a critical chronic intestinal inflammatory condition. It is characterized by epithelial barrier disruption, alterations in immune regulation with symptoms of passive leaky diarrhea, and abdominal pain (Abraham and Cho, 2009). UC normally affects the colon and small intestine. However, CD could affect the whole GI tract from the mouth till the anus. Moreover, UC affects the inner lining of the colon while CD can occur in all layers of the bowel walls.

IBD is one of the most general gastrointestinal diseases in the developed countries. Statistical data shows IBD affects 1 to 4 million individuals in the USA and about 2.2 million individuals in Europe. The worldwide incidence rate is about 10 to every 100000 people (Ingersoll et al., 2012). The most susceptible age for IBD is 15 to 30 years old. For the two different conditions UC and CD, similar symptoms are discovered including abdominal pain, diarrhea, fatigue, weight loss, and skin rashes (Hanauer and Sandborn, 2001). At the moment,

there is no effective clinical therapy or treatment for IBD and IBD generally needs a lifetime of care. Moreover, surgery is required for up to 75% of patients with CD and 25% of those with UC long term. Therefore, IBD a serious clinical problem plaguing the health and economy (Baumgart and Carding, 2007; Baumgart and Sandborn, 2007; Xavier and Podolsky, 2007). It is crucial and important to investigate on the pathogenesis and new therapy of IBD.

### *2.1.2 Pathogenesis of IBD*

Three essential factors of pathogenesis of IBD have been reported: (1) the disruption of intestinal barrier function; (2) exposure of luminal contents to immune cells in the lamina propria; and (3) an exaggerated immune response (Groschwitz and Hogan, 2009). Among these factors, numerous patients suffered from the disruption of intestinal barrier function which leads to leak flux diarrhea. Intestinal barrier is the monolayer of the intestinal epithelium. It acts as a selectively permeable barrier which allows absorption of nutrients, electrolytes, water. At the meantime, it isolates harmful substance as microbiota from the internal area. Numerous studies have been done to identify and characterize the mechanisms of barrier disruption in IBD; whereas it is currently unclear which factor is responsible for inducing the barrier dysfunction.

The investigation of IBD has also revealed that mucosal immunity is involved in IBD pathogenesis. The innate immune response is a not-specific and fast response to the antigens, it normally acts as the first layer of defense. A lot of immune cells mediate the innate immune response, the most commons cells includes dendritic cells, neutrophils, monocytes, macrophages and natural kill cells (Medzhitov and Janeway, 2000). For the innate immune

response, the antigens are recognized by the toll-like receptors (TLR) on the surface of cell and NOD-like receptors in the cytoplasm (Abreu et al., 2005). It has found that TLR and NOD are crucial for the immune system and the alteration of these receptors could induce inflammation.

In addition to the innate immune response, adaptive immunity is a more specific and slower system. It depends on the T immune cells. T cells induce by cytokines as IL-12 during inflammation, and it further produce IFN- $\gamma$ , IL-2 and IL-17. As an anti-inflammatory cytokine, IFN- $\gamma$  active macrophages and induce the expression of Class II major histocompatibility complex (MHC II). It is find that IFN- $\gamma$  and IL-17 are both at high level during IBD.

In IBD patients, both innate immune response and adaptive immune response are activated, and it is believed to be mediated by Th17 cells. However, there are still a lot of information remain unknown about the pathogenesis about IBD, and more research are needed to discover the disease.

### *2.1.3 Genetics of IBD*

Because of the technological advances in DNA analysis and sequencing as well as the development of database, we have a great advance in understanding the genetics of IBD recently. The very first gene related to IBD was caspase recruitment domain family member 15 (CARD15), also known as nucleotide-binding oligomerization domain containing 2 (NOD2). NOD2 was first addressed as an intracellular receptor recognizing the muramyl dipeptide (MDP), which is a conserved motif found in peptidoglycan. MDP was found in both Gram-positive and Gram-negative bacteria, and further induces autophagy. Autophagy is an intracellular degradation system that delivers cytoplasmic constituents to the lysosome. It is important in removal of intracellular microbes and resistance of infection for human body. By

inducing autophagy with MDP, host can maintain and control the duplication of bacteria and modulate the immune response (Inohara et al., 2003). Within this pathway, NOD2 plays important roles in regulating the T-cell response (Wang et al., 2016). Further, it is found that NOD2 binds to MDP and trigger a nuclear factor NF- $\kappa$ B, which is part of a central signaling pathway and stimulates the transcription of pro-inflammatory genes and anti-inflammatory genes.

Others have also reported that two genes *ATG16L1* and *IRGM*, which are autophagy-related genes were highly involved in the immune responses during IBD (Rioux et al., 2007); (McCarroll et al., 2008). *ATG16L1* is essential for all forms of autophagy, and can decrease the risk of inflammation. *IRGM*, which is a member of p47 immunity-related GTPase family, leads to reduced protein expression.

The MDR1 gene that encodes *P*-glycoprotein 170 was also related to UC and CD. *P*-glycoprotein 170 is a transporter that controls the efflux of drugs and xenobiotic compounds from cells. Mice without MDR1 gene shows an increased risk of colitis (Panwala et al., 1998).

Additionally, IL23R gene that encodes the pro-inflammatory cytokine IL-23 was reported to involve in the generation of Th17 cells (Zhang and Li, 2014). Several other genes including IL23R, IL12B, JAK2, and STAT3 are related in the Th17 and IL-23 pathway in IBD. Moreover, CARD9, IL1R2, REL, SMAD3 and PRDM1 are also related to the regulation of immune system in IBD.

#### 2.1.4 Barrier Function and IBD

The intestinal epithelium is a monolayer that constitutes the barrier against the external environment. It acts as a barrier to prevent the passage of harmful materials such as foreign

antigens, microorganisms and their toxic products from invading into internal area. It also acts as a selective permeable filter which allows the translocation of dietary nutrients, electrolytes and water from the intestinal lumen to the circulation (Blikslager et al., 2007). There are two parallel trans-epithelial pathways for materials to go through the epithelial barrier: transcellular pathway and par-acellular pathway. The transcellular pathway transports material through the cell. It is usually regulated by selective transporters on the epithelial cell such as PepT1. The para-cellular pathway transports materials through the space between epithelial cells. It is primarily controlled by intercellular complexes. Intercellular complexes are protein-protein complex, such as tight junction, desmosomes, and adherens junctions. They help to link adjacent cells and seal the intercellular space. Among the three structures, adherens junctions and desmosomes are important for the linkage of epithelial cells. The tight junctions are connections between epithelial cells and play very important roles in regulating selective transportation (Forster, 2008). With both transcellular pathway and para-cellular pathway, the intestinal barrier controls the selective transportation and keeps the intestinal homeostasis.

Barrier function is essential to maintain good health, however, the breakdown or defect of the epithelial barrier has been demonstrated as a critical factor in the intestinal inflammatory bowel disease or other gastrointestinal diseases (Groschwitz and Hogan, 2009). Among the clinical symptoms of IBD, impaired absorptive functions and barrier dysfunction caused leak flux diarrhea are very serious (Hering et al., 2012). At the moment, a growing data suggest that increased intestinal permeability is a primary causative factor contributing to IBD pathogenesis. IBD patients are always found to be associated with an increased intestinal epithelial permeability (Wyatt et al., 1993). Several experimental studies with colitis models

also demonstrate the link between altered intestinal barrier function and IBD. IL-10 knockout mice which spontaneously developed IBD showed increased intestinal permeability (Madsen et al., 1999). MDR1a<sup>-/-</sup> (a transporter which may contribute to the physiology of the intestinal barrier) mice can spontaneously develop colitis when maintained under pathogen-free conditions (Resta-Lenert et al., 2005). Therefore, the barrier dysfunction caused by inflammation is both an essential consequence and cause of IBD.

### *2.1.5 microRNA and IBD*

MicroRNAs (miRNAs) are important groups of non-coding RNAs. They are 18–24 base pairs in length that can inhibit the expression of various mRNAs by binding to their 3'-untranslated regions (UTRs). Most eukaryotic cells use miRNAs to control vital functions including differentiation, proliferation, and apoptosis (Ambros, 2004; Filipowicz et al., 2005; Griffiths-Jones, 2004; Krek et al., 2005; Lagos-Quintana et al., 2001). miRNAs are transcribed by nuclear RNA polymerase II. These primary miRNAs are then modified by RNase III (Drosha) to form 70-bp molecules (precursor miRNAs). Exportin 5 and Ran-GTP facilitate translocation of such precursor miRNAs to the cytosol, where processing by RNase Dicer occurs. The resulting 20–22-nucleotide double-stranded RNAs become associated with the multiprotein complex termed “RNA-induced silencing complex micro-ribonucleoprotein” (RISC-miRNP). A helicase facilitates separation of the two RNA strands and binding of argonaute proteins stabilizes the association of miRNAs with RISC-miRNP. Mature miRNAs ultimately inhibit protein expression by reducing the stability of target mRNAs via binding to complementary sequences within 3'-UTRs. Such binding causes both translational inhibition and changes in the target levels of various mRNAs (Krek et al., 2005; Mutoh et al., 2005).

MiRNA dysregulation, mutation and dysfunction have been reported in many inflammatory diseases and cancer (Ambros, 2004; Filipowicz et al., 2005; Griffiths-Jones, 2004; Krek et al., 2005; Lagos-Quintana et al., 2001). In recent years, numerous studies have been done to investigate the role of miRNAs in the regulation of inflammation. Since Dicer is necessary for miRNA processing, the conditional deletion of this gene can be used for investigation of miRNA function in different organs. In 2010, it was found that the conditional ablation of Dicer1 in the intestinal epithelium increases inflammation and exhibits a disorganized epithelium (McKenna et al., 2010). Furthermore, it is shown that miRNA-150 expression increases in colon tissue after dextran sodium sulphate (DSS) treatment which induces inflammation and may serve as a new mechanism to active human IBD (Bian et al., 2011). On the other hand, miRNA-19a is significantly reduced in human colon tissue with colitis or mice tissue with DSS-treated colitis (Chen et al., 2013). These data suggest that miRNAs expression level is dysregulated during IBD and it may play an important role in controlling the inflammation. However, the mechanism is not known yet.

In addition, it is also found that lipopolysaccharide (LPS) which is the ligand of Toll-like receptor 4 (TLR4) increases the expression of some miRNAs in intestinal epithelial cells (IES) (O'Connell et al., 2007). It shows that the bacteria or their products may also affect miRNAs expression.

Altogether, these result suggested that miRNA play important roles in small intestinal homeostasis.

### *2.1.6 Structure of Intestine and Crypt-Villus Axis*

The human gastrointestinal tract (GI) refers to the structures through the mouth until the anus. Several important organs contribute to the GI tract such as stomach and intestine. The whole GI tract including the digestive organs and their accessories comprise the human digestive system and play an essential role in the human body. The GI tract can be split into two parts: the upper gastrointestinal tract and the lower gastrointestinal tract. The lower gastrointestinal tract includes most of the small intestine and all of the large intestine.

Small intestine is a long finger like organ. It is the most important part of the GI tract since most of digestion takes place here, and almost 90 percent of nutrients from food are absorbed here in the small intestine. Small intestine has three distinct portions, the duodenum, jejunum and ileum. The duodenum is the first section and the shortest section among the three. The other two sections are longer, and more digestion and absorption occurs here.

The small intestine has four layers: serosa, muscularis, sub mucosa and mucosa. Mucosa is the most inner layer that on the top towards the lumen. Mucosa secretes digestive enzymes and hormones, which is important for the digestion function. Under mucosa, the second layer is sub mucosa. Sub mucosa is a support of the mucosa, it is formed by dense irregular connective tissue and loose connective tissue. The third layer is the muscularis, which is the muscle layer. It has circular smooth muscle and longitudinal smooth muscle, and these muscle controls the movement of small intestine. Further, the last layer is serosa. Serosa is a smooth membrane consisting of epithelial cells. It is responsible for secretion of the serous fluid.

The mucosa of jejunum and ileum is arranged into two fundamental structures: villus and crypt. Villi are projections into the lumen with mature absorptive enterocytes, while crypts are

invaginations of the epithelium around the villi. Stem cells were found at the base of the crypts continually divide and provide the source of all the epithelial cells (Gordon, 1989; Mac Donal et al., 2008). Cell proliferation, lineage-specific differentiation, migration, and finally apoptosis and/or cell shedding are tightly related processes that regulated along the crypt-villus axis (Gordon and Hermiston, 1994). While a number of factors that regulate cell fate and differentiation in the intestine have been identified (Yang et al., 2001) (Korinek et al., 1998) (Mariadason et al., 2001), and the overall gene expression was found differentially expressed between the crypt and villus (Mariadason et al., 2005). As the crypt-villus are important for maintaining the structure and control the function of small intestine, it would be necessary to investigate on the crypt-villus axis.

In addition to the small intestine, another major structure of the lower gastrointestinal tract is the colon. Colon contributes to the electrolyte homeostasis of the body. Under normal condition, colon absorbs sodium, chloride and water. The colon segment is divided into two parts, proximal and distal colon. The proximal colon comprised the ascending colon and the distal colon included the transverse and descending colon. Different from small intestine, colon does not have a significant villi structure although it shares the similar crypt structure with the small intestine. Due to the structure variance, colon has the secretion function but lack of the absorption function.

## **2.2 Intestinal H<sup>+</sup>-Coupled Oligo-Nucleotide Transporter PepT1**

### *2.2.1 Function and Expression of PepT1*

At the time, it has become clear that the di-/tri-peptide transporter PepT1 may play an important role in the pathogenesis of intestinal inflammation (Ingersoll et al., 2012). PepT1

belongs to H<sup>+</sup>-coupled oligopeptide transporter (POT) superfamily. A principal function of the small intestine is absorption of dietary proteins; this is essential if good health is to be maintained. It is reported that PepT1 acts as an important role in the absorption process. It mediates the transportation of dietary di/tripeptides from intestinal lumen to circulation. PepT1 expresses in the normal small intestine, and the expression level increases from the duodenum to the ileum (Freeman et al., 1995; Ogihara et al., 1996a; Ogihara et al., 1999). In the normal colon, the expression level of PepT1 is normally minimal or absent (Charrier and Merlin, 2006; Ford et al., 2003; Joly et al., 2009; Shen et al., 2001; Ziegler et al., 2002). However, it has been previously shown that the expression of human PepT1 (hPepT1) is upregulated in chronically inflamed colonic epithelial cells. Immunohistochemistry showed that hPepT1 protein expression was increased in the colons of patients with ulcerative colitis and Crohn's disease compared to healthy individuals (Merlin et al., 2001). In these patients, PepT1 expression was evident primarily at the apical membrane of colonic epithelia, as is true of normal small intestinal epithelia, suggesting that hPepT1 expression is induced in colonic cells under inflammatory conditions (Merlin et al., 2001). In recent years, several studies have been done to investigate the mechanisms of the expression of colonic PepT1. It is found that upregulation of pro-inflammatory cytokines and hormones during IBD cause the increase of PepT1 expression. Tumor necrosis factor- $\alpha$  (TNF- $\alpha$ ) and interferon- $\gamma$  (IFN- $\gamma$ ) expression are amplified in IBD, and both cytokines exhibit function to induce PepT1 expression in human intestinal cell line Caco2-BBE (Buyse et al., 2003; Vavricka et al., 2006). Furthermore, the adipocyte-secreted hormone leptin, which is normally not existed in small and large intestines but can be detected in inflamed colonic tissue, has also been found to enhance hPepT1

expression. The same results are also found in Caco2-BBE cells (Nduati et al., 2007). These data demonstrate that colonic PepT1 abnormal expression is induced by pro-inflammatory cytokines or hormones under inflammatory condition, suggesting that it may play an important role in regulation of the inflammation. The function and effect of colonic PepT1 is herein explored.

### *2.2.2 PepT1 Transport Bacterial Di/Tri-Peptide*

The normal function of PepT1 is transportation of dietary di/tri-peptide. However, it is found that PepT1 can also transport bacterial di/tri-peptide. It is well-known that the amount of bacterial di/tripeptides is much lower in the small intestine than the colon because of the lower number of microbiota in small intestine. Since PepT1 expression is normally restricted to the small intestine where less bacterial peptides exist, there is only minimum bacterial peptide uptake in the normal small intestine. Nevertheless, this situation is altered in IBD patients with PepT1 overexpression in colon. The evident colonic PepT1 expression causes an increasing intracellular accumulation of prokaryotic peptides because of the transportation function. This bacteria products accumulation can then trigger downstream pro-inflammatory effects. Numerous studies has described that colonic PepT1 can transport small bacterial products including N-formylmethionyl-leucyl-phenylalanine (fMLP), muramyl dipeptide (MDP), and L-Ala- $\gamma$ -D-Glu-meso-diaminopimelic acid (Tri-DAP) and subsequently causes inflammatory signal transduction pathways which induce downstream inflammation (Charrier et al., 2006; Dalmaso et al., 2010a; Merlin et al., 1998; Vavricka et al., 2004). Therefore, it is interesting that colonic PepT1 is induced by inflammation regulated cytokines and it can subsequently exacerbate the inflammatory response. The specific mechanisms of overexpressed colonic

PepT1 induced inflammation are not defined yet. Studies have shown that when treated Caco2-BBE cells with fMLP, Tri-DAP or MDP, the NF- $\kappa$ B pathway is activated (Buyse et al., 2003; Dalmaso et al., 2010a; Vavricka et al., 2004). In addition to the NF- $\kappa$ B pathway, Tri-DAP mediated activation of MAPK pathway and induced expression of IL-8 and MCP-1 which are chemoattractant for neutrophils and monocytes (Dalmaso et al., 2010a; Vavricka et al., 2004). These chemoattractant exacerbated immune responses and induce inflammation.

Numerous studies have been done to identify and characterize the mechanisms of increased intestinal permeability in IBD. It is found that pro-inflammatory cytokines play an important role in the induction of barrier defects in IBD. TNF- $\alpha$  and IFN- $\gamma$  expression are induced in CD patients and both of them can subsequently induce barrier dysfunction in cell culture and animal models (John et al., 2011). Notably, treatment of anti-TNF- $\alpha$  initiated downregulated the inflammatory response, restored intestinal barrier function and leads to a decrease in intestinal permeability in IBD patients (Suenart et al., 2002). The transforming growth factor- $\beta$  (TGF- $\beta$ ), which is induced in IBD, mediates increasing of claudin-4 (tight junction protein) expression (Monteleone et al., 2008). Furthermore, barrier disruption is also found to be related to the gut microbiota. Abnormal gut microbiota caused by the chronic inflammation leads to alteration of tight junction and causes barrier dysfunction (Sepehri et al., 2007). As mentioned above, PepT1, a transporter of bacterial di/tri-peptide which is overexpressed in colonic epithelial cells in IBD, might be highly involved in the inflammation caused barrier dysfunction. Interestingly, it is reported that the activation of the NF- $\kappa$ B pathway, which can be mediated by overexpression of colonic PepT1, enhances epithelial barrier function (Han et al., 2009).

### *2.2.3 PepT1 and The Structure of Small Intestine and Colon*

The epithelium of the small intestine is organized into villi (finger like structure) and crypt (tubular structures surrounding villi). The villi-crypt structure of small intestine is maintained by a small number of continually divided stem cells near the bottom of the intestinal crypt. These stem cells migrate up along the crypt-villi axis and differentiate to reach full maturity at the top of villi in 36 to 72 hours (Leblond and Messier, 1958). Because of the diverse cell types, the functions of villi and crypt are different. The absorption function of small intestine is mostly fulfilled by the villi, which contains more matured absorptive epithelial cells. To the opposite, crypt plays an important role in secretion to protect the epithelial cells and stem cells.

Studies had suggested that PepT1 plays an important role in intestinal physiology and intestinal inflammation. However, the function of PepT1 on different sites of intestine remains poorly understood. To study the role of PepT1 on villi and crypt of small intestine, a method has been developed in the laboratory to isolate epithelial cells from different level of the villi and crypt (Weiser, 1973). Moreover, to study the mechanisms involved in the abnormal expression of PepT1 on surface and crypt structures of colon, the method to isolate crypt membrane is also developed by Wiener et al. (Weiser, 1973).

### *2.2.4 Colonic Epithelial PepT1 Expression Modifies Colonic microRNA Expression*

Furthermore, CD98 (SLC3A2), which is a transmembrane glycoprotein involved in intestinal inflammation, belongs to the same solute carrier superfamily (SLC superfamily) of PepT1 (SLC15A1). Overexpression of the intestinal epithelial CD98 is known to regulate colonic miRNA-132, 23a, and 23b expression during inflammation (Charania et al., 2012).

This regulation only happens to the colonic miRNAs, but not the other tissues. PepT1 may have the same function in regulation of miRNA due to the similar transmembrane protein structure. Moreover, PepT1 protein, as indicated previously, mediates transport of bacterial peptides by intestinal epithelial cells and results in downstream activation of inflammatory pathways. Therefore, the colonic hPepT1 overexpression might likely be highly involved in regulation of miRNA expression due to its ability to induce inflammation and transport bacteria products.

miRNAs are also highly related to the barrier function. It was found that the conditional ablation of *Dicer1* in the intestinal epithelium causes severe damage on epithelial barrier function (McKenna et al., 2010). It is also found that miRNA-122a plays an important role in the TNF- $\alpha$  modulation of intestinal tight junction barrier. Significantly increase of miRNA-122a expression is shown when the Caco2-BBE cells are treated with TNF- $\alpha$ . When change the TNF- $\alpha$  to anti-sense inhibition of TNF- $\alpha$ , the cell exhibits a lower permeability, which suggests that miRNA-122a expression induce an increase in intestinal barrier permeability (Ye et al., 2011). Furthermore, miRNA-146b is also found to be linked with barrier function. The overexpression of miRNA-146b is reported to protect epithelial barrier function and relieved inflammation in the inflammatory disease mice model by activation of the NF- $\kappa$ B pathway (Nata et al., 2013). Interestingly, the data showed that the activation of NF- $\kappa$ B pathway can also be mediated by overexpression of colonic PepT1 and enhances epithelial barrier function (Han et al., 2009).

These data suggest that there may be a relationship between inflammation triggered colonic PepT1 overexpression and inflammation regulated miRNA such as miRNA-146b since

both of them induce NF- $\kappa$ B pathway and then protect barrier function. Herein, I will investigate this mechanism between colonic overexpressed PepT1, miRNA and barrier function.

#### *2.2.5 Abnormal Expression of PepT1 Regulates Intestinal Inflammation*

To investigate the role of colonic PepT1 in different locations of intestine, our laboratory has previously generated a mouse line expressing hPepT1 specifically in intestinal epithelial cells. The gene encoding hPepT1 is linked to and controlled by the villin promoter in transgenic (Tg) mice. Villin, which is a tissue-specific cytoskeletal protein, is expressed within the intestinal epithelial cells and in the proliferative stem cells (Pinto et al., 1999). Therefore, the Tg mice express hPepT1 specifically in villi/surface and crypt of both small intestine and colon. The mice appeared healthy and exhibited normal body weight, breeding behavior and general appearance (Dalmaso et al., 2011). Western blotting confirmed expression of hPepT1 in the colon epithelial cells of Tg mice but not in the WT mice. Immunohistochemical analysis verified hPepT1 membrane staining of colon epithelial cells in Tg mice, but not in WT mice. In addition, compared to the WT mice, apical membrane vesicles prepared from colon of Tg mice expressed significantly higher levels of functional hPepT1. In summary, villin-hPepT1 mice express functional hPepT1 in the colonic mucosa, which is the same in IBD patients. Therefore, it could be used as an appropriate model to explore the function of over expressed hPepT1 in intestine.

Besides the PepT1 overexpressed mice, our laboratory has also obtained PepT1-knockout mice (KO) from Deltagen, Inc (San Mateo, CA). These mice were developed using a conventional transgenic and breeding strategy. The PepT1 gene was disrupted by

insertion of a lacZ reporter gene under the control of the endogenous PepT1 promoter. These mice were backcrossed for 10 generations to C57BL/6 mice (WT) to have the same genetic background in both the littermates (WT and PepT1 KO). Compared to the WT mice, the PepT1 KO mice lacked the expression of PepT1 protein in the intestine. These mice appeared healthy and exhibited normal body weight, breeding behavior and general appearance (Hu et al., 2008). Nevertheless, PepT1 deletion reduced the intestinal uptake and effective permeability of the model dipeptide GlySar (Hu et al., 2008). Therefore, it could be used as a good model to explore the effect of PepT1 absence on intestine.

### **2.3 Ste20 Like Proline/Alanine Rich-Kinase SPAK**

#### 2.3.1 Overview of SPAK

Yeast ste20 kinases and mammalian homologs p21-activated kinase (PAK) and germinal center kinase (GCK) can act as mitogen-activated protein kinase kinase kinase kinase (MAP4K). They have been described to play a regulating and mediating function in barrier-related functions (Kyriakis, 1999). Lymphocyte-oriented kinase (LOK) and ste20 like kinase (SLK) can affect actin cytoskeleton reorganization during cell adhesion (Widmann et al., 1999) (Ip and Davis, 1998). However, PAK can increase the endothelial permeability (Stockton et al., 2004) (Stockton et al., 2007).

Ste20 like proline/alanine rich-kinase (SPAK), one of two forms of subfamily VI of germinal center kinase (GCK VI) is an MAPK kinase kinase which contains an N-terminal series of proline/alanine repeats (PAPA box) followed by a catalytic domain, a nuclear localization signal, a potential caspase-cleavage motif, and a C-terminal regulatory region (Johnston et al., 2000). The colonic isoform of SPAK, which lacks the PAPA box and

the F- $\alpha$  helix loop in the catalytic subdomain IX, was cloned and characterized by our group (Yan et al., 2007) (Yan and Merlin, 2008). Recently, we have demonstrated that under inflammatory conditions, TNF- $\alpha$  is a key regulator of SPAK expression (Yan and Merlin, 2008).

### 2.3.2 SPAK and IBD

SPAK plays important roles in multiple physiological processes including cell differentiation (Johnston et al., 2000), cell transformation and proliferation (Li et al., 2004), and regulation of chloride transport (Piechotta et al., 2002). Our previous data showed that SPAK expression is increased in colonic mucosa from CD (Yan et al., 2009) and UC (Yan et al., 2008) patients, and from DSS-colitis (Yan et al., 2007), as well as in pro-inflammatory signal TNF- $\alpha$  (Yan et al., 2008) and hyperosmotic medium (Yan et al., 2009) treated intestinal epithelial cells (IEC), but the underlying mechanisms are yet to be defined and our understanding about SPAK is still limited. Therefore, we would like to investigate its involvement in IBD.

## 2.4 Mice Model of Inflammatory Bowel Disease

IBD has been investigated for years. Although there have been several significant findings and explanations about it such as the involvement of NOD2 and NF $\kappa$ B pathway, relatively little is understood regarding the mechanisms of the disease. A range of mouse models has been used to study the pathways or therapeutics that is thought to protect intestinal epithelial cells from damage or stress response. The mostly used mouse models are induced by dextran sodium sulfate (DSS) or trinitrobenzene sulfonic acid (TNBS). More extended animal

models including transgenic animals like IL-10 deficient mice, TNF $\Delta$ ARE mice (Wirtz and Neurath, 2007).

#### *2.4.1 Dextran Sulfate Sodium (DSS)-Induced Colitis Model*

Dextran sodium sulfate (DSS) is a sulfated polysaccharide with anticoagulant properties to induce colitis. It is believed that DSS is directly toxic to gut epithelial cells of the basal crypts and thus harm the integrity of the mucosal barrier. The clinical observation of DSS treated animals are very similar to human IBD pathologies. The symptoms include weight loss, shorten of intestine and villus, diarrhea, and rectal bleeding. Hence, such a model is the most widely used mouse model for investigation of IBD. It has been proved that DSS-induced mice model is particularly appropriate for study of contribution of innate immune mechanisms of colitis and it is useful in study of epithelial repair mechanisms. By using different cycles and approaches to treat the mice, we could obtain acute colitis model or chronic colitis model (Wirtz and Neurath, 2007).

#### *2.4.2 TNBS-Induced Colitis Model*

Haptinizing agent 2,4,6-trinitrobenzene sulfonic acid (TNBS) dissolved in ethanol and intrarectally administered to a mouse through a special catheter is a suitable method to induce colitis. Ethanol is required to break the mucosal barrier, whereas TNBS is believed to haptinize colonic autologous or microbiota proteins rendering them immunogenic to the host immune system. The clinical observation of TNBS induced colitis model is similar to DSS induced model, which include weight loss, shorten of intestine and villus, diarrhea, and rectal bleeding. However, TNBS model normally shows more severe damage in the colon compared to the DSS model. It is believed that TNBS-induced mice model could be used to study T helper

cell-dependent mucosal immune responses and other aspects of gut inflammation including cytokine secretion, mechanisms of oral tolerance, cell adhesion and immunotherapy (Wirtz and Neurath, 2007).

#### *2.4.2 Indomethacin-Induced Colitis Model*

Indomethacin (INN) is a nonsteroidal drug with anti-inflammatory anti-pyretic and analgesic properties. It is commonly used to decrease the fever, pain and other effects caused by inflammation. Interestingly, small intestinal inflammation as Crohn's disease could be induced by two 24 hour apart subcutaneous injections of indomethacin in rat (Yasuoka et al., 2003). Although the reason that caused the inflammation is not clear yet, it is believed that the injection of indomethacin could significantly increase the mucosal permeability of small intestine and further cause damage and inflammation condition to the small intestine. These symptoms make it an appropriate model for Crohn's disease research and could be used for new drug or therapy investigation.

### **3 Experiment**

#### **3.1 Animals**

All animal procedures were conducted in accordance with the National Institutes of Health Guidelines for the Care and Use of Laboratory Animals and approved by the Georgia State University Institutional Animal Care and Use Committee.

##### *3.1.1 C57BL/6 Mice*

C57BL/6 mice (aged 8 to 10 weeks; weight, 18 to 22 g; n=6 mice per group), obtained from Jackson Laboratories (Bar Harbor, ME), were group housed under a controlled temperature (25°C) and photoperiod (12:12-hour light-dark cycle) and allowed unrestricted

access to standard mouse chow and tap water. Mice were allowed to acclimate to these conditions for at least 3 weeks before inclusion in the experiments.

### *3.1.2 SPAK KO Mice*

The SPAK knockout mice on a C57BL/6 background were a kind gift from Dr. Eric Delpire (Vanderbilt University, Nashville, TN). Genomic DNA from tail snips was extracted using the RED Extract-Amp Tissue PCR Kit (Sigma, St Louis, MO) according to the manufacturer's protocol. The primers used for identifying SPAK KO mice were 5'-CGTTGACATTTAAGTTGGCYYCTG-3' (forwards) and 5'-TCACTTCATCAGGAATCTCCG-3' (reverse). Specific PCR products for each target gene were obtained under the following conditions: 94°C for 3 min, 94°C for 15 s, 55°C for 30 s, 72°C for 1 min, and 72°C for 10 min for a total of 40 cycles. All mice were housed in groups of 5 per cage at Georgia State University under controlled conditions of 12:12 h dark/light, 5% humidity and 25°C. Animal experiments were approved by the Institutional Animal Care and Use Committee of Georgia State University (Atlanta, GA), and performed in accordance with the guide for the Care and Use of Laboratory Animals by U.S. Public Health Service. All procedures were approved and registered in the protocol IACUC ID: A14007.

### *3.1.3 PepT1 KO Mice*

PepT1 KO mice obtained from Deltagen (San Mateo, CA) were backcrossed with WT (C57BL/6) animals to obtain the same genetic background in both controls (WT and PepT1 KO). Genomic DNA from tail snips was extracted using the RED Extract-Amp Tissue PCR Kit (Sigma, St Louis, MO) according to the manufacturer's protocol. The primers used for identifying PepT1 KO mice were 5'-GGGCCAGCTCATTCCTCCCCTCAT-3',

5'-AGTGTGGGCTGGTGTGAGACACGTGT-3' (forwards) and  
5'-CAGGGGGAGAGAGAAACAGAGTTAG-3' (reverse). Specific PCR products for each target gene were obtained under the following conditions: 94°C for 3 min, 94°C for 15 s, 55°C for 30 s, 72°C for 1 min, and 72°C for 10 min for a total of 40 cycles. All mice were housed in groups of 5 per cage at Georgia State University under controlled conditions of 12:12 h dark/light, 5% humidity and 25°C. Animal experiments were approved by the Institutional Animal Care and Use Committee of Georgia State University (Atlanta, GA), and performed in accordance with the guide for the Care and Use of Laboratory Animals by U.S. Public Health Service. All procedures were approved and registered in the protocol IACUC ID: A14007.

## **4 RESULT 1: Knockout of Ste20-Like Proline/Alanine-Rich Kinase (SPAK) Attenuates Intestinal Inflammation in Mice**

Published as **Yuchen Zhang**, Sarah Ingosell, Stephen Yang, Hamed Laroui, Mark Baker, Yutao Yan, Knockout of Ste20-Like Proline/Alanine-Rich Kinase (SPAK) Attenuates Intestinal Inflammation in Mice. *The American Journal of Pathology*, Vol. 182, No.5, May 2013

*Note: Elsevier, the publisher of The American Journal of Pathology, automatically granted the authors the permission for using article in a thesis and/or dissertation*

### **4.1 Abstract**

Inflammatory bowel diseases are characterized by epithelial barrier disruption and alterations in immune regulation. Ste20-like proline/alanine-rich kinase (SPAK) plays a role in intestinal inflammation, but the underlying mechanisms need to be defined. Herein, SPAK knockout (KO) C57BL/6 mice exhibited significant increases in intestinal trans-epithelial resistance, a marked decrease in para-cellular permeability to fluorescence isothiocyanatedextran, and altered apical side tight junction sodium ion selectivity, compared with wild-type mice. Furthermore, the expression of junction protein, claudin-2, decreased. In contrast, expressions of occludin, E-cadherin, b-catenin, and claudin-5 increased significantly, whereas no obvious change of claudin-1, claudin-4, zonula occludens protein 1, and zonula occludens protein 2 expressions was observed. In murine models of colitis induced by dextran sulfate sodium and trinitrobenzene sulfuric acid, KO mice were more tolerant than wild-type mice, as demonstrated by colonoscopy features, histological characteristics, and myeloperoxidase activities. Consistent with these findings, KO mice showed increased IL-10

levels and decreased pro-inflammatory cytokine secretion, ameliorated bacterial translocation on treatment with dextran sulfate sodium, and regulation of with no lysine (WNK) kinase activity. Together, these features may reduce epithelial permeability. In conclusion, SPAK deficiency increases intestinal innate immune homeostasis, which is important for control or attenuation of pathological responses in inflammatory bowel diseases.

## **4.2 Introduction**

Inflammatory bowel diseases (IBDs), principally Crohn's disease (CD) and ulcerative colitis (UC), are characterized by epithelial barrier disruption and alterations in immune regulation with symptoms of passive leaky diarrhea and abdominal pain (Abraham and Cho, 2009).

The intestinal epithelium lies at the interface between the intestinal microbiome and the gastrointestinal associated lymphoid tissues and is drawing increasing attention as it represents interplay between genetic and environmental factors. Its tight junction, not like epithelial cell itself, forms a selectively dynamic permeable barrier with the ability to alter its permeability in response to extracellular stimuli, exhibiting both size and charge selectivity. Increased intestinal permeability has been exhibited in both CD and UC patients and their first degree relatives with a variety of underlying mechanisms (Coyne et al., 2002; Schmitz et al., 2000; Sydora et al., 2007; Yan et al., 2008). For example, pathogens and bacterial toxins, pro-inflammatory cytokines, like interferon-gamma (IFN- $\gamma$ ), interleukin (IL)-12, IL-1 $\beta$  and tumor necrosis factor-alpha (TNF- $\alpha$ ) (Berkes et al., 2003; Elson, 1996a; Marchiando et al., 2010; Plevy et al., 1997a; Taddei et al., 2008), can alter barrier function by modifying tight junction proteins. Also, genetic studies in IBD patients, as well as some animal models of

IBD, such as the IL-10<sup>-/-</sup> (Kennedy et al., 2000) and TLR<sup>-/-</sup> mouse models (Fukata et al., 2005), highlight the importance of genetic background on the increased para-cellular permeability.

However, increased intestinal permeability is not enough to predispose onset of IBD (Weber and Turner, 2007). Amplitude respects of evidence implicate abnormal host-microbial interactions in the pathogenesis of IBD. Patients with IBD have antibodies against microbial antigens such as *Saccharomyces cerevisiae* oligomannan (anti-*Saccharomyces cerevisiae* antibodies [ASCA]), *Escherichia coli* outer membrane protein C (OmpC), and *Pseudomonas fluorescens* I2 sequence (Chassaing and Darfeuille-Michaud, 2011). Cells derived from inflamed intestinal tissues of IBD patients are activated by exposure to sonicated samples of autologous or heterologous intestinal microflora, whereas cells from normal individuals respond only to sonicates of heterologous microflora (Duchmann et al., 1997), so intestinal inflammation might also arise from lack of tolerance to antigens present in autologous microflora.

The bowel is the largest immunological organ of the body, with continuous interaction between the mucosal immune system and the intestinal flora. IBD is commonly regarded as the consequences of an enhanced inflammatory response or the lack of a down regulatory response to bacteria abnormality (Sartor, 2008; Xavier and Podolsky, 2007) which may follow or precede the macroscopic lesions.

Ste20 like proline/alanine rich-kinase (SPAK), one of two forms of subfamily VI of germinal center kinase (GCK VI), plays important roles in multiple physiological processes including cell differentiation (Johnston et al., 2000), cell transformation and proliferation (Li

et al., 2004), and regulation of chloride transport (Piechotta et al., 2002). Our previous data showed that SPAK expression is increased in colonic mucosa from CD (Yan et al., 2009) and UC (Yan et al., 2008) patients, and from DSS-colitis (Yan et al., 2007), as well as in pro-inflammatory signal TNF- $\alpha$  (Yan et al., 2008) and hyperosmotic medium (Yan et al., 2009) treated intestinal epithelial cells (IEC), but the underlying mechanisms are yet to be defined.

In the present study, we investigated the effect of knocking down SPAK on the pathogenesis of IBD. We found that mice deficient in SPAK increased intestinal barrier function due to decreased permeability and changes in ion selectivity. SPAK knockout mice were more tolerant to experimental colitis, due to the immune homeostasis maintenance, regulation of junction proteins and intestinal bacteria composition.

### **4.3 Results**

#### *Characterization of SPAK expression in SPAK KO mice*

KO mice showed 5-fold decreases of SPAK mRNA transcripts (Figure 4-1A) and no protein expression was observed compared with WT mice (Figure 4-1B). Immuno-staining of colon sections showed SPAK staining mainly in the muscularis, muscularis mucosa, and epithelial layers in WT mice. However, KO mice showed decreased SPAK expression ubiquitously (Figure 4-1C).

#### *Knockdown of SPAK increases intestinal barrier function*

We hypothesized that SPAK may play a role in epithelial barrier function *ex vivo*. As shown in Figure 4-1D, knock down of SPAK significantly increases the TER to  $415.36 \pm 45.85 \Omega/\text{cm}^2$ , compared to the TER ( $278.08 \pm 53.27 \Omega/\text{cm}^2$ ) in WT mice. Since TER

depends on paracellular size selectivity and ion selectivity (Madara, 1990), the enhanced TER may be due to alteration of size or ion selectivity. To further explore the mechanisms underlying the barrier function increase, we examined the transepithelial permeability in vivo as shown in Figure 4-1E. WT mice showed an FITC-dextran level of  $894.56 \pm 105.25$  mU of FITC/ml protein. In comparison, there was a ~four-fold decrease in SPAK KO mice ( $241.56 \pm 96.36$  mU of FITC/ml protein). These results indicated that knockdown of SPAK decreases transepithelial permeability in vivo. To further evaluate the effects of SPAK expression on intestinal barrier function, the ion selectivity of tight junction was examined. We found that there was no significantly different transepithelial current in KO mice and WT littermates (Figure 4-1G) for the basolateral side ( $-12.263 \pm 2.135$   $\mu$ A vs.  $-12.201 \pm 2.312$   $\mu$ A). However, there was a significant change of transepithelial current for the apical side in KO ( $-23.336 \pm 4.516$   $\mu$ A) and WT mice ( $-27.6203 \pm 6.219$   $\mu$ A), almost no ion sodium flux change through apical side of epithelial cells in KO mice when the sodium concentration in the apical membrane was changed. These results indicate that SPAK knockdown affects intestinal barrier function by modulating tight junction size selectivity and ion charge selectivity.

#### *Characterization of tight junction proteins*

To explore the underlying mechanisms of knock down of SPAK in the retention of intestinal barrier function, we characterized the tight junction proteins using immunofluorescence, real time PCR and western blots (Figure 4-2). The expressions of junction proteins  $\beta$ -catenin, claudin-2 decreased in KO mice at mRNA and protein levels. In contrast, expression of occludin, E-cadherin and claudin-5 increased significantly, whereas the change of expressions of Claudin-1, Claudin-4, ZO-1 and ZO-2 was not noticeable.

*Signaling transduction pathways are involved in the integrity of intestinal barrier function*

We then examined the expression and activity of mitogens activated protein kinases (MAPKs) and WNK1-SPAK-NKCC1 axis. As shown in figure 4-3, there were no significant differences in the expression and the activity of MAPK kinases including p-ERK1/2, total ERK1/2, p-JNK, total JNK, p-p38 and total p38, indicating these tested MAPK pathways are not involved in the KO-related maintenance of barrier function. For the WNK1-SPAK-NKCC1 axis, we did not see a significant effect of SPAK on phosphorylation and expression of NKCC1; however, there was a dramatic increase of WNK1 phosphorylation, indicating its enhanced activity in KO mice.

*Knockdown of SPAK attenuates experimental colitis*

With DSS treatment, KO mice showed a marked amelioration in diarrhea and rectal bleeding (data not shown), and in body weight loss than WT mice (supplemental data). In addition, DSS caused a significant reduction in colon length (supplemental data), which was more severe in WT mice compared with KO mice.

Histological staining (Figure 4-4A) showed an intact epithelium, well-defined crypt architecture, no edema, and no neutrophil infiltration into the mucosa or submucosa, and no ulcers or erosions in WT mice. In contrast, water-treated KO mouse colon sections exhibited an intact epithelium with a relatively longer crypt length, a thinner submucosa or lamina propia. Colon tissue from DSS-treated WT mice had extensive inflammatory lesions throughout the mucosa, a large infiltration of immune cells including neutrophils and lymphocytes was seen, and both ulcers and shortening/loss of crypts were focally apparent. In KO mice treated with DSS, ulcers and shortening and loss of crypts progressed to less

extensive areas of mucosa; submucosal edema was less severe, relatively less immune cell infiltration was observed. Overall epithelium architecture was not damaged. Similar histological characteristics were noticed in TNBS colitis mouse model (Figure 4-4A). Colonoscopy analysis demonstrated that both WT and KO animals showed no evidence of macroscopic inflammation, displaying a semi-translucent mucosa characteristic of a healthy colon (Figure 4-4B). However, DSS induced a rapid and progressive severe, ulcerating, colonic inflammation with bloody diarrhea in both WT and KO mice. However, KO mice exhibited attenuated intestinal inflammation, including decreased colonic inflammation with non-prominent mucosal edema and spontaneous bleeding compared to WT mice. TNBS treated mice demonstrated similar miniature colonoscopy features (Figure 4-4).

MPO activity was measured as an indicator of tissue damage and the extent of infiltration by inflammatory cells. No significant MPO changes were noticed between untreated WT ( $2.46 \pm 2.04$  mUnits/ $\mu$ g protein) (Figure 4-4C) and KO mice ( $2.86 \pm 1.56$  mUnits/ $\mu$ g protein). MPO values increased dramatically in DSS-treated mice in comparison with controls, but DSS-treated KO mice showed significantly lower MPO values ( $23.59 \pm 3.58$  mUnits/ $\mu$ g protein) than DSS-treated WT mice ( $61.39 \pm 21.28$  mUnits/ $\mu$ g protein), indicating less neutrophil infiltration into the mucosa and submucosa of KO mice than WT mice. Figure 4-4D shows the survival curves of WT and KO mice after DSS treatment; 5 % of KO mice died during this period, whereas 35 % WT mice succumbed, indicating a lower mortality of KO mice during recovery. These data suggest that knock down of SPAK has a role in intestinal recovery and healing following acute colitis. The pattern of MPO activities and the recovery were similar in TNBS-induced colitis (Figure 4-4).

*SPAK knockdown decreased and delayed the enhancement of inflammatory cytokines production induced by DSS*

In order to investigate the mechanisms underlying the attenuated intestinal inflammation in KO mice, we quantified the production of colonic cytokines. As shown in Figure 4-5, the cytokine productions were low and similar at resting condition in both KO and WT mice with the exception that IL-6 secretion in KO mice was significantly decreased. With DSS treatment, the production of all of the cytokines tested was enhanced significantly in both WT and KO mice, but compared to WT mice, KO mice demonstrated significantly lower pro-inflammatory cytokine production of IFN- $\gamma$ , IL-1 $\beta$  and TNF- $\alpha$ ; however, the production of IL-12, IL-6, IL-8 and IL-17 did not show significant difference between KO and WT mice. Further, anti-inflammatory cytokine IL-10 demonstrated significant higher expression in KO mice than in WT mice under DSS treatment. To further determine if knockdown of SPAK can postpone the production of cytokines, we performed real-time PCR to monitor the expression of cytokines at different time points. In WT mice, the mRNA expression of the cytokines tested started as early as the first day (3 days for IL-12). We found that the expression of IFN- $\gamma$ , TNF- $\alpha$  and IL- $\beta$  at mRNA level was delayed to the third day after DSS treatment, further, no significant production of IL-12 was noticed until 5 days of DSS treatment at mRNA level (Figure 4-5B).

*Knock down of SPAK attenuates commensal bacterial translocation in DSS-induced colitis*

The imbalance between innate and adaptive immunity caused by luminal bacteria is thought to be a main contributor to the onset of IBD (Macdonald and Monteleone, 2005). We examined the translocation of luminal bacteria in KO and WT mice. First, significant

differences were noticed in CFU levels in any organs tested in KO and WT mice. KO mice harbored a significantly decreased bacterial load in comparison with WT mice. CFU levels increased markedly in all DSS-treated mice, but KO animals showed significantly lower CFU levels than WT in all organs tested (Figure 4-6A). Bacterial 16S rRNA PCR confirmed these results. 40 cycles of amplification did not generate visible products in either WT or KO mice; however, DSS-treated samples yielded strong DNA bands in both WT and KO mice. Furthermore, KO mice exhibited significantly less intense product bands than WT mice (Figure 4-6B). Next, we performed FISH and immunostaining on the same slides to visualize translocated bacteria (Figure 4-6C). We obtained results similar to those shown by CFU analysis, with few bacterial translocations in both KO and WT mice, but significantly fewer bacteria in KO mice compared to WT mice, without DSS treatment. Bacterial translocation was apparent upon DSS treatment in both KO and WT mice, and was significantly lower numbers of bacteria in KO mice. Further, from FISH and Muc2 staining in same slide, we found a bacterial composition change, in WT mice, mucosa-associated bacteria were mainly rod shaped and co-localized with intestinal mucus with or without DSS treatment, however, in KO mice, rod or forsium shaped bacteria did or did not co-localize with mucus.

#### 4.4 Discussion

Our SPAK KO mouse model demonstrated significantly enhanced TER with dramatically decreased para-epithelial permeability, and almost diminished apical side sodium ion selectivity; further, SPAK KO mice displayed different cytokines production and mucosa associated bacteria adherence and translocation in comparison with WT mice. Similar to some other KO colitis models, such as *Mdr1a*<sup>-/-</sup> (Collett et al., 2008) and *IL-10*<sup>-/-</sup> (Kennedy et al., 2000) mouse models, the SPAK KO mouse model is involved not only in intestinal barrier function regulation, but alteration of the mucosa-associated bacteria and the immune responses.

The underlying mechanisms of the gain of intestinal barrier function in KO mice are complicated. First, there were very low and not significant differences in cytokine secretion in WT and KO mice at resting condition (with the exception of IL-6). With DSS treatment, the production of inflammatory mediators increased dramatically, however, KO attenuated significantly the increased extent of some proinflammatory cytokines' production (IFN- $\gamma$ , IL-12, TNF- $\alpha$  and IL-1 $\beta$ ), but boosted significantly the increase of anti-inflammatory cytokine IL-10. The levels of proinflammatory cytokines are always consistent with severity of histological damage in the colon, emphasizing their important roles not only in the pathogenesis of colitis (Elson, 1996b; Plevy et al., 1997b; Sartor, 1994), but as intervention targets against colitis (Kurtovic and Segal, 2004). Anti-inflammatory cytokine IL-10 also plays important roles in regulating barrier function (Sydora et al., 2007), Enhanced production of IL-10 in KO mice, together with relative decreased proinflammatory cytokine production of TNF- $\alpha$ , IFN $\gamma$ , IL-12 and IL-1 $\beta$ , contributes to the attenuated DSS-colitis.

Another possible mechanism is that SPAK may alter the permeability of IEC by regulating the expression of junction proteins, which could result in modification of the contact of luminal food antigens and bacterial antigens with immune cells, resulting in sensitivity changes to colitic diseases (Aono and Hirai, 2008; Gassler et al., 2001), such as DSS-colitis. Occludin, the first tight junction protein identified, was found to play a controversial role in barrier function. In some studies (McCarthy et al., 1996), overexpression of occludin in Madin-Darby canine kidney (MDCK) cells enhanced TER, while synthetic peptides mimicking the extracellular loop structure of occludin have been found to increase permeability in A6 epithelial cells by disrupting normal loop-loop interactions (Wong and Gumbiner, 1997). E-cadherin forms homophilic cell-cell interactions and intracellularly binds to  $\beta$ -catenin which link the transmembranous E-cadherin via catenin to the actin cytoskeleton (Halbleib and Nelson, 2006). Several studies have reported reduced expression of E-cadherin in inflamed epithelium of patients with Crohn's disease and ulcerative colitis (Gassler et al., 2001; Jankowski et al., 1998; Kucharzik et al., 2001). Recently, polymorphisms in the *CDH1* gene, resulting in truncated and intracellularly mis-localized E-cadherin, have been identified in patients with Crohn's disease (Muise et al., 2009). We found low expression of  $\beta$ -catenin in KO mice, which is not consistent with notion that  $\beta$ -catenin was reported to negatively regulate intestinal barrier function (Manicassamy et al., 2010; Nava et al., 2010), therefore the study of the involved mechanisms is necessary. ZO-1 and ZO-2 are critical in the regulation of intestinal barrier function (Fanning and Anderson, 2009), but we did not find any differences between WT and KO mice. Further, claudin-5 is

increased in KO mice, which is in agreement with previous studies demonstrating over expression of claudin-5 increases barrier function (Taddei et al., 2008).

It is well known that ion selectivity of tight junctions plays an important role in the integrity of epithelial cells, thus in TER (Balda et al., 1996; Cereijido et al., 1978). Specifically, the tight junction family claudin plays an important role in the regulation of ion selectivity to mediate TER (Van Itallie and Anderson, 2004; Yu et al., 2003). Additionally, IFN- $\gamma$  and IL-1 $\beta$  regulate TER, not only through size selectivity, but also ion selectivity by regulating claudins (Coyne et al., 2002; Madsen et al., 1997). Our data show that SPAK can significantly decrease expression of pore-forming claudin-2, rendering the intestine firmer, both in epithelial size selectivity and in ion selectivity.

A complex shift in intestinal bacteria composition (Bloom et al., 2011; Chassaing and Darfeuille-Michaud, 2011; Lathrop et al., 2011; Sartor, 2008) is a requisite, perhaps even a central factor in compromising intestinal barrier function, and initiation and perturbation of IBD. Classically, the beneficial effect exerted by the antibiotics in the treatment of IBD and experimental colitis models have been mainly attributed to their antimicrobial properties. DSS can facilitate penetration of bacteria through mucus layer prior to reaching the epithelial cells to initiate the onset of inflammation (Johansson et al., 2008b). Tremendous evidence from IBD patients and experimental colitis models demonstrate that the bacterial load and composition in individual with different genetic backgrounds varies widely, which suggests genetics can interfere with the load and composition, rendering the different sensitivity. It is therefore compelling to study the bacterial component in SPAK engineered mouse models. Mucosa-associated bacteria may have more physiological relevance in IBD, as these

communities are thought to be stable and in actual physical association with the host epithelium. Our data demonstrate that there is much less bacterial translocation in the epithelium, which can explain the partially attenuated inflammatory features. Further, bacteria in KO mice display different features, in terms of bacterial shape and co-localization with mucus. The detailed mechanism of SPAK-specific bacteria in intestinal inflammation is yet to be defined.

In addition, it is accepted that MAPKs are involved in the intestinal barrier functions (Yan and Polk, 2002), and SPAK can activate ErK (Cardone et al., 2010), p38 (Yan et al., 2007), JNK (Polek et al., 2006) under different stimulations. However, we did not find expression and activity differences in KO and WT mice, which demonstrated that the protective phenomenon in KO mice is not due to MAPK kinase activation. The axis WNK-SPAK-NKCC1 has drawn increasing attention since Gordon's hypertension syndrome was found due to the dysregulation of this axis (Vitari et al., 2005). SPAK functions as an upstream kinase of NKCC1, a cation-channel regulator, which is involved in the transport of sodium, potassium and chloride. Thus far, there was no direct evidence about the involvement of NKCC1 in epithelial barrier function. SPAK is regarded as one of the substrates of WNK1 (Vitari et al., 2005). It activates the serum- and glucocorticoid-inducible protein kinase SGK1 (Xu et al., 2005), leading to activation of the epithelial sodium channel. WNK1 along with WNK4 stimulates clathrin-dependent endocytosis of renal outer medullar potassium (ROMK1) (He et al., 2007). WNK1 can also interact with intersectin (ITSN) (Huang et al., 2008), SGK1 (Kim et al., 2009), ROMK (Kahle et al., 2004) and ITSN, (Momboisse et al., 2009) which are reported to regulate epithelial barrier function.

In conclusion, SPAK regulates IEC barrier function by modulating the size selectivity and the ion selectivity of tight junctions. Knockdown of SPAK increases intestinal innate immune homeostasis, which is important in control or attenuation of pathological responses in IBD.

## **4.5 Materials and Methods.**

### ***Mouse model***

C57black/6 mice (8-10 wk, 18–22 g) obtained from Jackson Laboratories (Bar Harbor, ME), were group housed under a controlled temperature (25°C) and photoperiod (12:12-h light-dark cycle) and allowed unrestricted access to standard mouse chow and tap water. They were allowed to acclimate to these conditions for at least 7 days before inclusion in the experiments. Since genetically engineered mice have become essential tools in both mechanistic studies and drug development, we were gifted SPAK knockout mouse model in C57black/6 mouse by collaboration with Dr Eric Delpire (Vanderbilt University). All animal experiments were approved by The Institutional Animal Care and Use Committee of Emory University, Atlanta and were in accordance with the guide for the Care and Use of Laboratory Animal, published by the U.S. Public Health Service.

### ***Immunohistochemistry***

Immunostaining assays were performed according to the standard protocol with relevant primary antibodies [Abs; SPAK and mucin 2 Abs (Santa Cruz Biotechnology, Santa Cruz, CA) and zonula occludens protein 1 (ZO-1), ZO-2, occludin, E-cadherin, b-catenin, claudin-1, claudin-2, claudin-4, and claudin-5 Abs (Invitrogen, Carlsbad, CA)], Alexa Fluor 488/568 secondary Abs (Invitrogen), and rhodamine/phalloidin or Alexa Fluor 488 phalloidin (Invitrogen), as previously described, to visualize actin. Samples were mounted in Prolong Gold Antifade Reagent and analyzed by a Zeiss Axioskop 2 Plus microscope (Carl Zeiss MicroImaging, Inc., Thornwood, NY).

### ***Real time PCR***

For real-time PCR, total RNA from mouse colonic mucosa was reverse transcribed using the Thermoscript RT-PCR System (Invitrogen). Real-time PCR was performed using the iQ SYBR Green Supermix kit (Bio-Rad, Hercules, CA) with the iCycler sequence detection system (Bio-Rad) with specific primers (Table 1). Real-time PCR data were presented using the DDCT method, with 36B4 gene levels serving as the internal standard.

### ***Western blots***

All of the Western blot analyses were performed based on the standard protocol with the relevant antibodies: SPAK, WNK1, *p*-WNK1 (Thr60), sodium-potassium-chloride cotransporter isoform-1 (NKCC1; Cell Signaling Technology Inc., Danvers, MA), glyceraldehyde-3-phosphate dehydrogenase (Millipore, Billerica, MA), ZO-1, ZO-2, occludin, E-cadherin, b-catenin, claudin-1, claudin-2, claudin-4, and claudin-5 (Invitrogen). Total extracellular signal-regulated kinase (ErK)1/2, *p*-ERK1/2 (Thr177), c-Jun N-terminal kinase (JNK), *p*-JNK (Thr183), p38, *p*-p38 (Tyr182) (Santa Cruz Biotechnology), and NKCC1 phosphorylation was analyzed by anti-phosphorylated-threonine antibody with lysate immunoprecipitated by NKCC1 antibody.

### ***Ex vivo transepithelial resistance (TER) assay***

Since transepithelial barrier dysfunction is probably the first reaction in intestinal inflammation, followed by immune reaction, it is always reasonable to check the intestinal barrier status when SPAK expression alters. It is known that TER is dominated by the resistance of the paracellular pathway, including size selectivity and ion selectivity. To confirm our previous data that SPAK can decrease barrier function *in vitro* (Yan et al., 2007), we performed *ex vivo* experiments to determine the effect of SPAK expression on mouse

barrier function. Distal colonic mucosa was obtained by blunt dissection stripping from muscularis and serosa, mounted in Ussing chambers and incubated in Kreb's solution (128mM NaCl, 4.7mM KCl, 1.2mM KH<sub>2</sub>PO<sub>4</sub>, 1.2mM MgSO<sub>4</sub>, 10mM Glucose, 2.5mM CaCl<sub>2</sub>, 23mM NaHCO<sub>3</sub>) at 37°C, constantly saturated with an atmosphere of 95% O<sub>2</sub>/5% CO<sub>2</sub>. Voltage-sensing electrodes consisting of Ag/AgCl pellets and current-passing electrodes made of silver wire are connected by agar bridges containing 3 M KCl and interfaced *via* DM-MC6 head-stage amplifiers (Physiologic Instruments, San Diego, CA) to a microcomputer-controlled VCC-MC6 voltage/current clamp (Physiologic Instruments, San Diego, CA). The current between the two compartments was monitored and recorded at 5-s intervals, whereas the voltage was continuously clamped to zero. The total resistance between the apical and basal compartments was determined at 37°C from the current evoked by a 5-μA bipolar current pulse at time 0 and at 20-sec intervals for 10 min.

#### ***In vivo permeability assay***

*In vivo* permeability assays were performed as previously described. (Yan et al., 2011)

#### ***Ex vivo ion selectivity assay***

The ion selectivity of tight junctions was examined in Caco2-BBE monolayers and mice colon mucosa by determining dilution potentials by replacing the apical and basolateral solution, while keeping the other side (basolateral or apical solution) bathed in Ringer's solution (150 mM NaCl, 2 mM CaCl<sub>2</sub>, 1 mM MgCl<sub>2</sub>, 10 mM glucose, 10 mM HEPES, pH 7.4) or Kreb's solution. For 2:1 NaCl dilution potentials, the 150 mM NaCl was replaced with 75 mM NaCl in Ringer's solution or the 128mM NaCl was replaced with 52mM NaCl in Kreb's solution, and the osmolality was maintained with mannitol.

### ***Induction and assessment of DSS/TNBS colitis***

Colitis was induced by the addition of 3% (w/v) DSS (mol. wt., 50,000; ICN Biochemicals, Aurora, OH) to the drinking water or by colonic injection of 150 mg/kg body weight of trinitrobenzene sulfonic acid (TNBS; Sigma-Aldrich, St. Louis, MO) dissolved in 50% ethanol. Colitis was assessed 8 days after DSS treatment or 48 hours after TNBS administration, as previously described (n = 6 mice per group). Direct visualization of the colon was performed using the Coloview system (Karl Storz Veterinary Endoscopy, Goleta, CA). Neutrophil infiltration into the colon was quantified by measurement of myeloperoxidase (MPO) activity, as previously described. To study the effects of SPAK on the healing phase of intestinal inflammation, we monitored the survival status of the mice for another week after DSS/TNBS withdrawal. For histological assessment of colitis, specimens from proximal and distal parts of colon were stained with H&E, and histological features were analyzed on these microscopic sections, as previously described, according to the severity of the induced damage.

### ***Mouse colonoscopy***

Endoscopy was performed on mice to follow the progression of colitis. Direct visualization of the colon in vivo was performed using the Coloview System (Karl Storz Veterinary Endoscopy, Goleta, CA). If fecal material obstructed the endoscope, colons were flushed with saline. Before colonoscopy, all mice were anesthetized by inhalation of 1.5% to 2% (w/v) isoflurane, and 3- to 4-cm-long colon segments, from the anal verge to the splenic flexure, were visualized after inflation of each colon with air. All colonoscopic procedures were digitally recorded on an AIDA-vet PC (Karl Storz Veterinary Endoscopy, Goleta, CA).

### ***MPO activity***

Neutrophil infiltration into the colon was quantified by measuring MPO activity, as previously described. (Yan et al., 2011)

### ***Colon organ culture***

Colon organ cultures were prepared from age-matched wild type or SPAK KO mice in the following manner. Colons, not including the cecum, were dissected from mice and flushed with cold PBS to remove fecal matter. Each colon was then cut into 2-mm squares, washed in a large volume of PBS plus 5% fetal calf serum, and resuspended in RPMI-1640 supplemented with 10% fetal calf serum, 50 mmol/L 2-ME, penicillin (100 U/mL), streptomycin (100 U/mL), and ciprofloxacin (100  $\mu$ g/mL). Equivalent amounts of tissue (200 mg) were distributed into tissue culture plates (Falcon 3046; Becton Dickinson Labware) containing 5 mL of media alone or media supplemented with LPS (10  $\mu$ g/mL) or Con A (5  $\mu$ g/mL). Cultures were incubated at 37°C in 5% CO<sub>2</sub>. Supernatants were harvested after 18 hours, and cytokine levels were quantified using a mouse pro-inflammatory 7-plex MSD Tissue Culture Kit (MSD, Gaithersburg, MD) with Sector Imager 2400 software (MSD).

### ***Bacterial translocation assay***

Mucosa-associated bacteria may have more physiological relevance in IBD (Sun et al., 2011), because these communities are thought to be stable and in actual physical association with the host epithelium. The small intestine and colon were washed thoroughly with PBS to remove the fecal bacteria before the bacterial translocation assay. Colony-forming units (CFUs) in freshly isolated small intestine, colon, spleen, and liver tissues were then determined via homogenization of material PBS/0.01% Triton X-100, followed by serial

dilution plating on nonselective Luria-Bertani agar, as previously described. (Vijay-Kumar et al., 2007)

#### ***PCR of bacterial 16S rRNA genes***

Mucosa was sampled from an identical surface area in the dissected colon. The colon fragment was washed twice thoroughly with PBS and then DNA was prepared with the Wizard SV Genomic DNA Purification System (Promega, Madison, WI). DNA was analyzed by PCR with universal primers directed against a region of the 16S ribosomal RNA gene common to most bacteria: forward, 5'-CCATGAAGTCGGAATCGCTAG- 3'; and reverse, 5' -ACTCCCATGGTGTGACGG- 3' (bp, 1302 to 1394 in bacteria EU622773). The PCR products were analyzed by agarose gel electrophoresis.

#### ***FISH and immunohistochemistry***

The Fluorescence *in situ* hybridization assay was performed using an Alexa Fluor 555 (Invitrogen)-conjugated eubacterial (EUB; bp 337-354); the NON-EUB-Alexa Fluor 555 probe was used as a negative control. Immunofluorescence staining with anti-Muc2 antibody (Santa Cruz Biotechnology, Santa Cruz, CA) and Hoechst 33258 (Invitrogen, Carlsbad, CA) was performed on the same slides, following a protocol previously described (Johansson et al., 2008a).

#### ***In vitro and ex vivo ion selectivity assay***

As we mentioned, TER is determined mainly by IEC size selectivity and ion selectivity, since we already examined the effect of size selectivity on barrier function, we would perform *ex vivo* ion selectivity assay to examine their effects on TER. The ion selectivity of tight junctions was examined in Caco2-BBE monolayers and mice colon mucosa by

determining dilution potentials by replacing the apical and basolateral solution, while keeping the other side (basolateral or apical solution) bathed in Ringer's solution (150 mM NaCl, 2 mM CaCl<sub>2</sub>, 1 mM MgCl<sub>2</sub>, 10 mM glucose, 10 mM HEPES, pH 7.4) or Kreb's solution. For 2:1 NaCl dilution potentials, the 150 mM NaCl was replaced with 75 mM NaCl in Ringer's solution or the 128mM NaCl was replaced with 52mM NaCl in Kreb's solution, and the osmolality was maintained with mannitol. For assay in Caco2-BBE monolayers in Ringer's solution, the voltage between the two compartments was monitored and recorded at 5-s intervals, while the current was continuously clamped to zero. For assay in colonic mucosa in Kreb's solution, the current between the two compartments was monitored and recorded at 5-s intervals, while the voltage was continuously clamped to zero. Following the completion of each dilution potential study, the monolayers will be re-fed with control medium for 1 h. The TER will then be measured to determine the integrity of the cell monolayers.

### ***Statistical analysis***

Values are expressed as mean  $\pm$  SEM. Statistical analysis was performed using unpaired two-tailed Student's *t* test by InStat v3.06 (GraphPad, San Diego, CA) software. *P* < 0.05 was considered statistically significant.

### **4.6 Acknowledgments**

We thank Sarah A. Ingersoll, Didier Merlin, and Andrew T. Gewirtz for critically reading the manuscript.

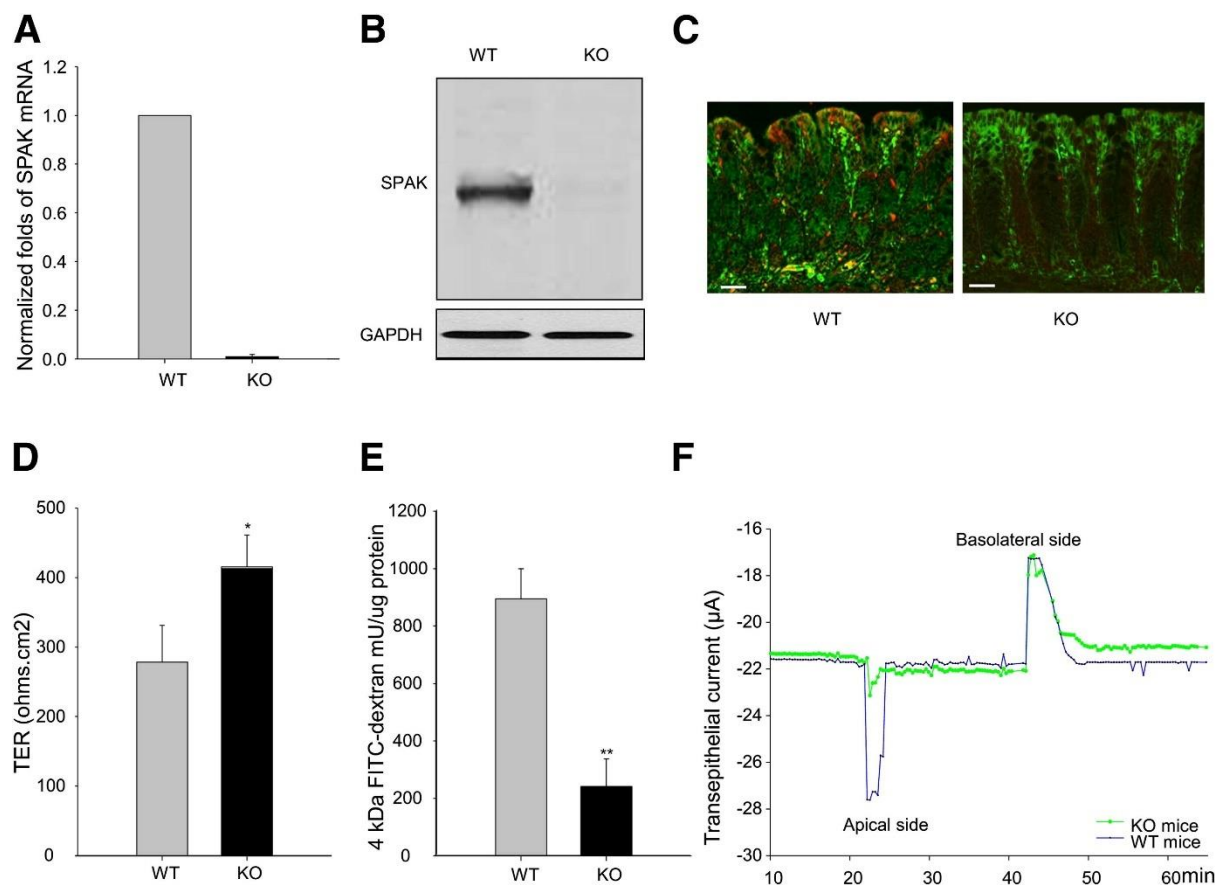
This article is dedicated to the memory of Dr. Shanthi Sitarman, a brilliant scientist, a dedicated physician, a passionate humanitarian, and a dearest friend.

Table 4.1 Primers Used for the Quantification of Inflammatory Mediators

Name	Nucleotide sequence
Mouse SPAK	
Forward	5'-CGTTGACATTTAAGTTGGCYCTG-3'
Reverse	5'-TCACTTCATCAGGAATCTCCG-3'
34B4	
Forward	5'-TCCAGGCTTTGGGCATCA-3'
Reverse	5'-CTTTATCAGCTGCACATCACTCAGA-3'
TNF- $\alpha$	
Forward	5'-AGGCTGCCCCGACTACGT-3'
Reverse	5'-GACTTTCTCCTGGTATGAGATAGCAAA-3'
IFN- $\gamma$	
Forward	5'-CAGCAACAGCAAGGCGAAA-3'
Reverse	5'-CTGGACCTGTGGGTTGTTGAC-3'
KC	
Forward	5'-CTTGAAGGTGTTGCCCTCAG-3'
Reverse	5'-TGGGGACACCTTTTAGCATC-3'
IL-6	
Forward	5'-ACAAGTCGGAGGCTTAATTACACAT-3'
Reverse	5'-TTGCCATTACACAACCTCTTTTC-3'

Name	Nucleotide sequence
IL-10	
Forward	5'-GGTTGCCAAGCCTTATCGGA-3'
Reverse	5'-ACCTGCTCCACTGCCTTGCT-3'
IL-12	
Forward	5'-AGACCCTGCCCATTGAACTG-3'
Reverse	5'-GAAGCTGGTGCTGTAGTTCTCATATTT-3'
IL-17	
Forward	5'-CAGGAACCCTCATCCTTCAA-3'
Reverse	5'-ATTCCCAAGCCCAGAATCTT-3'
IL-1 $\beta$	
Forward	5'-GGGCCTCAAGGAAAAGAATC-3'
Reverse	5'-AGCTGACTGTCCTGGCTGAT-3'
EUB	5'-GCTGCCTCCCGTAGGAGT-3'
EUB control	5'-CGACGGAGGGCATCCTCA-3'

EUB, eubacteria; KC, keratinocyte-derived chemokine.



**Figure 4.1** SPAK is involved in the regulation of barrier function of IECs *in vivo*.

Deficiency of SPAK expression in C57BL/6 mouse is demonstrated by quantitative PCR (A), Western blot analysis (B), and immunofluorescence (C; green represents actin; red, SPAK). D: SPAK KO mice display significantly decreased TER compared with WT mice. E: SPAK deficiency significantly reduces the flux of 4-kDa FITC-dextran. F: Transepithelial current at both the apical and basolateral side of IECs, as described in *Materials and Methods*. SPAK KO mice showed diminished transepithelial current at the apical side, but no difference at the basolateral side. Scale bars: 20  $\mu\text{m}$  (C). \* $P < 0.05$ , \*\* $P < 0.01$ . GAPDH, glyceraldehyde-3-phosphate dehydrogenase.

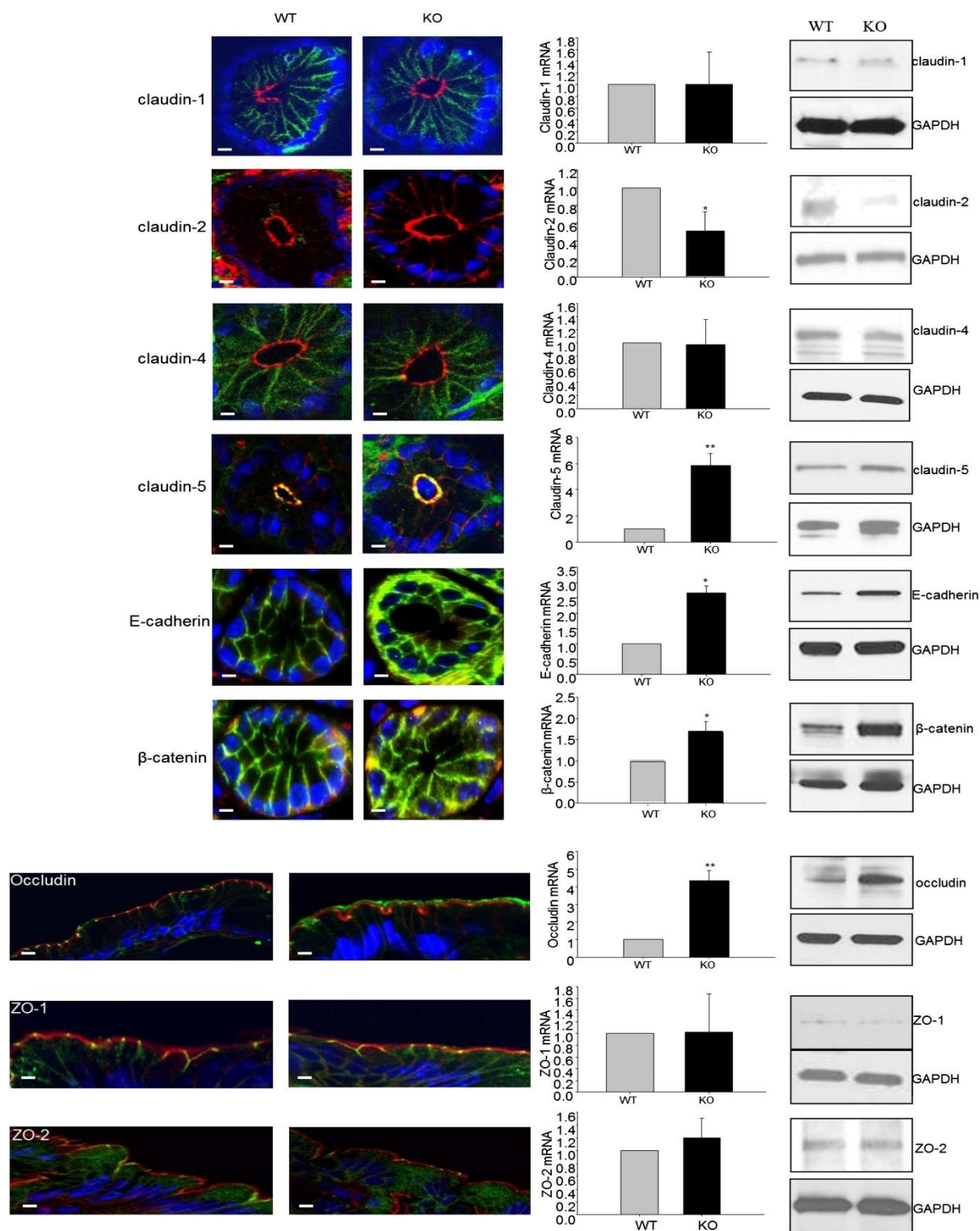


**Figure 4.2 SPAK is involved in expression modulation of junction proteins.**

Immunofluorescence, Western blot analyses, and real-time PCR were performed to quantify the expression of IEC junction proteins. Protocols in detail are in *Materials and Methods*. For immunofluorescence, green represents actin; red, relevant molecules; blue, nuclei. Scale bars: 5  $\mu\text{m}$ . \* $P < 0.05$ , \*\* $P < 0.01$ . GAPDH, glyceraldehyde-3-phosphate dehydrogenase.

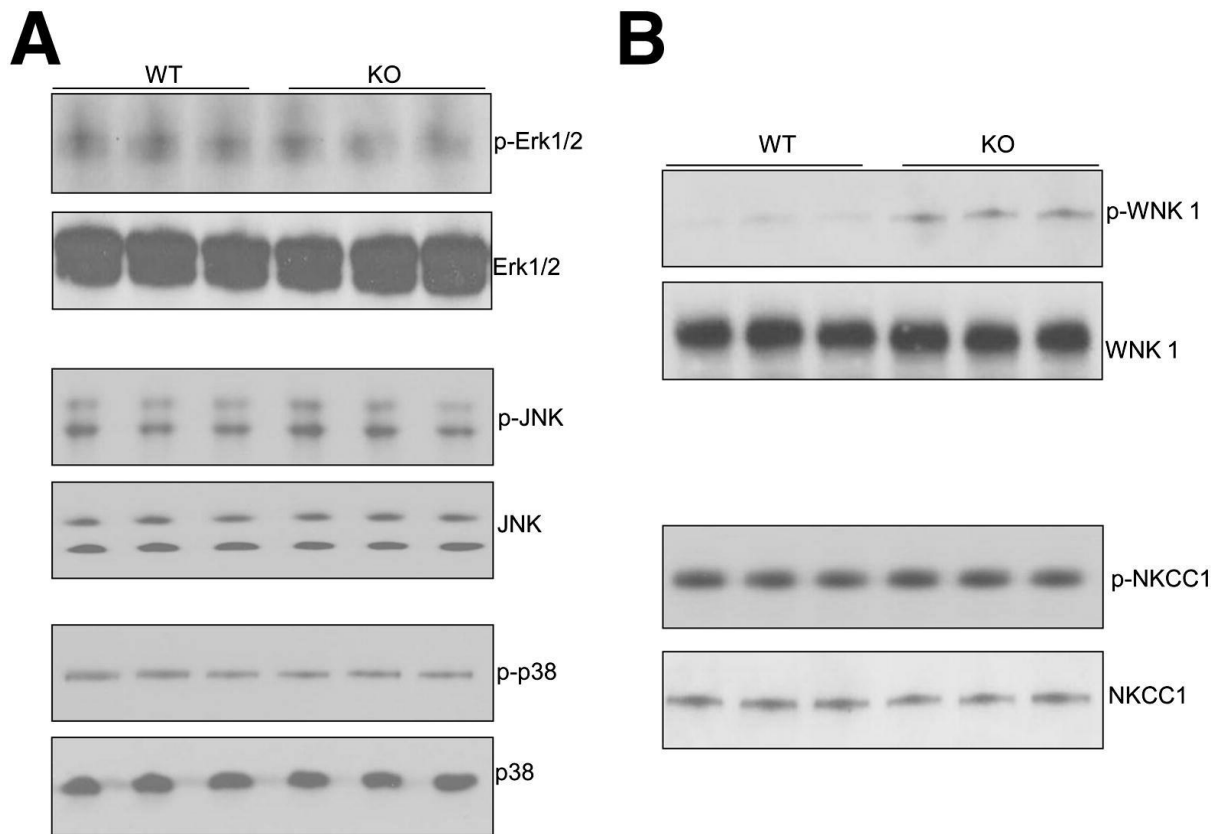


**Figure 4.3 Deficiency of SPAK regulates WNK function.**

**A:** Western blot analyses showed no effect of SPAK deficiency in expression and phosphorylation of Erk, JNK, and p38. **B:** However, SPAK deficiency modulates WNK1 expression and activity, but not its substrate, NKCC1.

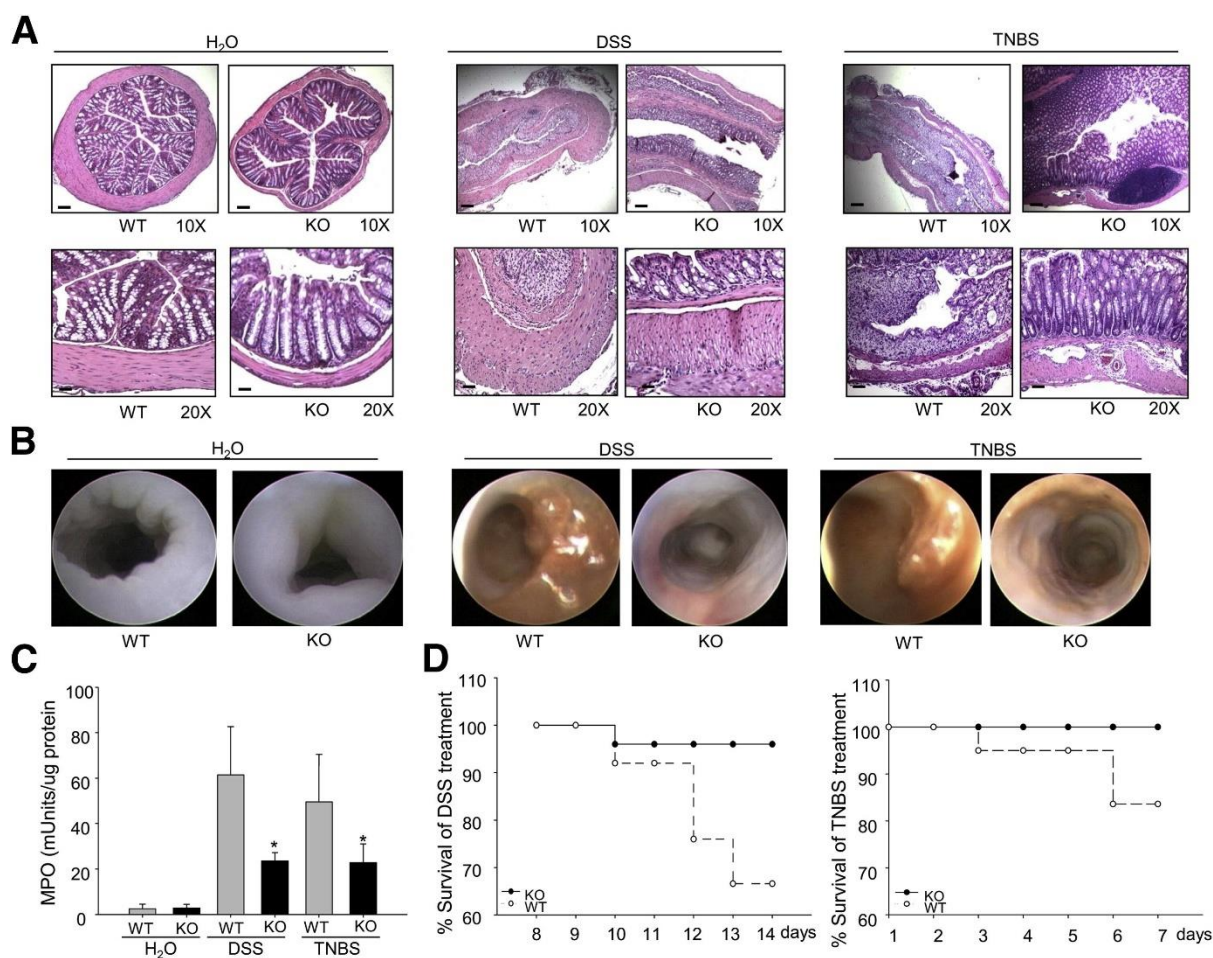


**Figure 4.4 SPAK KO mice exhibit attenuated inflammation.**

**A:** Representative photomicrographs of paraffin-embedded, H&E-stained sections of distal colon from mice treated with DSS for 7 days or treated with TNBS for 48 hours. Original magnification:  $\times 10$  (**top panels**);  $\times 20$  (**bottom panels**). **B:** Intestinal inflammation was evaluated macroscopically *in vivo* using a murine miniature endoscope. Representative images from six different mice treated with DSS for 7 days or treated with TNBS for 48 hours are shown. **C:** WT and KO mice were administered water or 3% DSS for 7 days or 150 mg/kg body weight of TNBS for 48 hours, and distal colon tissue was collected and analyzed for MPO activity. Data are expressed as means  $\pm$  SEM ( $n = 6$  mice per group). Statistical analysis was

performed using an unpaired two-tailed Student's *t*-test. **D**: After 7 days of 3% DSS or 48 hours of TNBS, mice were given tap water and observed for recovery. Scale bars: 80  $\mu\text{m}$  (top lane, **A**); 20  $\mu\text{m}$  (bottom lane, **A**). \**P* < 0.05.

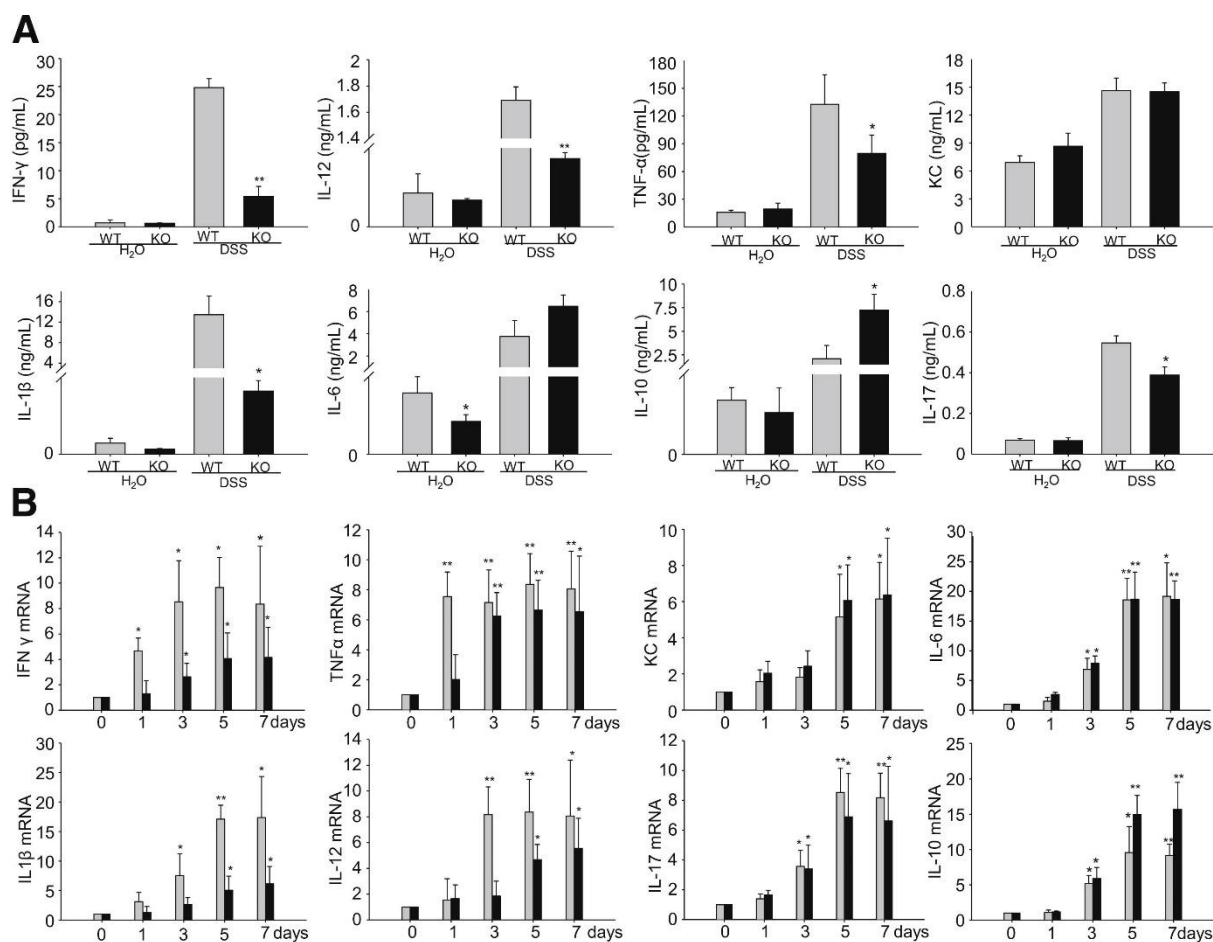


**Figure 4.5** SPAK deficiency decreased and delayed the enhancement of inflammatory cytokine production induced by DSS.

**A:** Cytokine levels were screened using a mouse proinflammatory multiplex MSD tissue culture kit. Statistical analyses were performed between WT and KO mice. In each case, the productions of cytokines in mice were compared between WT and KO mice under tap water treatment and DSS treatment for 7 days. **B:** Quantitative PCR measurements of cytokine transcripts were performed using colonic tissue from WT and KO mice that had been treated with DSS for different time points. Data are expressed as means  $\pm$  SEM ( $n = 6$  mice per group). Statistical analyses were performed separately for WT and KO mice. In each case, the production of cytokines in mice treated with DSS at the various time points (days 1, 3, 5, and 7)

were compared with the production in tap water-treated mice (day 0). \* $P < 0.05$ , \*\* $P < 0.01$ .

KC, keratinocyte-derived chemokine.

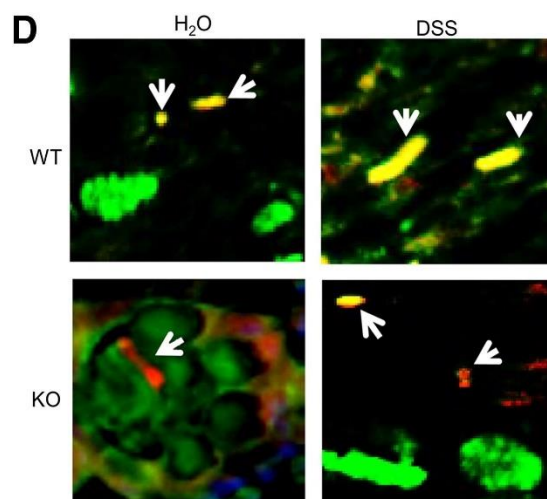
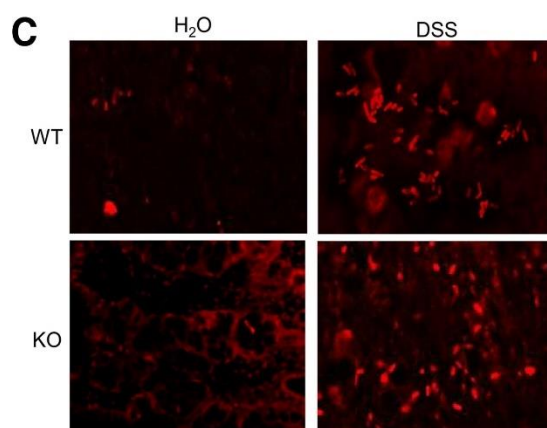
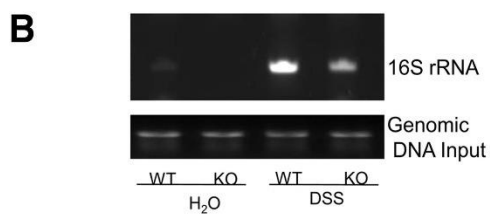
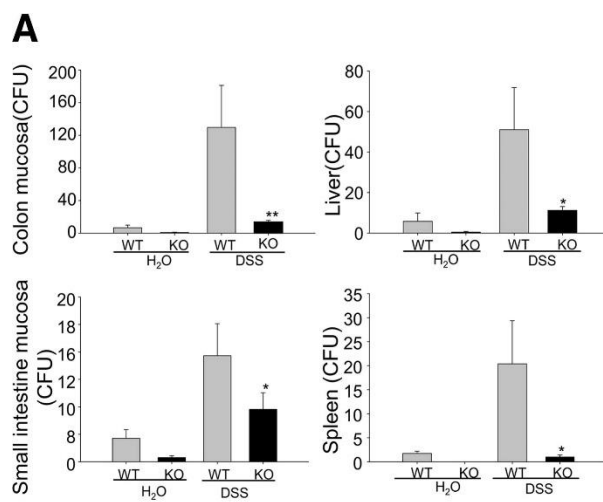
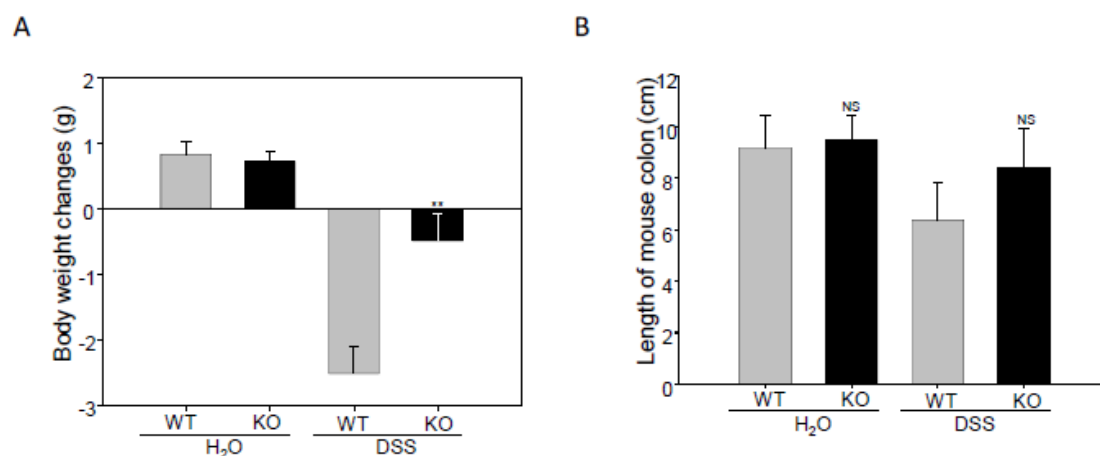


**Figure 4.6 Deficiency of SPAK decreases the luminal bacteria burden and translocation.**

**A:** Colon mucosa, small-intestinal mucosa, spleen, and liver tissue from SPAK KO mice or WT littermates were homogenized and cultured on nonselective media. CFUs were counted. Data are expressed as means  $\pm$  SEM ( $n = 6$  mice per group). Statistical differences of KO versus WT mice, with or without DSS treatment, are reported. Data are pooled from three independent experiments. **B:** PCR of bacterial 16S RNA gene using genomic DNA isolated from equal surface areas of colonic mucosa. Amplification was performed for 35 cycles. **C:** SPAK deficiency attenuated translocation of luminal bacteria into the colon mucosa. FISH with the probe of Alexa Fluor 555–conjugated EUB was performed for each slide. There was a sparse presence of bacteria (red) in untreated WT and KO mice. After DSS treatment, there was a dramatic increase of translocation of bacteria in both WT and KO mice; furthermore, significantly fewer bacterial colonies were observed in KO mice compared with WT mice. **D:** The bacterial composition differed between KO and WT mice. FISH with the probe of Alexa Fluor 555–conjugated EUB and mucus staining with Muc2 antibody visualized by Alexa Fluor 488–conjugated secondary antibody were performed for each slide. In WT animals, mucosa-associated bacteria were mainly rod shaped and colocalized with intestinal mucus (**arrows**), regardless of whether the animals were exposed to DSS. However, in KO mice, the bacteria were either rod or oval shaped and did not always colocalize with mucus. \* $P < 0.05$ , \*\* $P < 0.01$ . rRNA, ribosomal RNA.

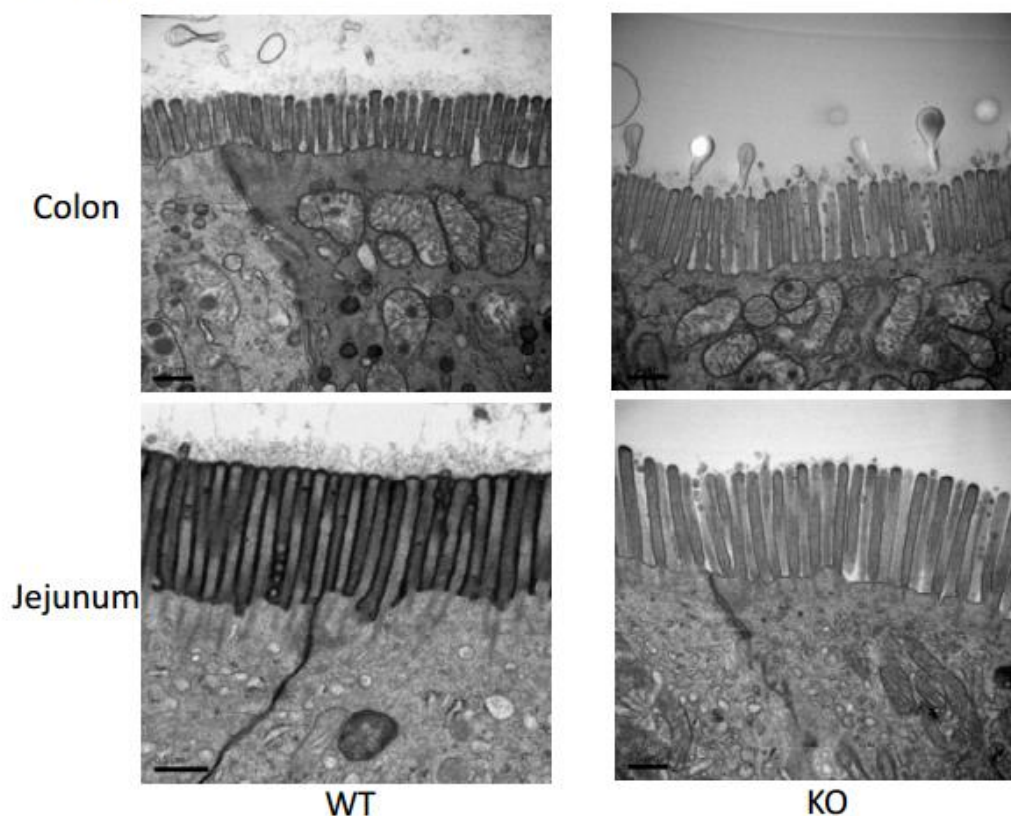
Supplemental Figure S1



#### Supplemental Figure 4.1 Body weight measurements.

**A:** Body weight measurement in WT and KO mice with 3% DSS treatment for 7 days or with 150 mg/kg body weight of TNBS treatment for 48 hours. **B:** Measurement of mouse colon length in WT and KO mice with 3% DSS treatment for 7 days or with 150 mg/kg body weight of TNBS treatment for 48 hours. Data are expressed as means  $\pm$  SEM ( $n = 4$  mice per group). Statistical differences of KO versus WT mice are reported. Data are pooled from three independent experiments.  $**P < 0.01$ .

Supplemental Figure S2: Electron microscopy



**Supplemental Figure 4.2 An IEC ultrastructure examination reveals abnormal morphological characteristics in enterocytes in KO compared with WT littermates.**

Intestine tissues were dissected into 1- to 2-mm cubes while immersed in 2.5% glutaraldehyde buffered with 0.1 mol/L sodium cacodylate (pH 7.2). Samples were stored in the same fixative overnight at 4°C. Samples were then washed with the same buffer and postfixed in 1% buffered osmium tetroxide, dehydrated through a graded ethanol series to 100%, and embedded in Eponate 12 resin (Ted Pella Inc. Redding, CA). Ultrathin sections were cut on a Leica UC6rt ultramicrotome (Leica Microsystems, Buffalo Grove, IL) at 70 to 80 nm and counterstained with 4% aqueous uranyl acetate and 2% lead citrate. Sections were examined using a Hitachi H-7500 transmission electron microscope (Hitachi High Technologies of America Inc. Schaumburg, IL) equipped with a Gatan BioScan

charge-coupled device (CCD) camera (Gatan, Inc, Warrendale, PA). Examination of IEC ultrastructure by electron microscopy showed abnormal morphological characteristics and slightly increased size of microvilli at the apical membranes of enterocytes in KO compared with WT littermates.

## **5 RESULT 2: PepT1 Expression Helps Maintain Intestinal Homeostasis by Mediating the Differential Expression of miRNAs along the Crypt-Villus Axis**

Published as **Yuchen Zhang**, Emilie Viennois, Mingzhen Zhang, Bo Xiao, Moon Kwon Han, Lewins Walter, Pallavi Garg, Didier Merlin. PepT1 Expression Helps Maintain Intestinal Homeostasis by Mediating the Differential Expression of miRNAs along the Crypt-Villus Axis. *Scientific Reports*. 6, Article number: 27119 (2016)

*Note: NatureResearch, the publisher of Scientific Reports, automatically granted the authors the permission for using article in a thesis and/or dissertation.*

### **5.1 Abstract**

In the jejunum, PepT1 is particularly enriched in the well-differentiated absorptive epithelial cells in the villi. Studies of expression and function of PepT1 along the crypt-villus axis demonstrated that this protein is crucial to the process of di/tripeptide absorption. We recently exhibited that PepT1 plays an important role in multiple biological functions, including the ability to regulate the expression/secretion of specific microRNAs (miRNAs) and the expression levels of multiple proteins. In this study, we observed that PepT1 knockout (KO) mice exhibited reduced body weight and shorten intestinal microvilli. We then examined the expression levels of various miRNAs and their target proteins along the crypt-villi axis in the jejunum of PepT1 KO mice. We found that PepT1 KO altered the distribution of miRNAs along the crypt-villus axis and changed the miRNA profiles of both villi and crypts. Using miRNA-target prediction and 2D-DIGE/mass spectrometry on villi and crypts samples, we found that ablation of PepT1 further directly or indirectly altered

expression levels of certain protein targets. Collectively, our results suggest that PepT1 contributes to maintain balance of homeostasis and proper functions in the small intestine, and dysregulated miRNAs and proteins along the crypt-villus axis are highly related to this process.

## 5.2 Introduction

One of the most significant functions of small intestine is the absorption of the nutrients including di/tri-peptides from the diet. This process is mediated by peptide transport activity (Adibi, 2003; Mathews and Adibi, 1976). The trans-membrane protein, *intestinal H<sup>+</sup>-coupled oligo-peptide transporter* (PepT1), which is a member of the SLC15 family of proton-oligopeptide cotransporters, has been found to mediate this activity. PepT1 transports di/tri-peptides (but not free amino acids or peptides with more than three amino residues) from the intestinal lumen into epithelial cells (Fei et al., 1994) (Liang et al., 1995). Moreover, it was recently shown that PepT1 also transport anti-inflammatory tri-peptides (*e.g.*, KPV and VPY (Dalmaso et al., 2008; Kovacs-Nolan et al., 2012)), peptidomimetic drugs (*e.g.*,  $\beta$ -lactam antibiotics, antiviral drugs and antineoplastic agents (Brodin et al., 2002; de Vruet et al., 1998; Friedman and Amidon, 1989; Kramer et al., 1990)), and bacterial proinflammatory peptides [*e.g.*, muramyl dipeptide (MDP) (Vavricka et al., 2004), formyl-methionyl-leucyl-phenylalanine (fMLP) (Charrier et al., 2006), and *L*-Ala- $\gamma$ -D-Glu-meso-DAP (Tri-DAP) (Dalmaso et al., 2010a)]. The absorption of bacterial oligopeptides was found to further trigger NF- $\kappa$ B signaling and induce inflammation (Dalmaso et al., 2010a; Dalmaso et al., 2011; Ingersoll et al., 2012). These results indicate that PepT1, through its transporter activity, plays an important role in the intestine under

physiological and pathological conditions, and this protein may thus be a candidate target for therapeutic applications.

It has been reported that PepT1 is mostly expressed in the small intestine, but in limited level or absent in the colon, kidney, pancreas and bile duct(Bockman et al., 1997; Groneberg et al., 2001; Knutter et al., 2002; Ogihara et al., 1996b; Shen et al., 1999). However, the expression of colonic PepT1 is known to be induced under conditions of chronic inflammation, such as inflammatory bowel disease (IBD)(Merlin et al., 2001),(Wojtal et al., 2009). Our group and others have also demonstrated that PepT1 is expressed in immune cells, such as macrophages, that are closely related to the lamina propria of the small and large intestines(Ayyadurai et al., 2013; Charrier and Merlin, 2006; Smythies et al., 2005).

In the small intestine, PepT1 is mostly expressed in the ileum and jejunum, associated with lipid rafts(Groneberg et al., 2001),(Nguyen et al., 2007). In the jejunum, PepT1 is particularly enriched in the villi, but poorly or not expressed in the goblet cells and less-differentiated epithelial cells of the crypts(Groneberg et al., 2001),(Nguyen et al., 2007). The expression/function of PepT1 along the crypt-villus axis suggests that the protein is specific to the well differentiated absorptive epithelial cells, strengthening the notion that PepT1 is important to the absorption process(Groneberg et al., 2001; Nguyen et al., 2007).

We recently demonstrated that PepT1 plays important roles in multiple biological functions in the small intestine. The expression of PepT1 regulates the expression/secretion of specific microRNAs (miRNAs), to thereby regulate the expression levels of multiple proteins(Ayyadurai et al., 2014). Intestinal miRNA expression is essential for maintaining intestinal homeostasis. In the intestinal epithelium, conditional ablation of Dicer1, which is

obligatory for miRNA processing, was reported to trigger increased inflammation and disorganization of the epithelium (Cobb et al., 2005; McKenna et al., 2010). Hence, it is crucial to investigate the effect of PepT1 expression on the miRNA expression and the crosstalk between these miRNAs and their target proteins.

Maintaining the intestinal homeostasis is crucial for a physiological equilibrium. A breach on that equilibrium can facilitate development of intestinal diseases such as inflammatory bowel disease. To get a better understanding of PepT1 functions and their influence on the small intestinal homeostasis, we first investigated miRNA expression patterns along the crypt/villus axis in the jejunum of wild-type (WT) mice, where PepT1 is highly expressed. We then examined the expression levels of various miRNAs and their potential target proteins along the crypt/villus axis in the jejunum of PepT1 KO mice, in an effort to identify PepT1-dependent miRNAs in this tissue. Our results support the emerging idea that PepT1 plays an important role in multiple biological processes, as we show for the first time that it critically regulates directly or indirectly the miRNA and protein expression along the crypt/villus axis in the jejunum, and thus helps maintain intestinal homeostasis.

### 5.3 Results

#### *PepT1 knockout reduces body weight and size of intestinal microvilli*

To study the role of PepT1 in small intestinal homeostasis toward the crypt-villus axis during intestinal epithelial cell differentiation, we obtained PepT1 KO mice from Deltagen (San Mateo, CA). Homozygous PepT1 KO mice were identified using a multiplex RT-PCR strategy (Figure 5-1a). Mice verified as homozygous and their WT controls were used for further study. Western blotting and qRT-PCR indicated that PepT1 protein and mRNA, respectively, were not expressed in the small intestines of PepT1 KO mice, but were expressed in their WT controls (Figure 5-1b, c). PepT1 expression was much lower in the colon than in the small intestine of WT mice, even with this residual PepT1 absent from colon tissue of PepT1 KO mice (Figure 5-1c). Histologic examination of small intestine sections showed no obvious differences between PepT1 KO and WT mice (Figure 5-1d). However, the body weight of PepT1 KO mice (n=9) was significantly lower than that of WT animals (n=9) at week 7 ( $16.48 \pm 0.70$  vs  $18.30 \pm 1.03$  g), week 8 ( $17.06 \pm 0.87$  vs.  $18.82 \pm 1.22$  g), week 9 ( $17.19 \pm 0.63$  vs.  $19.82 \pm 1.50$  g), and week 10 ( $17.38 \pm 0.07$  vs.  $20.23 \pm 1.31$  g) (Figure 5-1e). Furthermore, examination of ultrastructure by transmission electron microscopy showed abnormal morphology in PepT1 KO mice. The size of microvilli at the apical membranes of enterocytes was much lower in PepT1 KO than in WT animals ( $1.14 \pm 0.14$  vs.  $1.29 \pm 0.07$   $\mu\text{m}$ ; n=27) (Figure 5-1f, g), suggesting that knockout of PepT1 in the small intestine resulted in defective microvilli at the brush borders of apical surfaces of mouse villus enterocytes. Because microvilli greatly increase the surface area of the small

intestine for digestion/absorption, these data suggest that intestinal absorption is decreased in PepT1 KO compared with WT mice.

*Isolation of villi and crypt epithelial cells of the jejunum from WT and PepT1 KO mice*

Morphological alteration (shorten microvilli) in PepT1 KO mice has been described. To further evaluate if that change is associated to molecular alterations along the crypt-villus axis, we isolated villi and crypts from the jejunum of 8 week-old PepT1 KO mice and their WT controls using a low-temperature method (Flint et al., 1991), as described in the methods (Figure 5-2). Total RNA from sample 1 to sample 11 were isolated. qRT-PCR analysis showed that the levels of villus markers including PepT1 mRNA in WT animals and mucin 2 mRNA (Muc2) in both WT and PepT1 KO animals were enriched in sample 1 (Figure 5-3a, b and Supplementary Figure 5-1) but were less enriched in sample 11 (Figure 5-3a, b and Supplementary Figure 5-1). Conversely, the levels of mRNA encoding leucine-rich repeat containing protein-coupled receptor 5 (Lgr5), a stem cell marker located at the bottom of the crypts, were enriched in sample 11, but less enriched in sample 1 in both WT and PepT1 KO mice (Figure 5-3a, b). As PepT1 and Muc2 were shown to be markers of well differentiated intestinal epithelial cells (Buyse et al., 2001), (Chang et al., 1994), and as Lgr5 is a marker of crypt stem cells (Barker et al., 2007), these results suggest that sample 1 is the purest villus isolate whereas sample 11 is the purest crypt isolate. Figure 5-3c shows the visual appearance of the extracted villus and crypts fractions isolated from the jejunum of WT and PepT1 KO mice. Further qRT-PCR of the isolated samples confirmed that isolated villi from WT mice express high levels of PepT1 and Muc2 and low levels of Lgr5 when compared with isolated crypts (Figure 5-3d). The isolated villi from PepT1 KO mice exhibited higher levels of Muc2

expression and lower levels of Lgr5 expression when compared with isolated crypts, with neither villi nor crypts expressing PepT1 (Figure 5-3d). These results indicate that villi and crypts can be isolated from WT and PepT1 KO mice with high purity and quality. The differential expression of Muc2, Lgr5 and PepT1 along the crypt-villus axis in intact tissue from WT and PepT1 KO was confirmed by immunofluorescence (Figure 5-3e and Supplementary Figure 5-2a, b, c).

#### *Expression of miRNAs in crypt and villi epithelial cells from WT and PepT1 KO mice*

To investigate the miRNA expression profiles of intestinal epithelial cells (IEC) along the crypt-villus axis in WT and PepT1 KO mice, miRNA microarrays were analyzed in WT and PepT1 KO villi and crypts in the IEC. Large numbers of miRNA were differentially expressed, with an average of 239 microRNAs detected per sample.

Levels of specific miRNAs were compared pairwise among WT and PepT1 KO villi and crypts. The miRNAs with differential  $P$  value < 0.05 and of signal strengths > 500 were selected. Of the 239 targets assayed, 36 miRNAs showed significant differences in at least one of the comparisons (Supplementary Figure 5-3). The expression levels were further verified by qRT-PCR (Supplementary Figure 5-4).

#### *miRNAs expressed differently along crypt-villus axis in WT mice*

Of the 36 differentially expressed miRNAs, 20 were down-regulated in WT crypts compared with WT villi (Figure 5-4a1, with all 18 blue spots below the purple spots, and Figure 5-4a2, with the first two blue spots below the purple spots), 1 miRNA (miR-212-3p) showed the same level of expression in WT villi and crypts (Figure 5-4a2; the third blue spot, overlapping the purple spot), and 15 miRNAs were up-regulated in WT crypts relative to villi

(Figure 5-4a2, with blue spots 4 to 18 above the purple spots). Of the 20 miRNAs downregulated in crypts, 8 showed a >4.0-fold difference (miR-142-5p, miR-16-5p, miR-22-3p, miR-194-3p, miR-33-5p, miR-223-3p, miR-32-5p, miR-140-5p; Figure 5-4a1, blue spots), whereas, of the 15 miRNAs upregulated in crypts, 2 showed a >3.0-fold difference (miR-192-5p, miR-98-5p) (Figure 5-4a2, blue spots). Together these results demonstrate that miRNAs are differentially expressed along the crypt-villus axis in WT mice.

*PepT1 expression affects the normal miRNA distribution along crypt-villus axis*

The expression levels of the 36 differentially expressed miRNAs were also compared in PepT1 KO crypts and villi (Figure 5-4b). In contrast to WT mice, 17 miRNAs were down-regulated in PepT1 KO crypts compared with PepT1 KO villi (Figure 5-4b1 and Figure 5-4b2, with red spots below the green spots), 12 miRNAs demonstrated same expression level (Figure 5-4b1 and Figure 5-4b2, with red spots overlapping green spots), and 7 miRNAs were up-regulated in PepT1 KO crypts compared with PepT1 KO villi (Figure 5-4b1 and Figure 5-4b2 red spots above the green spots). Specifically, 5 miRNAs (miR-223-3p, miR-326-3p, miR-26a-5p, miR-103-3p, miR-98-5p; Figure 5-4a1 Blue spots vs Figure 5-4b1: Red spots) showed expression profiles along the crypt-villus axis in PepT1 KO opposite to those in WT mice. 6 miRNAs (miR-221-3p, miR-181-5p, miR-181b-5p, miR-712-5p, miR-345-5p, miR-100-5p; Figure 5-4a2 and Figure 5-4b2) showed a lower expression level in KO crypts than KO villi, but showed higher expression level in WT crypts than WT villi (Figure 5-4b2: Red spots vs Figure 5-4a2: Blue spots). Together, these results demonstrate that knockout of PepT1 markedly alters normal miRNA distribution along the crypt-villus

axis compared with WT mice (Figure 5-4b1 and Figure 5-4b2 vs Figure 5-4a1 and Figure 5-4a2).

*PepT1 expression altered miRNA profiles in both villi and crypts*

Comparisons of miRNA expression in PepT1 KO and WT villi showed that levels of 15 miRNAs were lower in villi from PepT1 KO mice than that from WT mice (Figure 5-4c1 and Figure 5-4c2; green spots below the purple spots), whereas levels of 11 miRNAs were higher in villi from PepT1 KO than from WT mice (Figure 5-4c1 and Figure 5-4c2; green spots above the purple spots). In addition, the expression levels of miRNAs also differed in crypts from PepT1 KO and WT mice. Specifically, 11 miRNAs were less expressed (Figure 5-4d1 and Figure 5-4d2; red spots below blue spots) and 14 miRNAs were more expressed (Figure 5-4d1 and Figure 5-4d2; red spots above blue spots) in crypt cells from PepT1 KO mice than in crypt cells from WT mice (Figure 5-4d).

*Overall distribution of miRNAs in crypt and villus cells from PepT1 KO and WT mice*

The overall distribution of miRNAs was further confirmed by principal component analysis (PCA), which demonstrates overviews of sample clusters based on the 50 miRNAs with the largest variations across all samples (Figure 5-5). The largest component in the variation is plotted along the X-axis and the second largest is plotted on the Y-axis. PCA analysis revealed that 15 samples can be roughly divided into 4 groups. miRNAs from PepT1 KO and WT villi were distinct from miRNAs from KO and WT crypts (Figure 5-5). Thus, in both PepT1 KO mice and their WT controls, there were significant differences in miRNA expression profiles between villi and crypts.

*Proteins are differently expressed along crypt-villus axis in WT mice*

In order to investigate whether miRNA alteration was accompanied by changes of protein expression, we further analyzed protein accumulation along the crypt-villus axis. Differential protein expression in crypt and villus cells from WT mice were analyzed by two-dimensional difference gel electrophoresis (2D-DIGE), as described in Methods section. Analysis of gel images showed 43 spots with >2.0-fold differences in spot intensity between WT villi and crypts (Supplementary Figure 5-5a). Of these 43 spots, 18 were up-regulated, and 25 were down-regulated in crypts relative to villi. 18 candidate spots were picked from the total 43 spots based on their reliability, location on the gel, intensity, and fold change (>2.24) for mass spectrometry.

To identify these selected spots, LC-MS was used, and 13 different proteins were identified. Of these, 7 proteins, Protein Hbb-bs (Hbb-bs), trypsin 1 (Prss1), fatty acid-binding protein (Fabp1), skeletal muscle alpha-actin mRNA (Acta1), family with sequence similarity 135 (Fam135a), laminin receptor (Rpsa), and Ras-related protein Rab-21 (Rab-21), exhibited significantly lower expression levels in WT crypts than in WT villi (Figure 5-6a, blue round spots below the purple square spots). 6 other proteins, proliferating cell nuclear antigen (Pcna), cytosolic non-specific di-peptidase (Cndp2), glycerol kinase (Gyk), 26S protease regulatory subunit 6A (Psmc3), 60S acidic ribosomal protein P0 (Rplp0), and gastrotropin (Fabp6), showed higher expression levels in WT crypt than in WT villus cells (Figure 5-6a, blue round spots above purple square spots). Spot number, GI accession number, gene symbol, protein name, protein molecular weight, isoelectric point (PI), average fold change, and overall trend of these spots are shown in Table 5-1. Thus, using 2D-DIGE/mass

spectrometry on isolated crypt and villus samples identified proteins with different expression levels along the crypt-villus axis in WT mice.

*PepT1 expression disturbs normal differential protein expression along crypt-villus axis*

2D-DIGE was also used to assess differential protein expression in the crypt and villus cells from PepT1 KO mice. Gel image analysis identified 72 spots with a >2.0-fold difference in spot intensity between PepT1 KO villi and crypts (Supplementary Figure 5-5b). Of these 72 spots, 28 were up-regulated and 44 were down-regulated in crypts relative to villi of PepT1 KO mice. 17 candidate spots were picked based on their reliability, location on the gel, intensity, and fold change (>2.15) for mass spectrometry.

LC-MS of the 17 spots identified 12 different proteins. Of these, 5 proteins, Hbb-bs, Prss1, Rpsa, eukaryotic translation initiation factor 4Aa1 (Eif4a1), and very long chain specific acyl-CoA dehydrogenase, mitochondrial (Acadvl), demonstrated lower expression levels in PepT1 KO crypts than in PepT1 KO villi (Figure 5-6b; red round spots below green square spots). 7 other proteins, fructose-bisphosphate aldolase (Aldob), tubulin alpha-1C chain (Tuba1c), Gyk, Fabp6, leukocyte elastase inhibitor A (Serpinb1a), dehydrogenase (Dhrs11), and Rplp0, showed higher expression levels in PepT1 KO crypts than in PepT1 KO villi (Figure 5-6b; red round spots above green square spots). Spot number, GI accession number, gene symbol, protein name, protein molecular weight, PI, average fold change, and overall trend of these spots are shown in Table 5-2.

Comparison of the differently expressed proteins along the crypt-villus axis in WT and PepT1 KO mice showed that PepT1 knockout had no effect on the expression of Hbb-bs, Prss1, Rpsa, Gyk, Rplp0, and Fabp6. Although Fabp1, Acta1, Fam135a, Rab21, PcnA,

Cndp2, and Psmc3 were differently expressed along the crypt-villus axis in WT mice (Figure 5-6a and Table 5-1), they showed similar expression levels along this axis in PepT1 KO mice (these proteins are not shown in Figure 5-6b and Table 5-2 because of their similar expression levels along the crypt-villus axis in PepT1 KO mice). Several other proteins, Eif4a1, Acadvl, Aldob, Tuba1c, Serpinb1a, and Dhhrs11, had similar expression levels along the crypt-villus axis in WT mice (these proteins are not shown in Figure 5-6a and Table 5-1 because of their similar expression levels different along the crypt-villus in WT mice), but were differentially expressed along this axis in PepT1 KO mice (Figure 5-6b and Table 5-2). Together, these results demonstrate that PepT1 expression dysregulates the normal differential expression of proteins along the crypt-villus axis.

*PepT1 expression altered normal protein profile in villus cells*

To investigate the effects of PepT1 knockout on protein expression in villus cells, protein expression was compared between PepT1 KO villi and WT villi. Representative 2D-DIGE gel images are shown in Figure 5-7a. Relative to WT, 14 proteins were up-regulated and 10 were down-regulated in PepT1 KO villi (Supplementary Figure 5-6a). 13 candidate spots were picked based on their reliability, location on the gel, intensity, and fold change ( $>2.09$ ) for mass spectrometry.

12 proteins were identified from the 13 selected spots using LC-MS. The expression levels of Rab-21, Serpinb1a, Aldob, Fam135a, Fabp1, Hbb-bs, Prss1, and glutathione S-transferase Mu1 (Gstm1) were lower in PepT1 KO than in WT villi (Figure 5-8a: green spots below the purple squares, Figure 5-9: Immunofluorescence staining showing lower expression of Rab-21 and Fabp1 in PepT1 KO than in WT villi); whereas the expression

levels of Actb, ATP synthase subunit beta, mitochondrial (Atp5b), Psmc3, and capping protein muscle Z-line, alpha 1 (Capza1) were higher in PepT1 KO villi than in WT villi (Figure 5-8a: green spots above the purple squares). Spot number, GI accession number, gene symbol, protein name, protein molecular weight, PI, average fold change, and overall trend are shown in Table 5-3. Together, these results demonstrate that PepT1 knockout modified normal protein expression in villus cells.

*PepT1 expression altered normal protein profile in crypt cells*

To investigate the effects of PepT1 KO on protein expression in crypts, protein expression levels were compared between PepT1 KO and WT crypts. Representative 2D-DIGE gel images are shown in Figure 5-7b. 2 proteins were up-regulated and 3 were down-regulated with volume difference in PepT1 KO crypts (Supplementary Figure 5-6b). 3 candidate spots were picked based on their reliability, location on the gel, intensity, and fold change (>2.03) for mass spectrometry.

LC-MS identified 3 proteins. The levels of Fabp6 and Gstm1 were lower (Figure 5-8b: red round spots below blue square spots), while the levels of Actb were higher (Figure 5-8b: red round spots above blue square spots), in PepT1 KO than in WT crypts. Spot number, GI accession number, gene symbol, protein name, protein molecular weight, PI, average fold change, and overall trend are shown in Table 5-4. Together these results demonstrate that PepT1 knockout modified normal protein expression in crypt cells.

Collectively, these results demonstrate that 3 proteins, Gyk, Rplp0, and Fabp6, show the same expression gradient along the crypt-villus axis in both PepT1 KO and WT mice, with much higher expression levels in crypts than in villi in both WT and PepT1 KO mice

(Figure 5-10a). 3 other proteins, Rpsa, Hbb-bs, and Prss1, were less expressed in crypts than in villi in both WT and KO mice (Figure 5-10b). However, the protein expression gradients of Serpinb1a, Aldob, Fam135a, Psm3, Actb and GStm1 differed between PepT1 KO and WT mice (Figure 5-10c, d). Together, these results demonstrate that protein expression differs along the crypt-villus axis, and knockout of PepT1 alters some of the protein expression gradient along this axis.

#### *PepT1 alters miRNA expression and their target protein expression*

The potential target genes of the 36 selected miRNAs were determined by 3 different algorithms, as described in the Materials and Methods section. The proteins identified on 2D-DIGE were examined in the target list for each miRNA. As mentioned in the Introduction, miRNAs and their target proteins showed reverse associations. Thus, we filtered the proteins that could be a target of a certain miRNA and showed reverse expression compared with that of miRNA.

4 pairs of miRNA and proteins were found to be related (Table 5-5). The expression of miRNA-221-3p was higher in crypts than in villi of WT mice, whereas it was higher in villi than in crypts of PepT1 KO mice (Figure 5-11a). This change in expression gradient was also reflected in the level of its target protein Serpinb1a (Figure 5-11b). Similarly, the expression of miR-200c-5p was higher in WT crypts than in WT villi, but the levels were similar in crypts and villi of PepT1 KO mice (Figure 5-11c). These findings were reflected by the expression of its target protein Rpsa (Figure 5-11d). Both miRNA-33-5p and its target protein Gyk showed the same gradient changes along the crypt-villus axis in WT and PepT1 KO mice (Figure 5-11e, f). Both miR-212-3p and its target Actb showed no expression gradient

along the crypt-villus axis in WT and PepT1 KO mice; however, the levels of expression of miR-212-3p were equivalently high in WT crypts and villi and equivalently low in PepT1 KO crypts and villi (Figure 5-11g, h). The expression of its target protein Actb was in agreement with miR-212-3p expression (Figure 5-11g, h). Together, these results suggest that knockout of PepT1 protein affects the expression of certain miRNAs, modifying the expression of their target proteins.

#### *PepT1 expression affects apoptosis and proliferation of IECs*

We have shown that PepT1 expression altered morphology of crypt-villus axis and molecular distribution of miRNA and protein. Further, we wanted to know if these changes are accompanied to modification of normal tissue homeostasis. Normal tissue homeostasis is determined by the balance between apoptosis and cell proliferation. A key feature of intestinal homeostasis is the ability to maintain epithelial integrity and trigger cell renewal along the crypt-villus axis. Here, we used TUNEL and Ki67 staining of small intestinal sections to assess IEC apoptosis and proliferation. As shown in Figure 5-12a, the apoptosis of IECs was higher in the villi of PepT1 KO mice than in those of WT mice. IEC proliferation was also increased in PepT1 KO mice compared to WT mice. Moreover, in contrast to WT mice, IEC proliferation was not largely restricted to crypt cells (Figure 5-12b). These results indicate that PepT1 expression modulates the balance of apoptosis and cell proliferation in the small intestine, and is thus likely to affect the overall function of the small intestine.

## 5.4 Discussion

We herein show that ablation of PepT1 expression does not significantly affect villus length in PepT1 KO mice. It does, however, affect the apoptosis and proliferation of IECs, suggesting that PepT1 contributes to maintaining intestinal homeostasis. The body weights of PepT1 KO mice were significantly lower than those of WT animals. This may reflect the decreased microvillus size observed in PepT1 KO mice, which would be likely to reduce their overall nutrient absorption and weight gain. These observations are in agreement with previous reports that mice lacking PepT1 exhibited reduced energy absorption (Kolodziejczak et al., 2013). We found that PepT1 expression exhibited a marked crypt-villus gradient. This is consistent with previous studies showing that PepT1 is abundant at the tip of the villus and decreases toward its base (Ogihara et al., 1999). These observations show that PepT1 is specific to the plasma membranes of the differentiated absorptive epithelial cells that form microvilli. Thus, a lack of PepT1 expression may limit microvilli development and decrease the overall capacity for intestinal absorption (Chen et al., 2010). These observations collectively suggest that PepT1 expression may affect major intestinal functions.

Protein expression along the crypt-villus axis is subject to a very dynamic regulatory process. The stem cells found at the base of the crypt continually divide and are the source of all epithelial cells (Gordon, 1989; Mac Donal et al., 2008). Cell proliferation, lineage-specific differentiation, migration, and apoptosis and/or cell shedding are all tightly interrelated along the crypt-villus axis (Gordon and Hermiston, 1994). A number of factors have been shown to regulate cell fate and differentiation in the intestine (Yang et al., 2001) (Korinek et al., 1998),

and the overall gene expression pattern has been shown to differ between crypts and villi (Mariadason et al., 2005).

miRNAs play critical roles in important biological processes, including development, differentiation, proliferation, and apoptosis (Lim et al., 2005), (Mirnezami et al., 2009), (Ruan et al., 2009). Our group previously showed that specific miRNA expression profiles are associated with the different differentiation statuses of IECs, and that miRNAs could contribute to determining the unique physiological characteristics of human IECs (Dalmasso et al., 2010b). Thus, we speculated that miRNAs could be involved in highly regulated process of protein expression/repression along the crypt-villus axis.

It is well known that the combined activities of various transcription factors modulate the expression of transcriptional targets in IEC along the crypt-villus axis (San Roman et al., 2015). Transcription factors are differentially expressed along the crypt and villus, presumably forming a basis for the differential protein expression between these cell types. It has been reported that miRNA expression is cell-type-specific (Sood et al., 2006). However, the miRNA expression levels in the various intestinal epithelial cell subtypes have not previously been studied along the crypt-villus axis.

Here, we describe cell fractionation experiments using mouse small intestinal epithelial cells, and report that miRNAs are differently expressed along the crypt-villus axis, where they are likely to play important roles in the expression/repression of various proteins, including transcription factors. We suggest that proper specification of the intestine during development relies on not only the action of transcription factors, but also the effects of these miRNAs. Moreover, we propose that tight control of the miRNA expression gradients along

the crypt-villus axis is crucial for the maintenance of normal intestinal epithelial integrity(Xiao and Wang, 2014).

To evaluate the potential interdependence of protein and miRNA expression levels along the crypt-villus axis, we used the PepT1 KO mice model. In our previous study, we demonstrated that overexpression of PepT1 in a specific tissue (colon) altered the overall miRNA expression in that tissue(Ayyadurai et al., 2014). In the present study, we observed that KO of PepT1, which is mostly expressed in villi, affected the expression levels and expression gradients of miRNAs in the small intestine. Interestingly, we observed that the lacking of PepT1 expression affect the normal miRNAs expression along the crypt-villus axis of WT mice. When comparing the same miRNAs, we observed a change of the miRNAs expression in crypt cell in mice lacking PepT1 expression in crypt cells. The later observation implies that PepT1 knockout could therefore conceivably dysregulate protein expression in crypt cells *via* the observed alterations in miRNA expression or through other miRNAs-independent pathways. Thus, PepT1 expression could impact the regulatory networks of crypt cells at least in part by modulating the steady-state levels of miRNAs in these cells. Consistent with this proposal, a recent study exhibited that viruses such as HIV disrupt normal host miRNA expression specifically in the proliferative crypt region. Notably, proper miRNA expression in this region controls the expression levels of genes involved in cell death and epithelial maturation, and thereby affects overall intestinal homeostasis(Gaulke et al., 2014). The PepT1 KO mice also exhibited disrupted miRNA expression profiles in their villus cells. We do not yet know whether this is a downstream effect of altered miRNA biogenesis in the crypt cells or a direct effect on villus cells.

We further observed that the protein expression gradients along the crypt-villus was altered in PepT1 KO mice compared to WT, suggesting that the homeostasis of the small intestine was affected in PepT1 KO mice. The altered proteins included Ras-related protein (Rab21), which belongs to a subfamily of Ras-superfamily small GTP-binding proteins. Rab21 plays an important role in regulating vesicular transport at the apical sides of polarized intestinal epithelial cells (Opdam et al., 2000), and acts as a signal transduction molecule in the development of the brush borders (microvilli) (Paradela et al., 2005). In PepT1 KO mice, Rab21 expression was ~ 4.58-fold lower than that in WT mice. This could explain why the microvilli in PepT1 KO mice are less developed than those of WT mice, which would affect intestinal absorption in these mice (Figure 5-9a). Another altered protein was fatty acid-binding protein (Fabp1), which shows high-level expression in villus cells but low-level expression in crypt cells of normal mice, and is used as a marker of cell differentiation (Carroll et al., 1990). We observed that Fabp1 expression was reduced in the villus cells of PepT1 KO mice, suggesting that such mice may exhibit altered cell differentiation along the crypt-villus axis (Figure 5-9b).

We herein report that PepT1 KO affects the expression levels and gradients of both miRNAs and proteins along the crypt-villus axis, and that there are correlations between the changes in miRNA and protein levels. For example, miR-221-3p and its protein target, *serpinb1a*, are expressed equally in the crypt and villus cells of WT mice but exhibit gradients between the crypts and villi of PepT1 KO mice. These results support our hypothesis that the absence of PepT1 expression dysregulates normal miRNA expression and alters the expression levels of their target proteins along the crypt-villus axis. The latter observation

implies that PepT1 KO could conceivably dysregulate protein expression in the crypt-villus axis via the observed alterations in miRNA expression. However, we cannot rule out that the observed dysregulated protein expression along the crypt-villus axis in PepT1 KO could also be miRNAs-independent. To determine whether this correlation between miRNA expression and target protein expression is direct, a transfect of certain miRNAs into isolated crypts or enteroids from WT and KO mice could be helpful and need to be further studied.

We found that PepT1 and the differential expression of its target miRNAs along the crypt-villus axis could contribute to cell fate decisions along the crypt-villus axis. Previous studies have shown that transcription factors are required for proper specification of cells along the crypt-villus axis(Nduati et al., 2007). Based on our present results, we demonstrate that miRNAs could post-transcriptionally modulate or fine-tune the dynamics of the cellular processes that occur along this axis. The disruption of normal miRNA expression along the axis, such as that seen in some pathologies like miRNA-135b overexpression in colon cancer(Khatri and Subramanian, 2013), may affect intestinal homeostasis and/or functions. Our results also suggest that PepT1 helps maintain small intestinal homeostasis and function by regulating miRNA/protein expression along the crypt-villus axis. These alterations could occur *via* the actions of PepT1 on transcription factors and/or miRNAs, or indirect through other pathways including other cellular components or immune cells, offering multiple combinations through which different cellular functions may be regulated.

Although PepT1 is found to be mostly expressed in the small intestine, low levels of PepT1 expression is also reported in the kidney, pancreas and bile duct(Bockman et al., 1997; Knutter et al., 2002; Shen et al., 1999). In the kidney, PepT1 is detected in the cortex. Since

another oligopeptide transporter PepT2 has greater abundance over PepT1 in kidney, we speculate that peptides are predominantly reabsorbed in kidney by PepT2. However, we cannot rule out the possibility that ablation of PepT1 in kidney or other organs will also play important roles in mediating their homeostasis.

## 5.5 Methods

### *Mouse model*

PepT1 KO mice obtained from Deltagen (San Mateo, CA) were backcrossed with WT (C57BL/6) animals to obtain the same genetic background in both controls (WT and PepT1 KO). Genomic DNA from tail snips was extracted using the RED Extract-Amp Tissue PCR Kit (Sigma, St Louis, MO) according to the manufacturer's protocol. The primers used for identifying PepT1 KO mice were 5'-GGGCCAGCTCATTCTCCCACTCAT-3', 5'-AGTGTGGGCTGGTGTGAGACACGTGT-3' (forwards) and 5'-CAGGGGGAGAGAGAAACAGAGTTAG-3' (reverse). Specific PCR products for each target gene were obtained under the following conditions: 94°C for 3 min, 94°C for 15 s, 55°C for 30 s, 72°C for 1 min, and 72°C for 10 min for a total of 40 cycles. All mice were housed in groups of 5 per cage at Georgia State University under controlled conditions of 12:12 h dark/light, 5% humidity and 25°C. Animal experiments were approved by the Institutional Animal Care and Use Committee of Georgia State University (Atlanta, GA), and performed in accordance with the guide for the Care and Use of Laboratory Animals by U.S. Public Health Service. All procedures were approved and registered in the protocol IACUC ID: A14007.

### ***Isolation of epithelium from crypts and villi of small intestine***

Epithelium was isolated from crypts and villi of the small intestines of 8 week-old WT and PepT1 KO female mice using the low-temperature method(Flint et al., 1991). Small intestines were cleaned and sliced into 2-3 mm sections. Pieces were washed in HBSS with 0.5 mM DTT for 5 min at 4°C with constant stirring at 200 rpm (Step 1). Detached tissues were collected as sample 1. Tissue pellets were transferred to 115 ml of chelating buffer (27 mM trisodium citrate, 5 mM Na<sub>2</sub>HPO<sub>4</sub>, 96 mM NaCl, 8 mM KH<sub>2</sub>PO<sub>4</sub>, 1.5 mM KCl, 0.5 mM DTT, 55 mM D-sorbitol, 44 mM sucrose, pH 7.3), incubated at 4°C for 20 min with constant stirring at 200 rpm, and re-collected as sample 2 (Step 2). The remaining pellets were re-suspended in 20 ml of fresh chelating buffer in a 50 ml centrifuge tube for washing. The tube was manually inverted 60 times and detached pieces were collected as sample 3 (Step 3). Next, 20 ml of fresh chelating buffer was added to the wash tube and manually washed for three times. Detached pieces were collected every time as sample 3 (Step 4). After manual washing, step 2 through step 4 was repeated three times to collect sample 4-9. Tissue pellets were further re-suspended in 20 ml chelating buffer in a 50 ml centrifuge tube and vigorously shaken by hand for 1 min. Detached pieces were collected as sample 10 (Step 5). Step 5 was then repeated to collect sample 11. Samples 1-11 collected from the separation procedures were re-suspended in 1 ml HBSS for further experimental use. The purity of villi and crypts was examined *via* microscopy and RT-PCR, and samples were stored at -80°C until use. See Figure 5-2.

### ***Sample collection and preparation***

Approximately 2.0 cm pieces of small intestine or villi/crypt samples collected from isolated small intestine were homogenized in RIPA buffer (150 mM NaCl, 0.5% sodium deoxycholate, 50 mM Tris-HCl, pH 8.0, 0.1% SDS, 0.1% Nonidet P-40) with one tablet of protease inhibitor. Homogenates were centrifuged at 12,000 rpm for 10 min at 4°C, and protein concentrations were measured using the DC protein assay kit (Bio-Rad, Hercules, CA). The protein solution was used either for Western Blot or 2-D analysis after 2-D clean-up. For 2-D clean-up, 230 mg of protein was precipitated, purified and cleaned using a specific kit (GE Healthcare Life Science, Piscataway, NJ), according to the manufacturer's protocol. Precipitated pellets were re-suspended in 65 µl of rehydration buffer (2M Thiourea, 7M Urea, 4% Chaps, 25 mM Tris-HCl, pH 8.8).

#### ***Sample labeling and two-dimensional gel electrophoresis***

WT villi (or WT crypts) sample (30 µg) was labeled with 200 pmol N-hydroxysuccinimidyl-ester of cyanine dye, Cy3, and 30 mg KO villi (or KO crypts) sample was labeled with 200 pmol N-hydroxysuccinimidyl-ester of cyanine dye, Cy5 (GE Healthcare Life Science, Piscataway, NJ). After quenching with 10 mM lysine, the labeled proteins were mixed. Sample buffer (7 M urea, 4 M thiourea, 4% CHAPS, 2% IPG buffer, pH 4-11, NL) and rehydration solution (7 M urea, 4 M thiourea, 4% CHAPS, 1% DTT, 1% IPG) were added to a final volume of 350 µl for each gel. First-dimension isoelectric focusing (IEF) was performed using 24 cm IPG strips (pH 4-7, GE Healthcare Life Sciences, Piscataway, NJ) in EttanIPGphor (GE Healthcare Life Sciences, Piscataway, NJ). Strips containing samples were equilibrated, reduced, alkylated and stained *via* sequential incubation in 1.5% DTT equilibration buffer (50 mM Tris-HCl, 6 M urea, 30% glycerol, and 2% SDS) and 4.5%

iodoacetamide equilibration buffer stained with bromophenol blue for 20 min each. Second-dimension electrophoresis was conducted on a 10% SDS polyacrylamide gel in the Ettan DALT II system separation unit (GE Healthcare Life Science, Piscataway, NJ).

Gel images were further acquired on a Typhoon Trio (GE Healthcare) at the appropriate wavelengths for Cy3 and Cy5 dyes, and analyzed using DeCyder image analysis software (V7.0, GE Healthcare). Next, gels were visualized with colloidal Coomassie staining (SimplyBlue, Invitrogen, Carlsbad, CA). Coomassie-stained gel was re-scanned with the Typhoon Trio Scanner, and the image matched and aligned with Cy3 and Cy5 fluorescence images. A list of proteins of interest showing >1.75-fold increase or decrease was collated, based on the analysis. 3D views of individual spots generated with DeCyder image analysis software (GE Healthcare) were also considered while selecting the list of proteins.

#### ***Spot picking and mass spectrometric protein identification***

The pick list was exported to Ettan Spot Picker (GE Healthcare), and protein spots excised and transferred to a microtiter plate using Ettan Spot Picker. Picked gel pieces were washed initially with dd H<sub>2</sub>O and subsequently with washing solution I (50% ethanol, 10% acetic acid) following by washing solution II (50% acetonitrile, 100 mM ammonium bicarbonate, pH 8.3). Cleaned gel pieces were finally dehydrated with 100% acetonitrile and dried under a speed-vac. Dried gels were either digested with trypsin or incubated at -80°C until trypsin treatment for mass spectrometry peptide analysis. Gel pieces were incubated with an appropriate amount of trypsin (Modified Trypsin Gold, Promega, Madison, WI) in ProteaseMax Surfactant (Promega, Madison, WI) at 37°C for 2-3 h. After incubation,

digested peptides were extracted with 2.5% trifluoroacetic acid, further purified and concentrated using ZipTip, a micro-reverse phase column (Millipore, Bilerica, MA), according to the manufacturer's protocol. Extracted peptides were subsequently analyzed with a 4800 MALDI-TOF/TOF tandem mass spectrometer (AB Sciex, Framingham, MA) in the MS/MS tandem mode. Protein identification was accomplished using Mascot search engine (Matrix Science Inc, Boston, MA) against Swiss-Prot or NCBI protein databases.

### ***RNA extraction and real-time reverse transcription-PCR***

Total RNA was extracted from mouse small intestine with the RNeasy Mini kit (Qiagen, Valencia, CA), according to the manufacturer's instructions, and yield and quality verified. cDNA was generated from total RNA using the maxima first-strand cDNA synthesis kit (Thermo Scientific, Glen-Burnie, MD). cDNA of miRNAs was generated from total RNA preparations using NCode miRNA first-Strand cDNA synthesis and qRT-PCR kits (Invitrogen, Carlsbad, CA). Levels of targets were quantified with real-time reverse transcription (RT-PCR) using Maxima SYBR Green/ROX qPCR Master Mix (Fermentas). Fold induction was calculated using the Ct method as follows:  $\Delta\Delta CT = (CT_{\text{target}} - CT_{\text{housekeeping}})_{\text{group1}} - (CT_{\text{target}} - CT_{\text{housekeeping}})_{\text{group2}}$ , and final data derived from  $2^{-\Delta\Delta CT}$ .

### ***Microarray analysis of miRNA expression***

Total RNA (50 ng) containing miRNA was extracted from small intestine of mice with the miRCURY RNA isolation kit-Tissue (Exiqon, Woburn, MA) according to the manufacturer's protocol for purification of miRNA from animal tissue. RNA yield and quality were verified. All miRNA PCR reactions were performed by Exiqon Services,

Vedvack, Denmark. RNA (10 ng) was reverse-transcribed in 50 µl reactions using the miRCURY LNA™ Universal RT microRNA PCR, Polyadenylation and cDNA synthesis kit (Exiqon). cDNA was diluted 100× and assayed in 10 µl reaction mixtures using the protocol for miRCURY LNA™ Universal RT microRNA PCR. Every microRNA was assayed once with qPCR on microRNA Ready-to-Use PCR, Mouse&Rat panel I+II using ExiLent SYBR® Green master mix. Negative controls, excluding the template from the reverse transcription reaction, were examined and profiled in a similar manner to samples. Amplification was performed in a LightCycler® 480 Real-Time PCR System (Roche) in 384-well plates. Amplification curves were analyzed using Roche LC software, both for determination of C<sub>q</sub> (with the second derivative method) and for melting curve analysis. Amplification efficiency was calculated using algorithms similar to those in LinReg software. Criteria for inclusion of an assay in the analysis included C<sub>p</sub> less than 37 and 5 less than that of negative control. Data that did not satisfy these criteria were omitted from further analysis. All data were normalized to the average of samples detected in all assays (average – assay C<sub>p</sub>), which was confirmed as the best normalizer using NormFinder.

### ***miRNA target prediction***

To determine the potential target genes of detected miRNAs, miRSearch V3.0 algorithms (Exiqon, Woburn, MA) (<https://www.exiqon.com/mirsearch>), miRDB database (<http://mirdb.org/cgi-bin/search.cgi>), and TargetScanMouse ([http://www.targetscan.org/mmu\\_61/](http://www.targetscan.org/mmu_61/)) were used.

### ***Hematoxylin and eosin (H&E) staining***

Mouse small intestines were fixed with 10%-buffered formalin for 24 h at room temperature and then embedded in paraffin. Tissues were sectioned at 6- $\mu$ m and stained with H&E using standard protocols. Images were acquired using an Olympus microscope equipped with a DP-26 Digital camera (Olympus, Tokyo, Japan).

### ***Immunohistochemistry***

Paraffin-embedded tissue sections were de-paraffinized in xylene and rehydrated in an ethanol gradient. For epitope retrieval, the sections were heated in 10 mM sodium citrate buffer (pH 6.0) for 10 min in a pressure cooker. The sections were then blocked with 5% goat serum in TBS and incubated for 1 hour at 37°C with anti-PepT1 (1:200; Santa Cruz, Dallas, TX), anti-Muc2 (1:600; Santa Cruz, Dallas, TX), or anti-Rab21 (1:600; Abcam, Cambridge, MA). After being washed with PBS, the sections were incubated with Alexa-Fluor 568 phalloidin (1:5000; Invitrogen Carlsbad, CA) and a horseradish peroxidase-conjugated secondary antibody for 45 minutes at room temperature in the dark. Sections were mounted in mounting medium containing 4', 6-diamidino-2-phenylindole (DAPI; Vector Laboratories, Burlingame, CA) and covered with coverslips. Images were acquired using an Olympus microscope equipped with a Hamamatsu Digital Camera ORCA-03G (Olympus, Tokyo, Japan).

### ***Terminal deoxynucleotidyl transferase deoxyuridine triphosphate nick-end labeling (TUNEL) staining***

For quantification of apoptosis among epithelial cells of the small intestine, paraffin sections were de-paraffinized and stained for apoptotic nuclei using an *In Situ* Cell Death Detection Kit (Roche Diagnostics, Indianapolis, IN) according to the manufacturer's

instructions. Images were acquired using an Olympus microscope equipped with a Hamamatsu black and white ORCA-03G digital camera (Olympus, Tokyo, Japan). The numbers of TUNEL-positive cells that overlapped with DAPI nuclear staining were counted per villus.

### ***Ki67 staining***

Mouse small intestinal tissues were formalin-fixed, paraffin-embedded, and sectioned. The sections were de-paraffinized in xylene and rehydrated in an ethanol gradient. For antigen retrieval, the sections were placed in 10 mM sodium citrate buffer (pH 6.0) and cooked with a pressure cooker for 10 minutes. The sections were blocked with 5% goat serum in TBS, and incubated with anti-Ki67 (1:100; Vector Laboratories, Burlingame, CA) for 1 hour at 37°C. After being washed with TBS, the sections were treated with the appropriate biotinylated secondary antibodies for 1 hour at 37°C, and color development was performed using a Vectastain ABC kit (Vector Laboratories, Burlingame, CA). The sections were then counterstained with hematoxylin, dehydrated, and coverslipped. Images were acquired using an Olympus microscope equipped with a DP-23 Digital camera (Olympus, Tokyo, Japan). The numbers of Ki-67-positive cells were counted per villus.

### ***Transmission electron microscopy (TEM)***

Small intestine tissues were dissected into 1 to 2 mm cubes while immersed in 2.5% glutaraldehyde buffered with 0.1 M sodium cacodylate (pH 7.2). Samples were stored in the same fixative overnight at 4 °C. Samples were then washed with the same buffer and post-fixed in 1% buffered osmium tetroxide, dehydrated through a graded ethanol series to 100%, and embedded in Eponate 12 resin (Ted pella Inc., Redding, CA). Ultrathin sections

were cut on a Leica UC6rt ultra microtome (Leica Microsystems, Buffalo Grove, IL) at 70-80 nm and counterstained with 4% aqueous uranyl acetate and 2% lead citrate. Sections were examined under a LEO906e transmission electron microscope (Carl Zeiss, Oberkochen, German) at a voltage of 80 kV.

### ***Western blot***

Collected proteins (30  $\mu$ g) were resolved on 12% polyacrylamide gels (Bio-Rad, Hercules, CA) and transferred to nitrocellulose membranes (Bio-Rad, Hercules, CA). Membranes were probed with anti-PepT1 primary antibody (dilution 1:1000; Santa Cruz, Dallas, TX). After three washes, membranes were incubated with the appropriate horseradish peroxidase-conjugated secondary antibodies (dilution 1:4000, GE Healthcare Biosciences, Pittsburgh, PA) and bands detected using the Enhanced Chemiluminescence Detection Kit (GE Healthcare Biosciences, Pittsburgh, PA).

### ***Statistical analysis***

Values were expressed as means $\pm$ s.e.m. Statistical analysis for significance ( $P<0.05$ ) was determined using two-tailed Student's *t*-test by GraphPad Prism 5 software. Differences were noted as significant with: \* $P<0.05$ , \*\* $P<0.005$ , \*\*\* $P<0.001$ .

## **5.6 Acknowledgments**

This work was supported by grants from the Department of Veterans Affairs (BX002526) and the National Institutes of Health of Diabetes and Digestive and Kidney (RO1-DK-071594 to D.M). E. Viennois and M. Zhang are recipients of a Research Fellowship Award from the Crohn's & Colitis Foundation of America. D. Merlin is a recipient of a Research Career Scientist Award from the Department of Veterans Affairs.

### **5.7 Author contributions**

YZ and DM conceived and designed the experiments, analyzed the data, and wrote the manuscript. YZ performed the experiments. BX, EV, MZ, MH, LW, PG contributed reagents and materials. All the authors participated in general discussions, read, commented and approved of the final the manuscript.

### **5.8 Competing financial interests**

The authors declare that they have no competing financial interests.

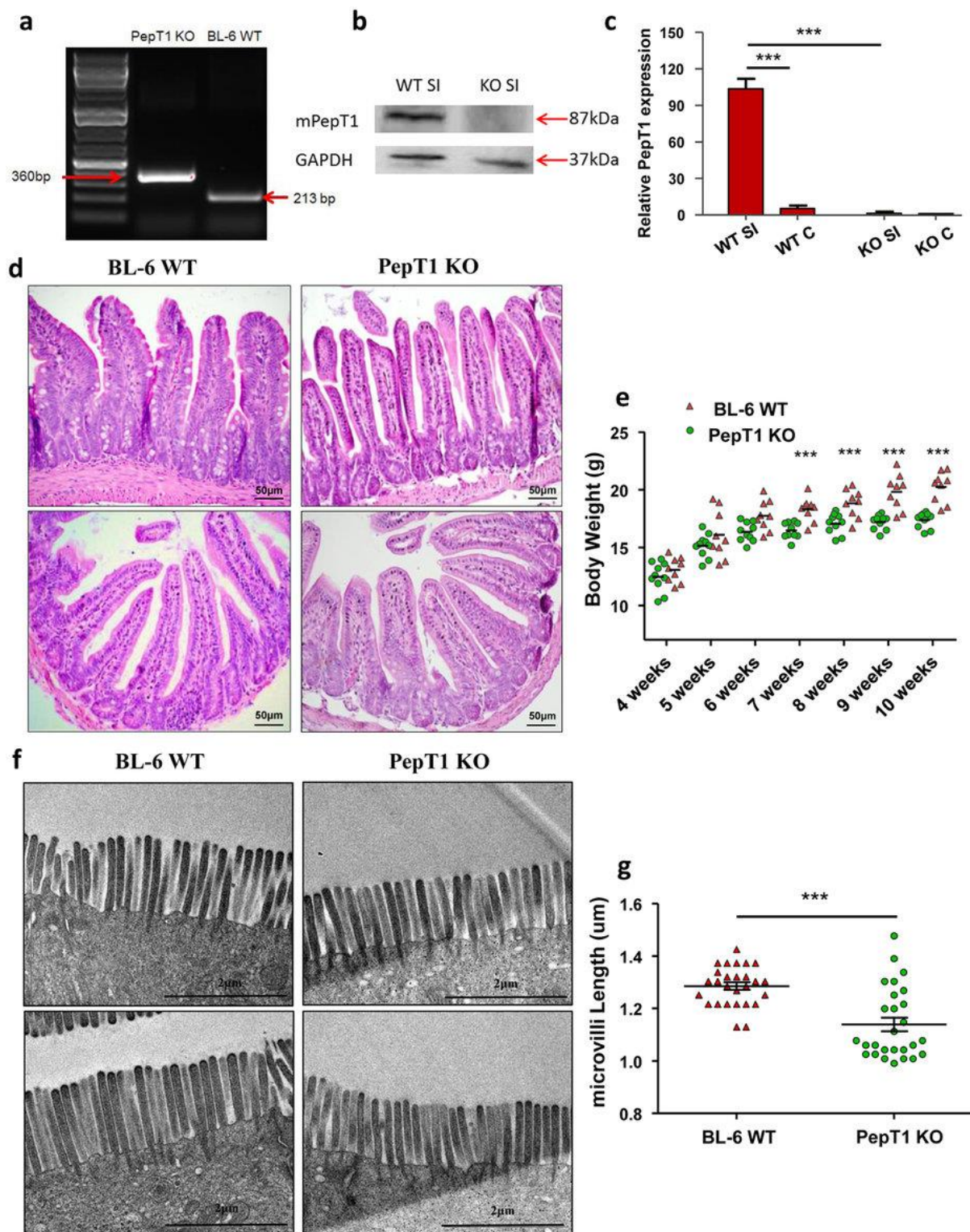


**Figure 5.1 PepT1 knockout reduces mouse body weight and the size of intestinal microvilli.**

*a.* Genotyping was performed on PepT1 KO and BL-6 WT mice. Homozygous PepT1 KO mice and appropriate BL-6 WT controls were used in our studies. *b* and *c.* PepT1 expression levels in the small intestines of PepT1 KO and BL-6 WT mice were detected by Western blotting (*b*) and qRT-PCR (*c*). *d.* Representative H&E-stained sections of small intestines from BL-6 WT and PepT1 KO mice showed no significant gross morphology difference. Original magnification, 20 $\times$ . Scale bars, 50  $\mu$ m. *e.* Body weights measured at the indicated ages were significantly higher in BL-6 WT mice than in PepT1 KO mice (PepT1 KO: n=9/group, BL-6 WT: n=9/group \*\*\* $P$ <0.001). *f* and *g.* Transmission electron photomicrographs showed abnormal morphology and smaller microvilli on the apical membrane of jejunal enterocytes from PepT1 KO mice compared to those of BL-6 WT controls. Scale bars, 2  $\mu$ m; n= 27 microvilli/group; and \* $P$ <0.05, \*\*\* $P$ <0.001.

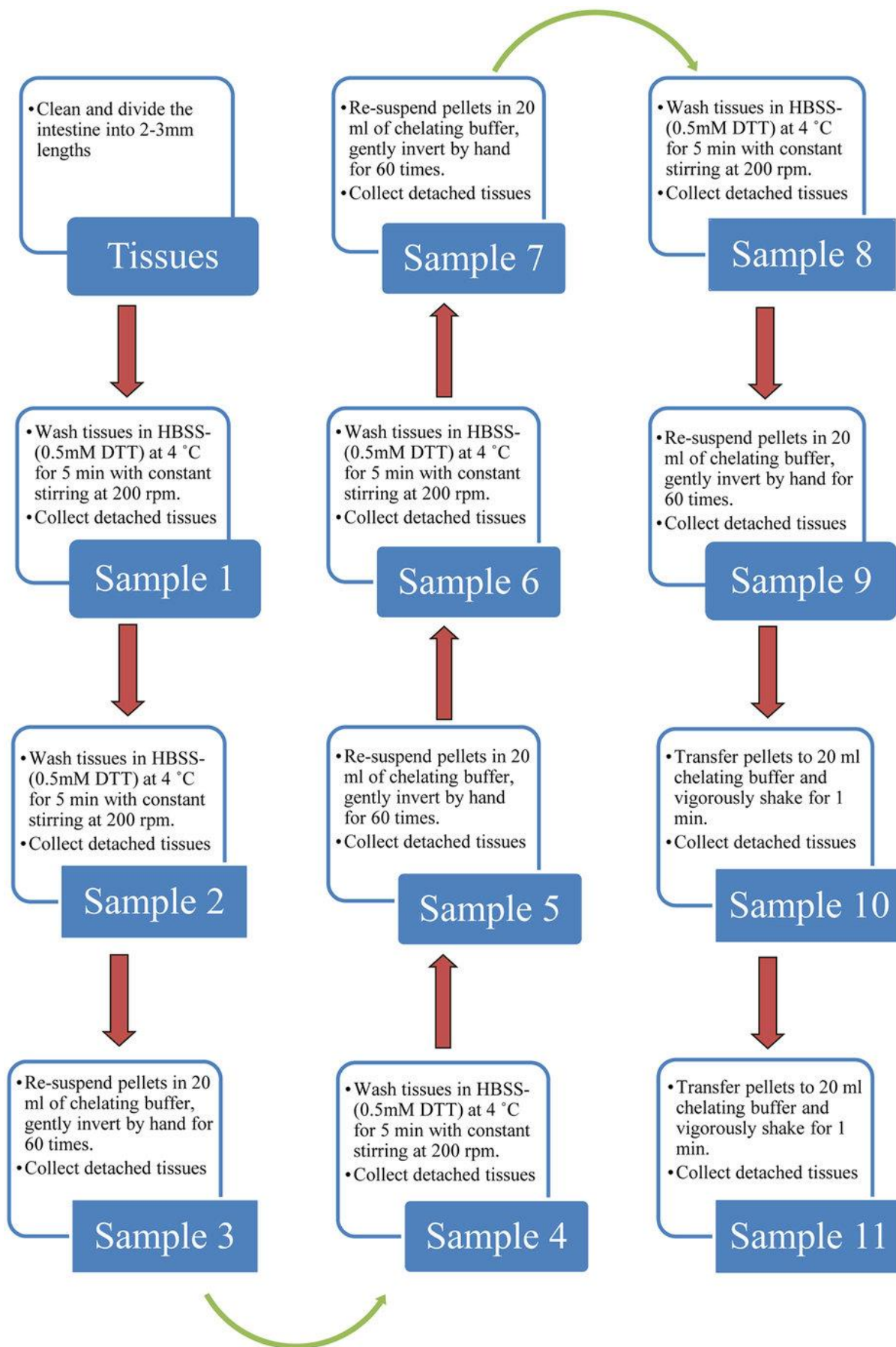


**Figure 5.2 Flow diagram of the low-temperature method used to obtain villi and crypts from intestinal epithelial cells at 4°C.**

Epithelia of the jejunum were isolated from crypts and villi of the small intestines of 8-week-old BL-6 WT and PepT1 KO female mice using the previously described low-temperature method(Flint et al., 1991).

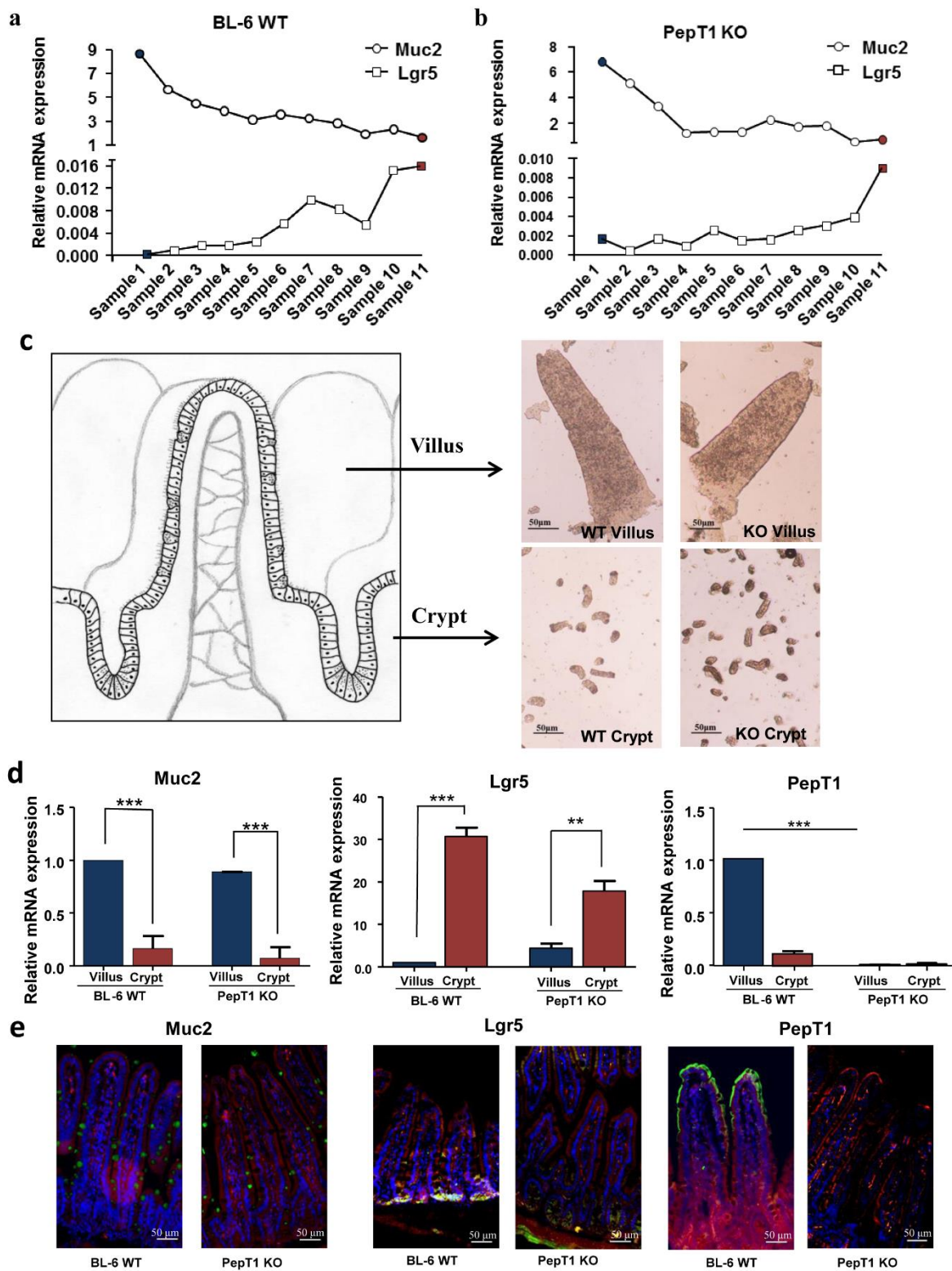


**Figure 5.3 Isolation of villi and crypt epithelial cells of the jejunum from BL-6 WT and PepT1 KO mice.**

*a.* Total RNAs were extracted from the different fractions collected from BL-6 WT mice using the low-temperature method, and the expression levels of Muc2 (as a villus marker) and Lgr5 (as a crypt marker) were assessed by qRT-PCR. *b.* Total RNAs were extracted from different fractions collected from PepT1 KO mice, and the expression levels of Muc2 (as a villus marker) and Lgr5 (as a crypt marker) were assessed by qRT-PCR. *c.* Pictures of selected villi and crypts fractions were taken with a Nikon Eclipse TS100 microscope at 10× magnifications. Scale bar, 50 μm. *d.* Total RNAs were extracted from selected villus and crypt fractions from BL-6 WT and PepT1 KO mice. The expression levels of Muc2, Lgr5 and mPepT1 in the villi (blue bars) and crypts (magenta) of BL-6 WT and PepT1 KO mice were further assessed by qRT-PCR (n= 5; and \*\* $P < 0.005$ , \*\*\* $P < 0.001$ ). *e.* The expression of Muc2, Lgr5 and mPepT1 in the tissue were confirmed by immunofluorescence. Muc2, Lgr5, mPepT1 were immunostained using anti-Muc2, anti-Lgr5 and anti-PepT1 (FITC, green), respectively, F-actin was stained using phalloidin (TRITC, red), and cell nuclei were stained using DAPI (blue). Separate pictures were taken at 20× for each filter, and the images were merged. Scale bar, 50 μm.

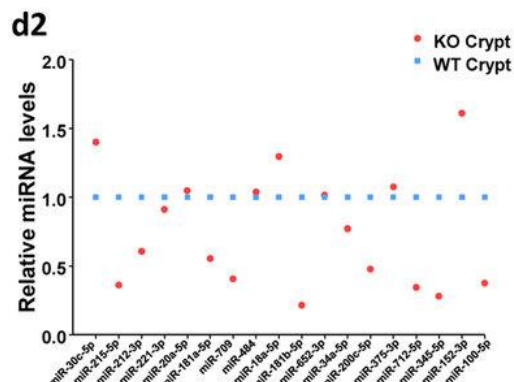
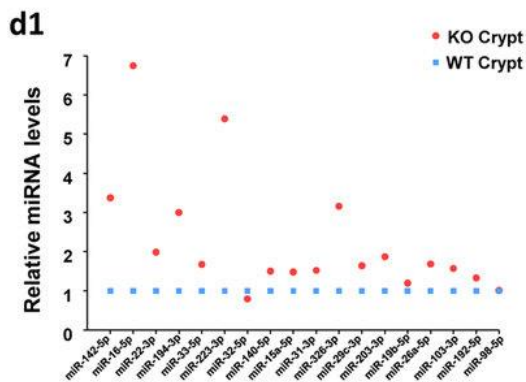
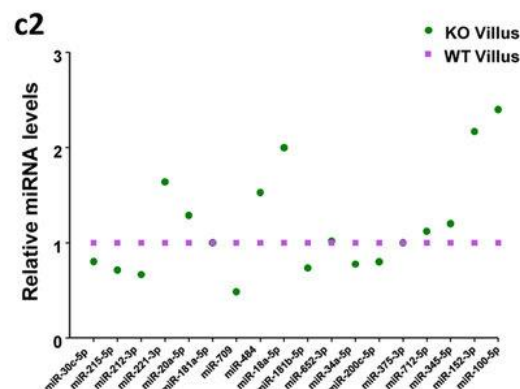
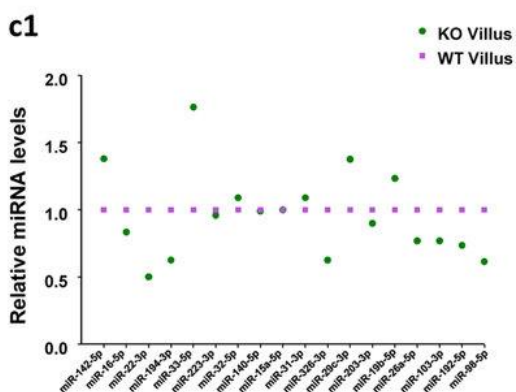
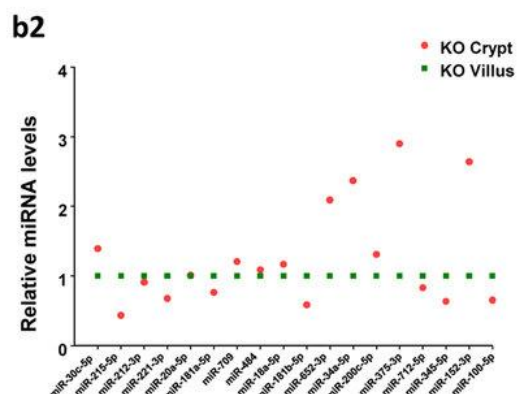
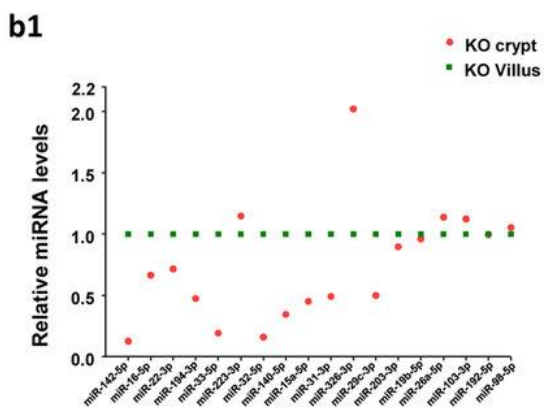
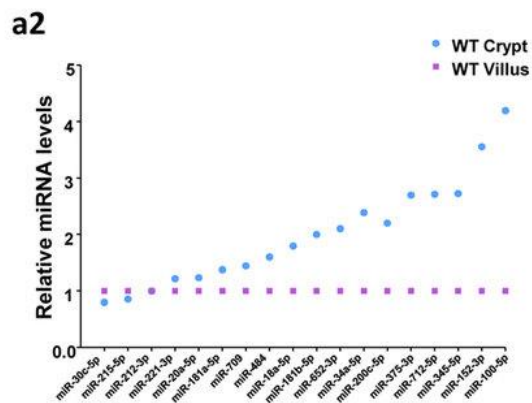
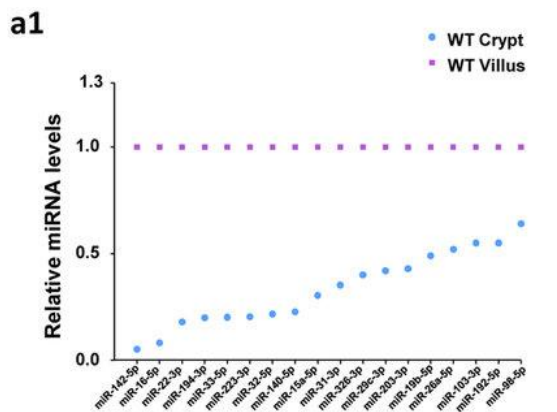


**Figure 5.4 Expression levels of miRNAs in crypt and villus epithelial cells from BL-6 WT and PepT1 KO mice.**

A total of 36 miRNA transcripts were found to be differentially expressed in the villi and crypts of BL-6 WT and PepT1 KO mice; those having  $P < 0.05$  and signal  $> 500$  are shown (n=4). *a1* and *a2*. In BL-6 WT crypts compared to BL-6 WT villi, 20 miRNAs were lower expressed (blue spots below purple spots), 1 displayed similar expression levels, and 15 were higher expressed (blue spots above purple spots). *b1* and *b2*. In PepT1 KO crypts compared to PepT1 KO villi, 17 miRNAs were lower expressed (red spots below green spots), 12 displayed similar expression levels in the two tissues, and 7 were higher expressed (red spots above green spots). *c1* and *c2*. In PepT1 KO villi compared to BL-6 WT villi, 15 miRNAs were down-regulated (green spots below purple spots), 10 displayed similar expression levels, and 11 were up-regulated (green spots above purple spots). *d1* and *d2*. In PepT1 KO crypts compared to BL-6 WT crypts, 11 miRNAs were down-regulated (red spots below blue spots), 11 displayed similar expression levels, and 14 were up-regulated (red spots above blue spots).

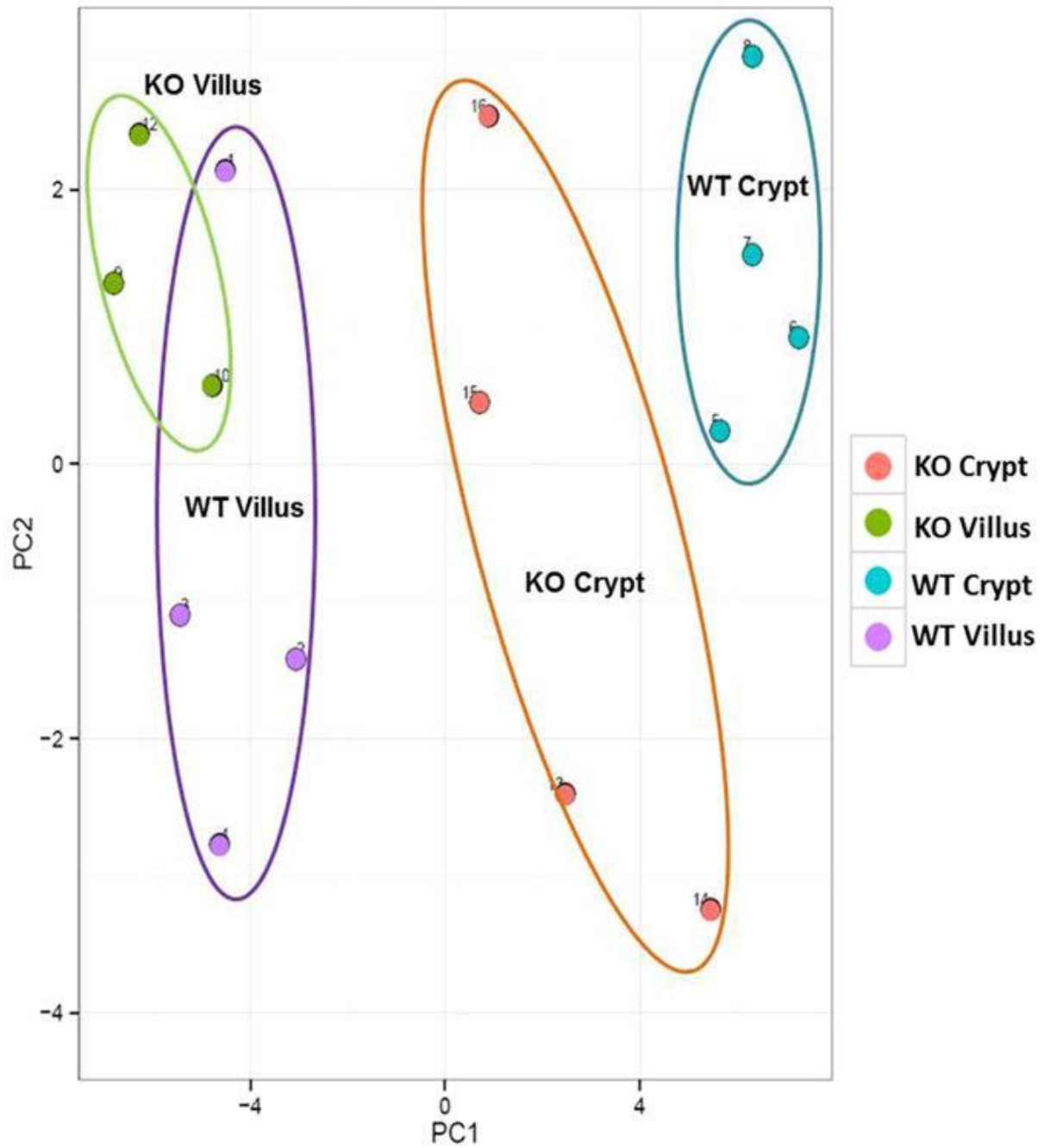


**Figure 5.5 Overall distribution of miRNAs in crypt and villus cells from PepT1 KO and BL-6 WT mice.**

Overall miRNA populations are shown as a Principal Component Analysis (PCA) plot including the top 50 miRNAs that showed the largest variations across all samples.

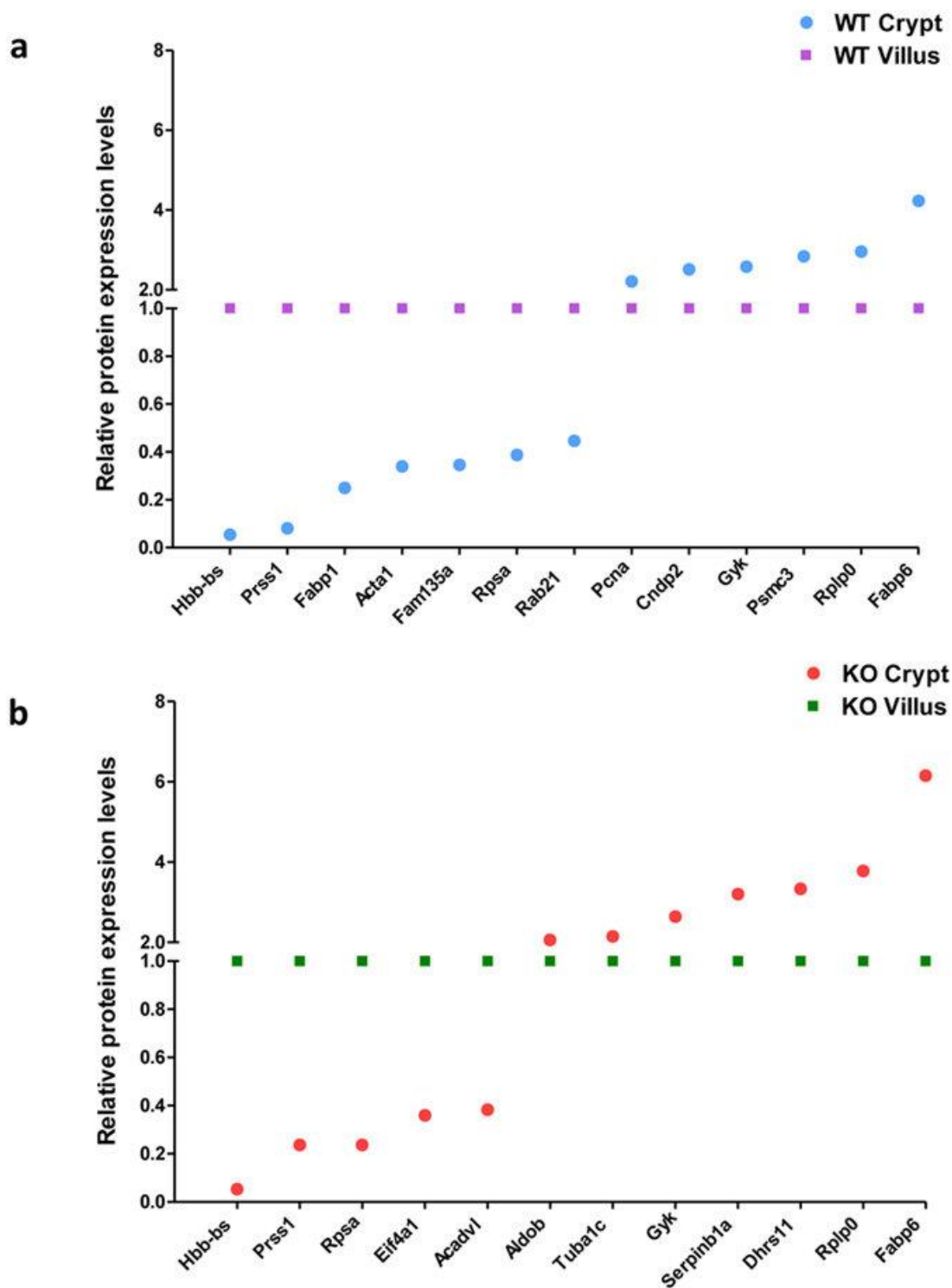


**Figure 5.6 Differential expression of proteins along the crypt-villus axis.**

*a.* In BL-6 WT crypts compared to BL-6WT villi, 7 proteins were lower expressed (blue spots below purple spots) and 6 proteins were higher expressed (blue spots above

purple spots). *b.* In PepT1 KO crypts compared to PepT1 KO villi, 5 proteins were lower expressed (red spots below green spots) and 7 proteins were higher expressed (red spots above green spots).

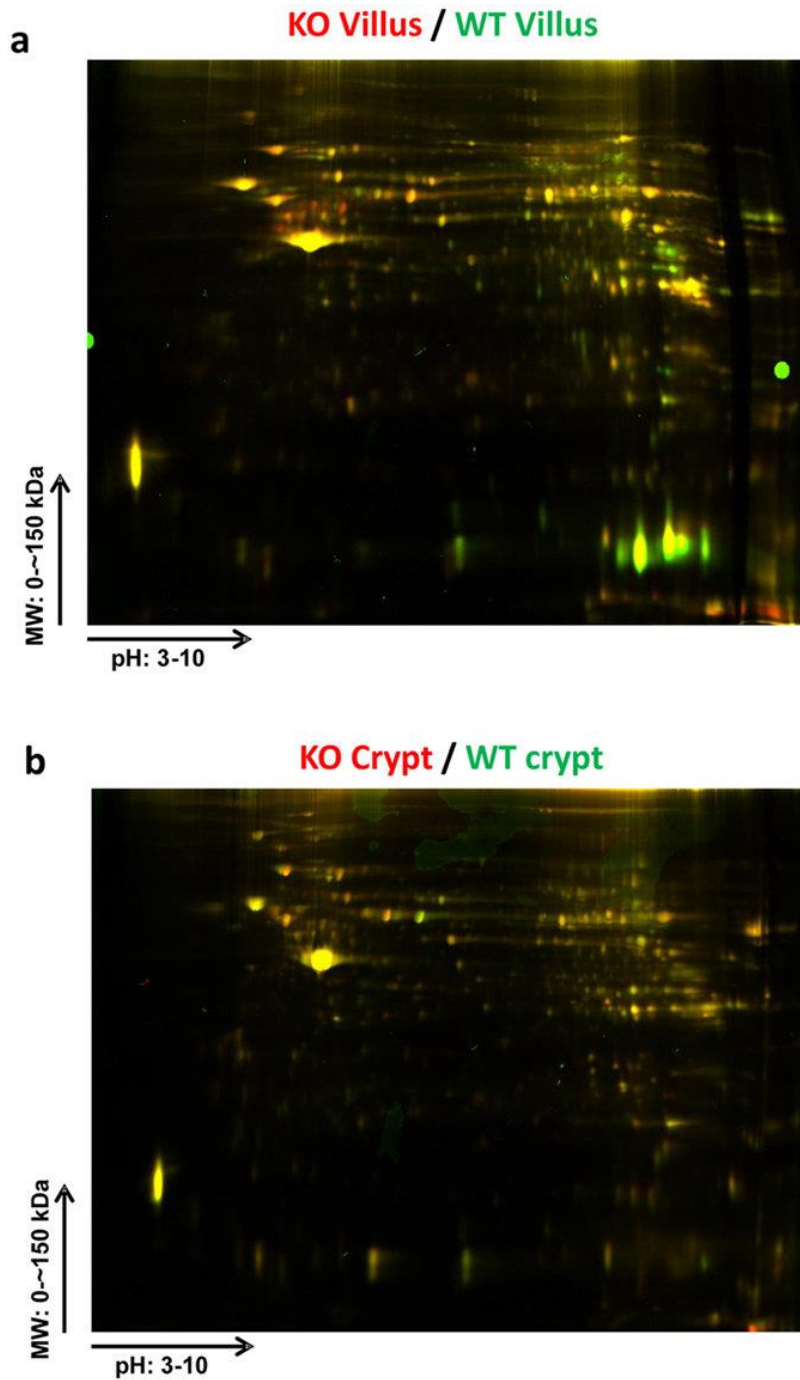


**Figure 5.7 2D-DIGE-based assessment of differential protein expression.**

*a.* Superimposed 2D-DIGE overlay image of protein accumulation in the villi of PepT1 KO (Cy5, red fluorescence) and BL-6 WT (Cy3, green fluorescence) mice. *b.* Superimposed

2D-DIGE overlay image of protein accumulation in the crypts of PepT1 KO (Cy5, red fluorescence) and BL-6 WT (Cy3, green fluorescence) mice.

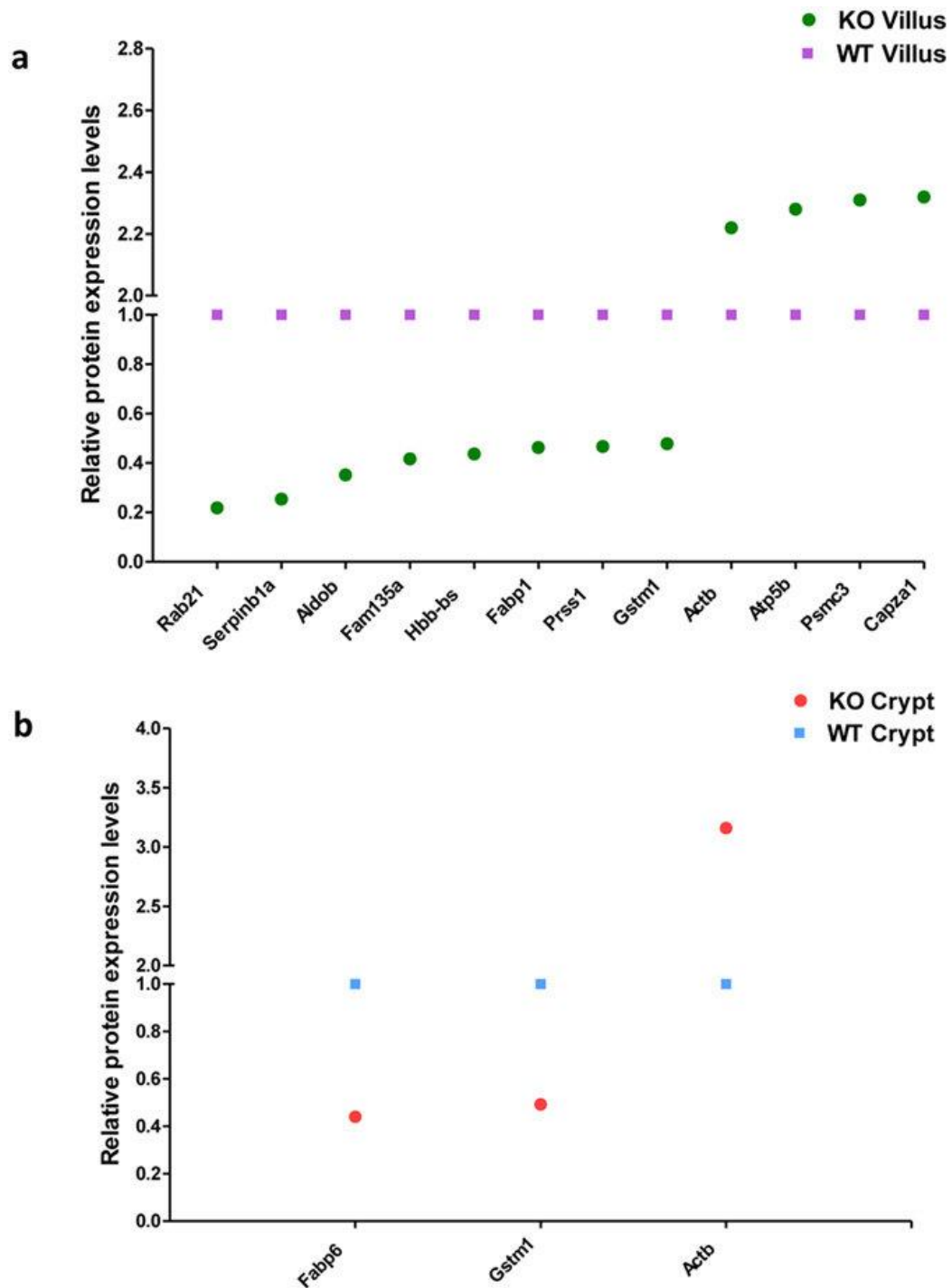


**Figure 5.8** The protein expression gradient differs along the crypt-villus axis of PepT1 KO and BL-6 WT mice.

*a.* In PepT1 KO villi compared to BL-6 WT villi, 8 proteins were down-regulated (green spots below purple spots) and 4 proteins were up-regulated (green spots above purple spots)

spots). *b.* In PepT1 KO crypts compared to BL-6 WT crypts, 2 proteins were down-regulated (red spots below blue spots) and 1 protein was up-regulated (red spots above blue spots).

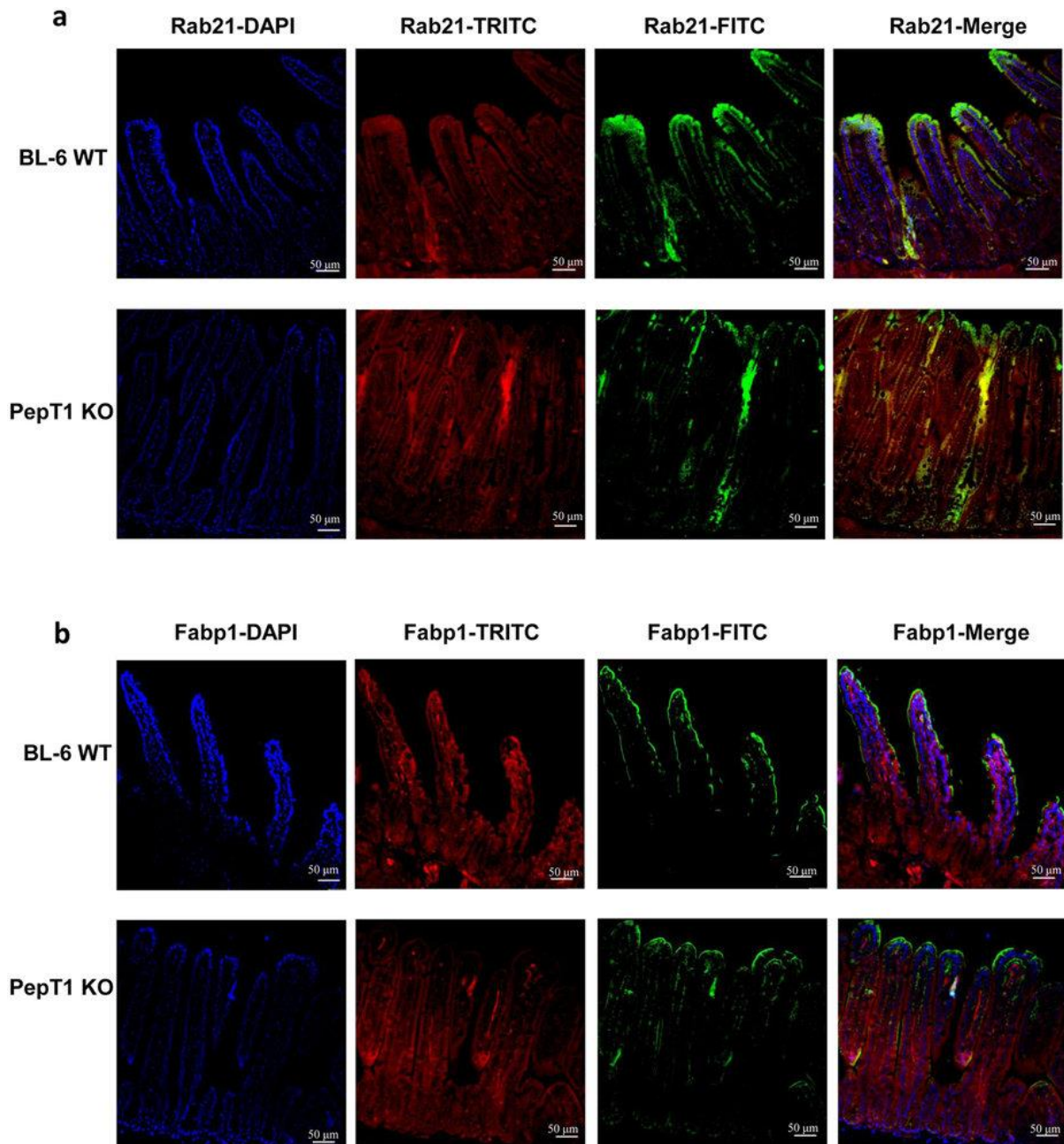


**Figure 5.9 PepT1 KO alters the protein expression levels of Rab21 and Fabp1.**

*a.* The expression of Rab21 was assessed by immunofluorescence. Rab21 was immunostained using anti-Rab21 (FITC, green), F-actin was stained using phalloidin (TRITC, red), and cell nuclei were stained using DAPI (blue). *b.* The expression of Fabp1 was assessed by immunofluorescence. Fabp1 was immunostained using anti-Fabp1 (FITC,

green), F-actin was stained using phalloidin (TRITC, red), and cell nuclei were stained using DAPI (blue). Separate pictures were taken at 20× for each filter, and the images were merged.

Scale bar, 50 μm.

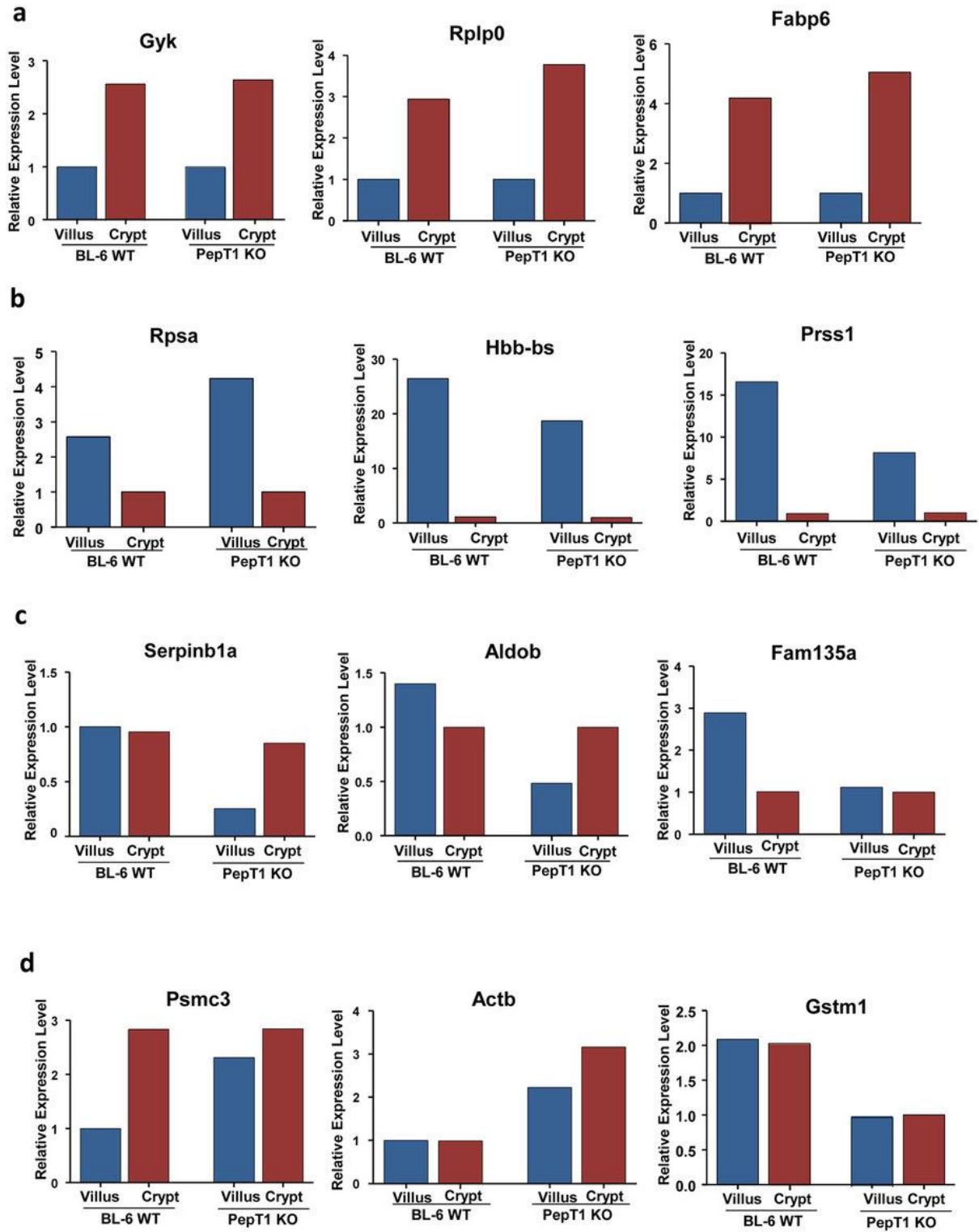


**Figure 5.10 PepT1 KO alters the profiles of specific proteins along the crypt-villus axis.**

*a* and *b*. The expression gradients of Gyk, Rplp0, Fabp6 (shown in A), Rpsa, Hbb-bs, and Prss1 (shown in B) along the crypt-villus axis are similar in PepT1 KO and BL-6 WT mice. *c* and *d*. The protein expression gradients of Serpinb1a, Aldob, Fam135a, Psm3, Actb and GStm1 differ between PepT1 KO and BL-6 WT mice.

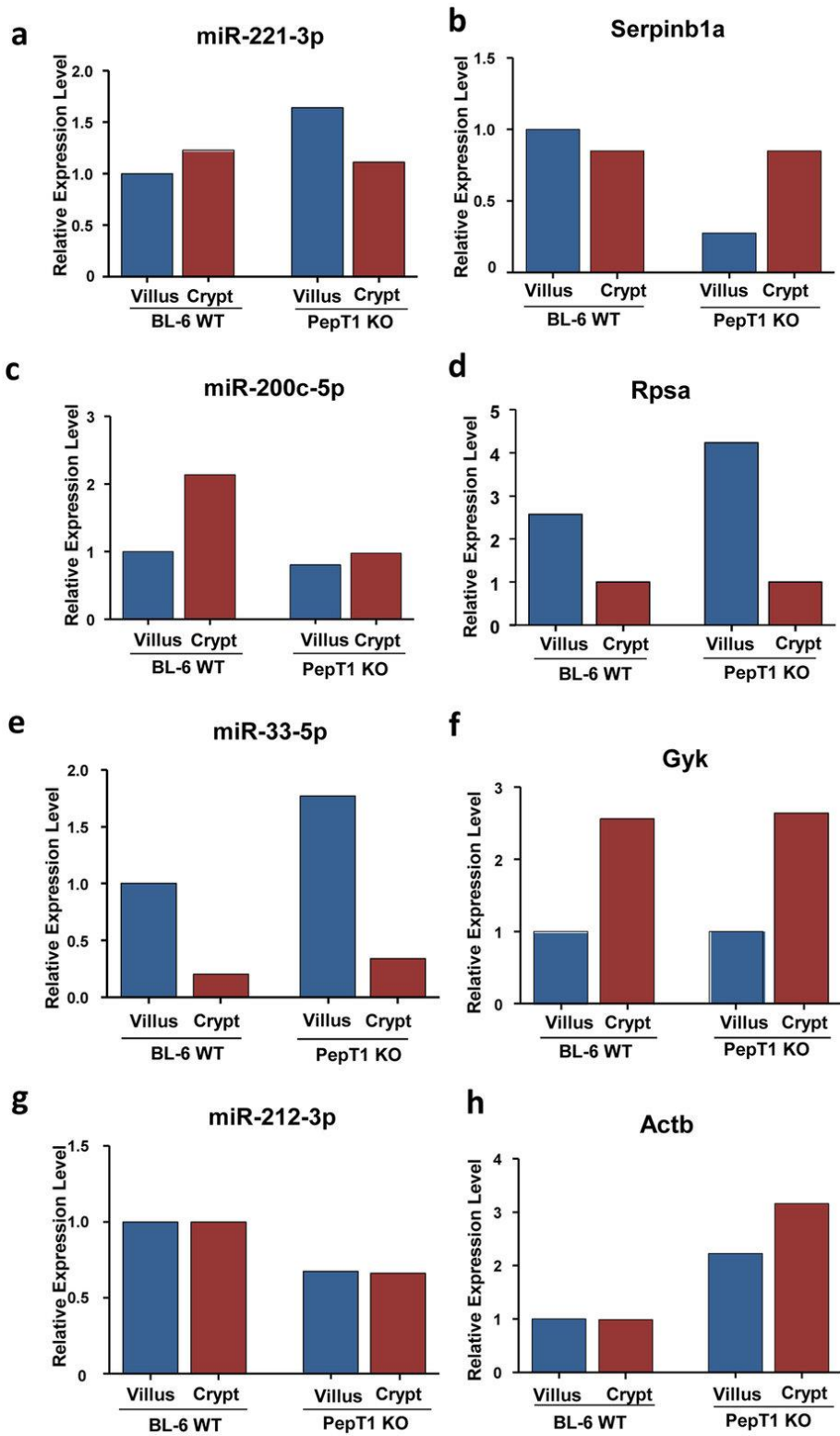


**Figure 5.11 PepT1 KO modulates the expression levels of certain miRNAs, thereby altering the expression levels of their target proteins.**

*a* and *b*. In BL-6 WT mice, miRNA-221-3p was higher in crypts than in villi. In PepT1 KO mice, in contrast, this miRNA was higher in villi than in crypts. This same pattern was reflected in the expression of its target protein, Serpinb1a. *c* and *d*. In BL-6 WT mice, miRNA-200c-5p was higher in crypts than in villi. This pattern was reflected in the expression of its target, Rpsa. *e* and *f*. Corresponding gradient changes along the crypt-villus axis were seen in miRNA-33-5p and its target, Gyk in both BL-6 WT mice and PepT1 KO mice. *g* and *h*. In both villi and crypts, miR-212-3p was higher in BL-6WT mice than in PepT1 KO mice, and this difference was reflected in the expression of its target, Actb.



**Figure 5.12 PepT1 KO increases small intestinal epithelial cell proliferation and apoptosis.**

*a.* Apoptotic small intestinal epithelial cells were quantified using a TUNEL assay (FITC, green) and nuclei were stained with DAPI (blue). *b.* Cells positive for both TUNEL and DAPI staining were counted and averaged per villus. *c.* The levels of epithelial cell proliferation in small intestine sections from BL-6 WT and PepT1 KO mice were assessed by immunohistochemistry using the proliferation marker, Ki67. *d.* Ki67<sup>+</sup> cells were counted and averaged per villus. Scale bars, 50  $\mu\text{m}$ ; \*\*  $P < 0.005$ .

Table 5.1 Identification of picked proteins differentially expressed between WT villus and WT crypt

Table 1- Identification of picked proteins differentially expressed between WT villus and WT crypt							
Spot No. <sup>a</sup>	Accession No. <sup>b</sup>	Gene <sup>c</sup>	Protein Name	Protein MW (kDa)	Protein PI	Average fold change <sup>d</sup>	Overall trend
1320	Q3TEN9	Gyk	Glycerol kinase	57.4	5.76	-2.58	Up
1400	NP_032974	Psmc3	26S protease regulatory subunit 6A	44.6	5.02	-2.84	Up
1800	B2CY77	Rpsa	Laminin receptor	32.8	4.87	2.58	Down
1952	P14869	Rplp0	60S acidic ribosomal protein P0	34.2	6.25	-2.96	Up
1961	Q61264	Acta1	Skeletal muscle alpha-actin mRNA	37.7	5.54	2.94	Down
2541	P35282	Rab21	Ras-related protein Rab-21	24.1	7.94	2.24	Down
2992	A0A087WQ08	Fam135a	Family with sequence similarity 135	30.5	7.01	2.89	Down
3086	Q9Z1R9	Prss1	protease, serine 1 (trypsin 1)	26.1	4.94	12.35	Down
3247	Q9D1A2	Cndp2	Cytosolic non-specific dipeptidase	52.7	5.66	-2.51	Up
3254	E9Q223	Hbb-bs	Protein Hbb-bs	11.1	6.37	18.52	Down
3261	P51162	Fabp6	Gastrotropin	14.5	6.15	-4.23	Up
3268	P17918	Pcna	Proliferating cell nuclear antigen	28.8	4.77	-2.21	Up
3281	P12710	Fabp1	Fatty acid-binding protein	14.2	8.56	4.01	Down

<sup>a</sup> Spot No. generated by DeCyder image analysis software (v 7.0, GE Healthcare), referencing the spots shown on the representative image in **Supplementary Fig. 5**.

<sup>b</sup> Accession number from NCBI database.

<sup>c</sup> Gene symbol from NCBI database. All genes are *Mus musculus*.

<sup>d</sup> Average ratio of protein expression.

Table 5.2 Identification of picked proteins differentially expressed between KO villus and KO crypt

Table 2- Identification of picked proteins differentially expressed between KO villus and KO crypt							
Spot No. <sup>a</sup>	Accession No. <sup>b</sup>	Gene <sup>c</sup>	Protein Name	Protein MW (kDa)	Protein PI	Average fold change <sup>d</sup>	Overall trend
1118	P50544	Acadv1	Very long-chain specific acyl-CoA dehydrogenase, mitochondrial	70.8	8.75	2.61	Down
1266	P68373	Tuba1c	Tubulin alpha-1C chain	49.9	5.10	-2.15	Up
1320	Q3TEN9	Gyk	Glycerol kinase	57.4	5.76	-2.64	Up
1496	Q8VH52	Eif4a1	Eukaryotic translation initiation factor 4A1	16.1	5.15	2.78	Down
1732	Q9D154	Serpinb1a	Leukocyte elastase inhibitor A	42.5	6.21	-3.20	Up
1794	Q3TJ66	Aldob	Fructose-bisphosphate aldolase	39.5	8.27	-2.06	Up
1800	B2CY77	Rpsa	Laminin receptor	32.8	4.87	4.23	Down
1952	P14869	Rplp0	60S acidic ribosomal protein P0	34.2	6.25	-3.78	Up
2346	Q9Z1R9	Prss1	protease, serine 1 (trypsin 1)	26.1	4.94	4.23	Down
2529	Q3U0B3	Dhrs11	Dehydrogenase	28.3	6.34	-3.33	Up
3254	E9Q223	Hbb-bs	Protein Hbb-bs	11.1	6.37	18.87	Down
3261	P51162	Fabp6	Gastrotropin	14.5	6.15	-6.16	Up

<sup>a</sup> Spot No. generated by DeCyder image analysis software (v 7.0, GE Healthcare), referencing the spots shown on the representative image in **Supplementary Fig. 5**.

<sup>b</sup> Accession number from NCBI database.

<sup>c</sup> Gene symbol from NCBI database. All genes are *Mus musculus*.

<sup>d</sup> Average ratio of protein expression.

Table 5.3 Identification of picked proteins differentially expressed between WT villus and KO villus

Table 3- Identification of picked proteins differentially expressed between WT villus and KO villus							
Spot No. <sup>a</sup>	Accession No. <sup>b</sup>	Gene <sup>c</sup>	Protein Name	Protein MW (kDa)	Protein PI	Average fold change <sup>d</sup>	Overall trend
1372	P56480	Atp5b	ATP synthase subunit beta, mitochondrial	56.3	5.34	-2.28	Up
1400	NP_032974	Psmc3	26S protease regulatory subunit 6A	44.6	5.02	-2.31	Up
1789	Q9D154	Serpinb1a	Leukocyte elastase inhibitor A	42.5	6.21	3.94	Down
1794	Q3TJ66	Aldob	Fructose-bisphosphate aldolase	39.5	8.27	2.84	Down
1870	Q3UAS2	Capza1	capping protein (actin filament) muscle Z-line, alpha 1	32.9	5.55	-2.32	Up
1875	Q3U804	Actb	Actin, Beta	41.8	6.30	-2.22	Up
2537	P10649	Gstm1	Glutathione S-transferase Mu 1	26.0	7.94	2.09	Down
2541	P35282	Rab21	Ras-related protein Rab-21	24.1	7.94	4.58	Down
2992	A0A087WQ08	Fam135a	Family with sequence similarity 135	30.5	7.01	2.4	Down
3254	E9Q223	Hbb-bs	Protein Hbb-bs	11.1	6.37	2.29	Down
3257	Q9Z1R9	Prss1	protease, serine 1 (trypsin 1)	26.1	4.94	2.14	Down
3281	P12710	Fabp1	Fatty acid-binding protein	14.2	8.56	2.16	Down

<sup>a</sup> Spot No. generated by DeCyder image analysis software (v 7.0, GE Healthcare), referencing the spots shown on the representative image in **Supplementary Fig. 6**.

<sup>b</sup> Accession number from NCBI database.

<sup>c</sup> Gene symbol from NCBI database. All genes are *Mus musculus*.

<sup>d</sup> Average ratio of protein expression.

Table 5.4 Identification of picked proteins differentially expressed between WT crypt and KO crypt

Table 4- Identification of picked proteins differentially expressed between WT crypt and KO crypt							
Spot No. <sup>a</sup>	Accession No. <sup>b</sup>	Gene <sup>c</sup>	Protein Name	Protein MW (kDa)	Protein PI	Average fold change <sup>d</sup>	Overall trend
1875	Q3U804	Actb	Actin, Beta	41.8	6.30	-3.16	Up
2537	P10649	Gstm1	Glutathione S-transferase Mu 1	26.0	7.94	2.03	Down
3235	P51162	Fabp6	Gastrotropin	14.5	6.15	2.27	Down

<sup>a</sup> Spot No. generated by DeCyder image analysis software (v 7.0, GE Healthcare), referencing the spots shown on the representative image in **Supplementary Fig. 6**.

<sup>b</sup> Accession number from NCBI database.

<sup>c</sup> Gene symbol from NCBI database. All genes are *Mus musculus*.

<sup>d</sup> Average ratio of protein expression.

Table 5.5 Expression of the miRNA and its corresponding protein target

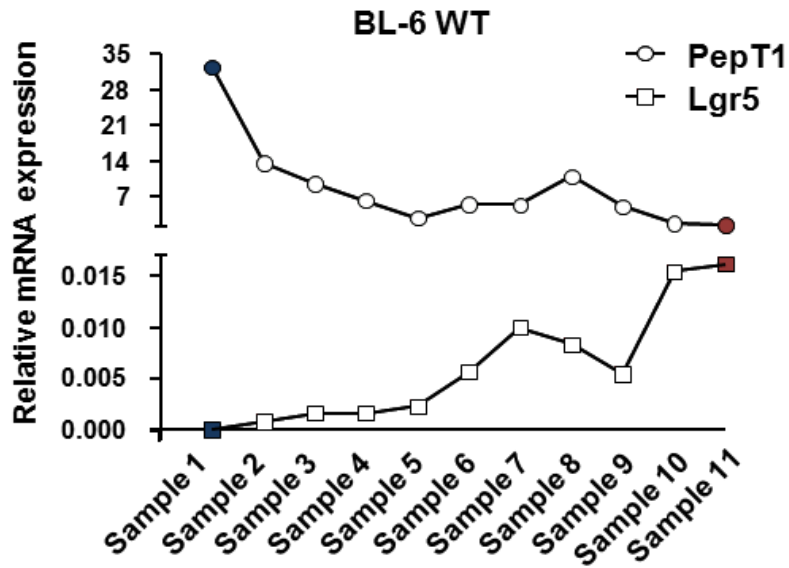
Table 5- Expression of the miRNA and its corresponding protein target											
Spot No. <sup>a</sup>	Protein Name	Gene <sup>c</sup>	Protein				miRNA	miRNA			
			Expression Level (Fold change) <sup>b</sup>					Relative Expression Level			
			WTV	WTC	KOV	KOC		WTV	WTC	KOV	KOC
1320	Glycerol kinase	Gyk	1	2.58	1	2.64	miR-33-5p	1	0.20	1.76	0.34
1789	Leukocyte elastase inhibitor A	Serpinb1a	1	0.85	0.25	0.85	miR-221-3p	1	1.22	1.64	1.11
1800	Laminin receptor	Rpsa	2.58	1	4.23	1	miR-200c-5p	1	2.20	0.80	1.05
1875	Actin, beta	Actb	1	1	2.22	3.16	miR-212-3p	1	1.06	0.67	0.61

Abbreviations: WTV: Wild-type villus, WTC: Wild-type crypt, KOV: PepT1 KO villus, KOC: PepT1 KO crypt

<sup>a</sup> Spot No. generated by DeCyder image analysis software (v 7.0, GE Healthcare), referencing the spots shown on the representative image in **Supplementary Fig. 5, 6**.

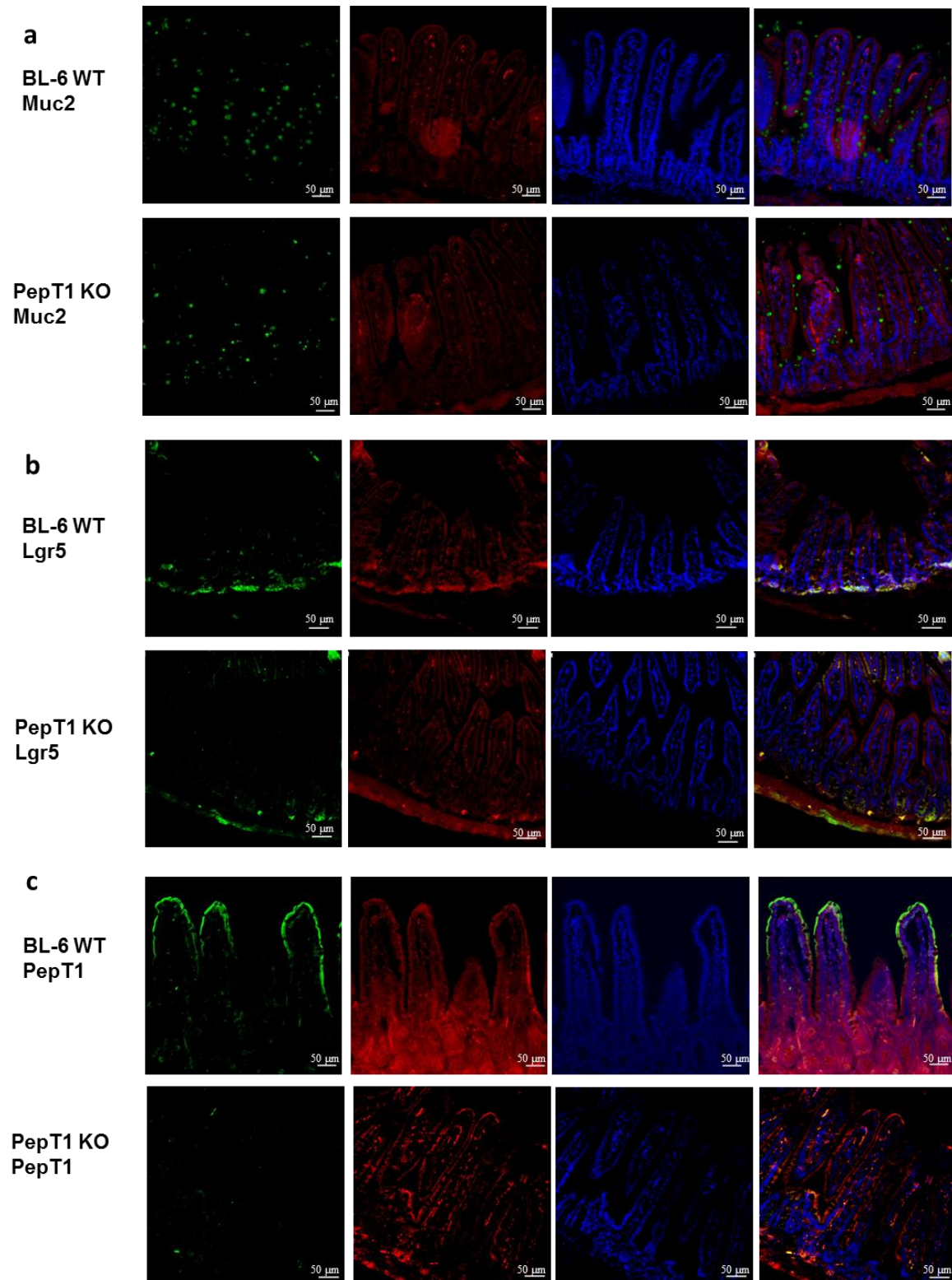
<sup>b</sup> Average ratio of protein expression.

<sup>c</sup> Gene symbol from NCBI database. All genes are *Mus musculus*.



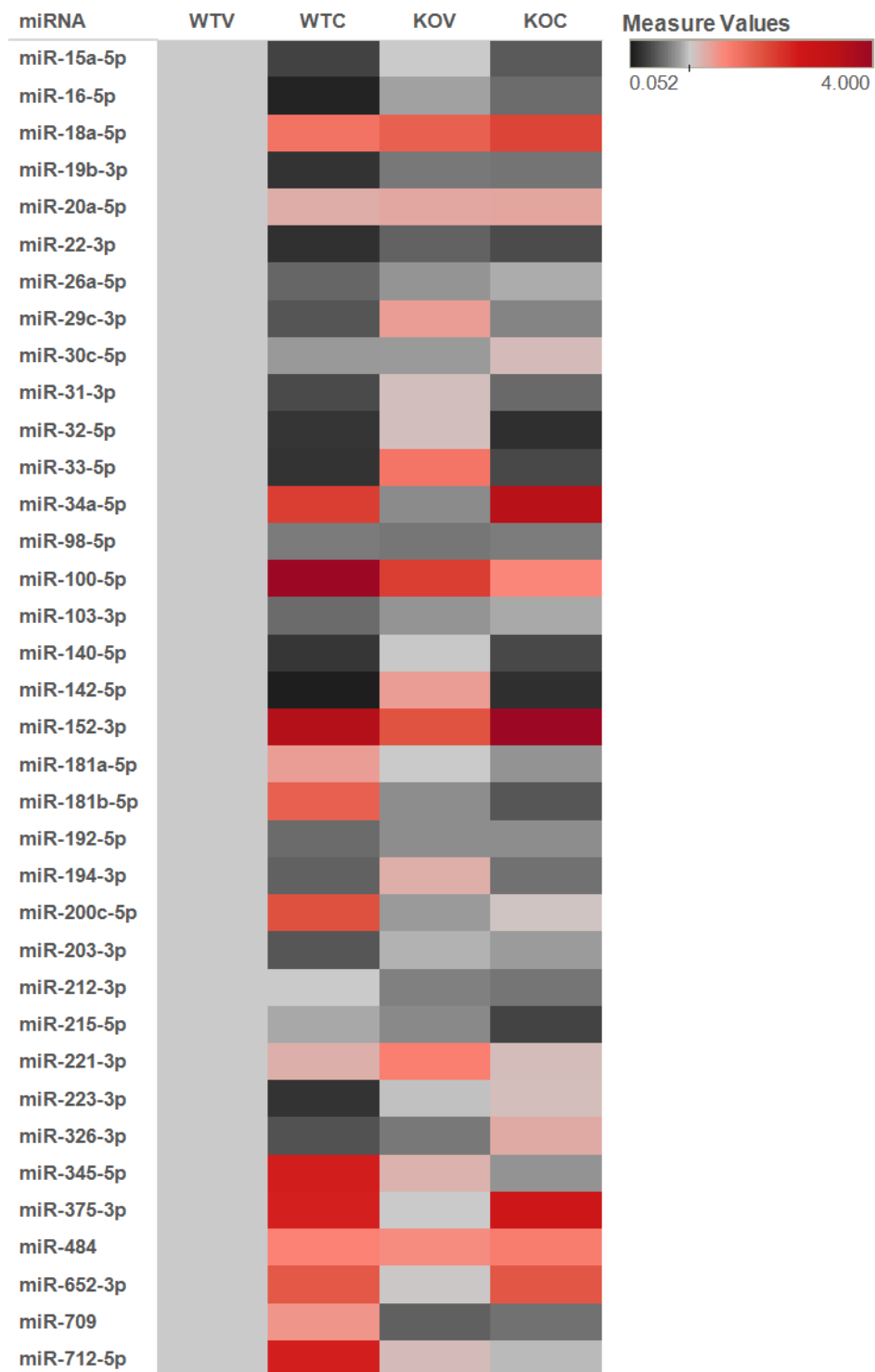
**Supplemental Figure 5.1 Expression of PepT1 and Lgr5 in isolated epithelial cells of the jejunum from BL-6 WT mice.**

Total RNAs were extracted from the different fractions collected from BL-6 WT mice using the low-temperature method, and the expression levels of PepT1 (as a villus marker) and Lgr5 (as a crypt marker) were assessed by qRT-PCR.



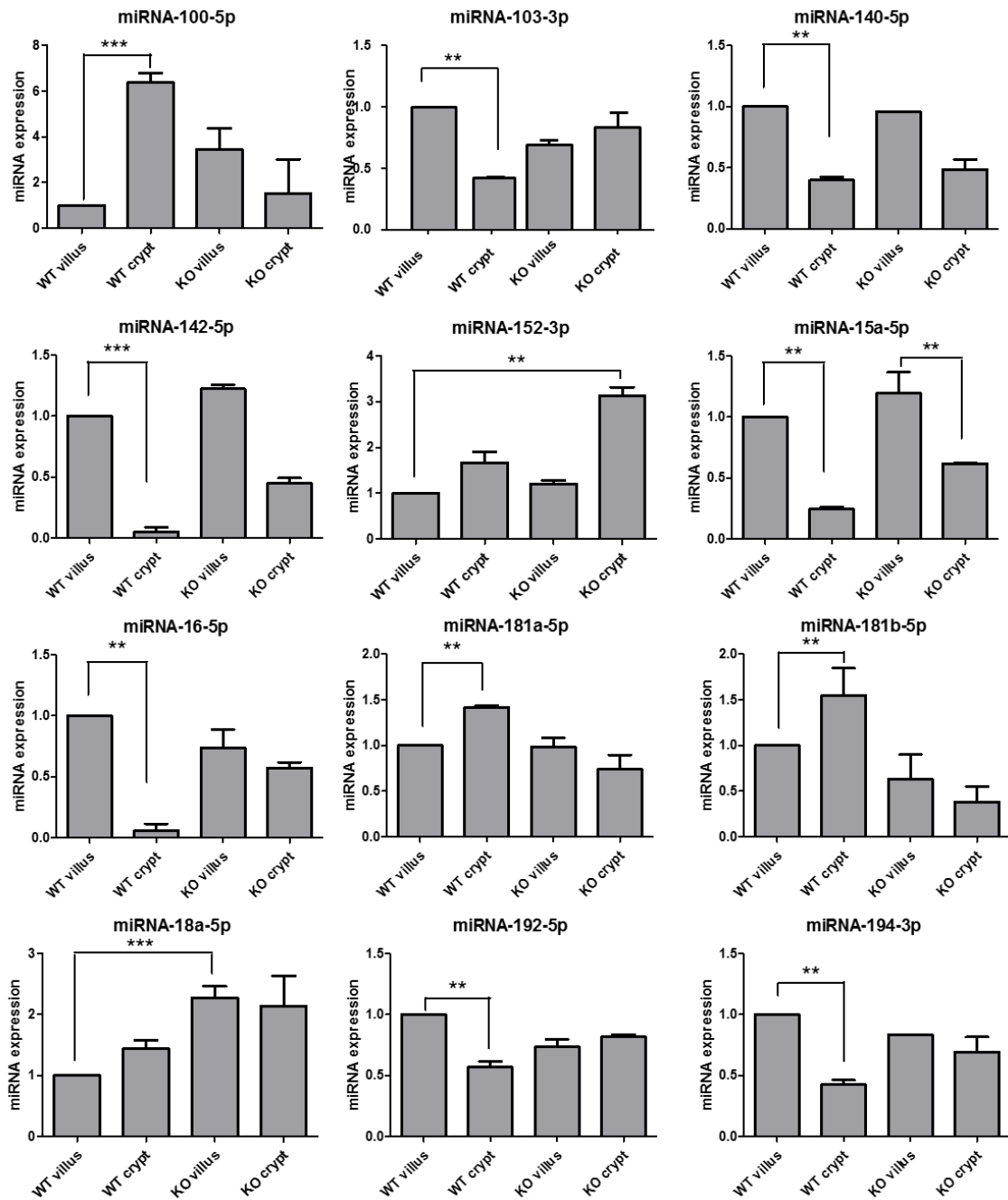
**Supplemental Figure 5.2 Expression of Muc2, Lgr5, and mPepT1 in WT and KO mice.**

The expression levels of (a) Muc2, (b) Lgr5, and (c) mPepT1 were assessed by immunofluorescence. Muc2, Lgr5 and mPepT1 were immunostained using anti-Muc2, anti-Lgr5, and anti-PepT1, respectively (FITC, green). F-actin was stained using phalloidin (TRITC, red), and cell nuclei were stained using DAPI (blue). Separate pictures were taken at 20× for each filter, and the images were merged. Scale bar, 50 μm.



**Supplemental Figure 5.3 Clustering graph of selected miRNAs.**

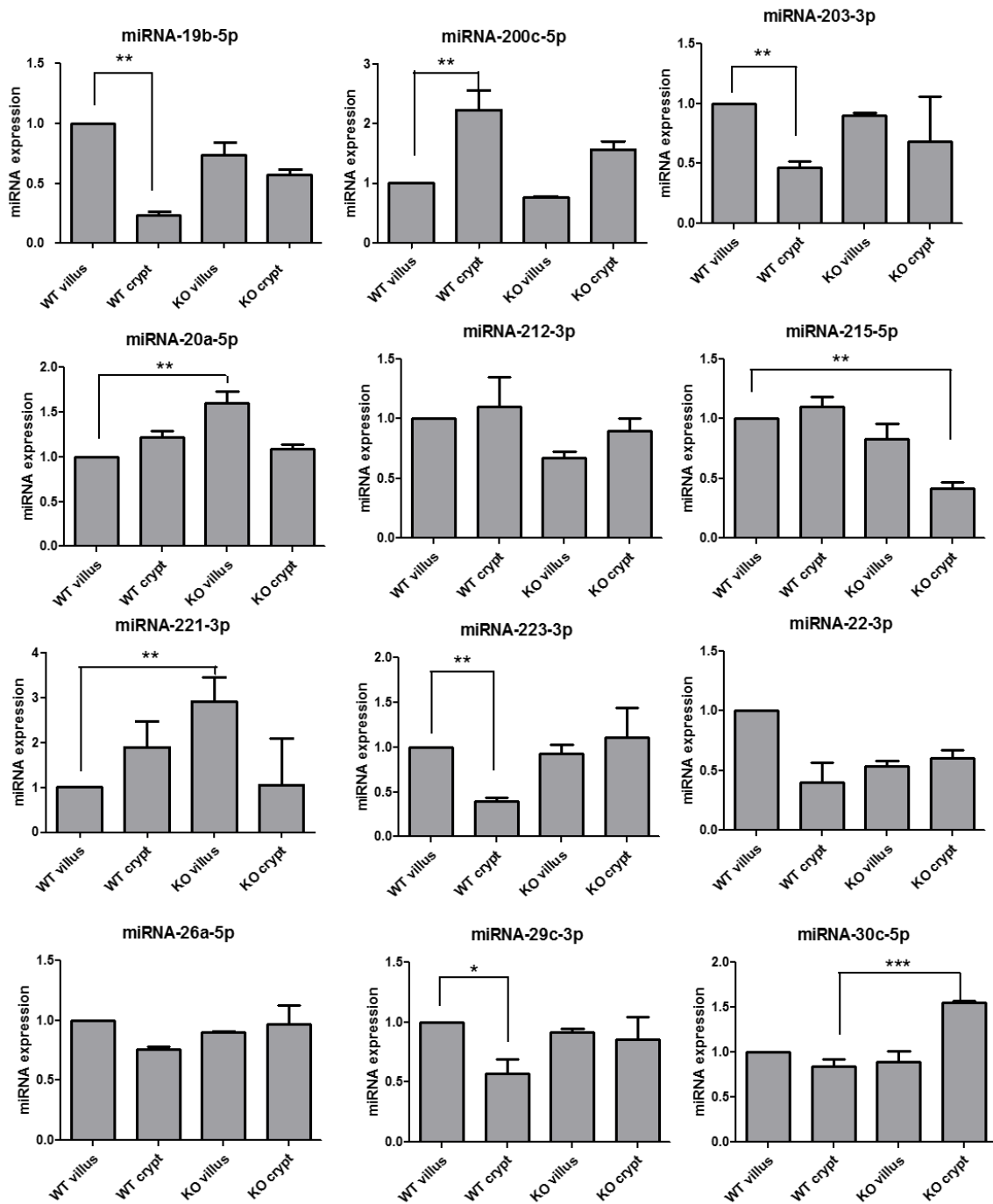
MicroRNA microarray results demonstrated that different miRNA profiles were observed in crypts and villi of WT and PepT1 KO mice. We selected miRNAs that exhibited  $P$  value  $<0.05$  and signal strengths  $> 500$ .



**Supplemental Figure 5.4 Expression levels of selected miRNAs in crypt and villus epithelial cells from BL-6 WT and PepT1 KO mice.**

The expression levels of 36 selected miRNAs were verified by qRT-PCR (n= 5/group;

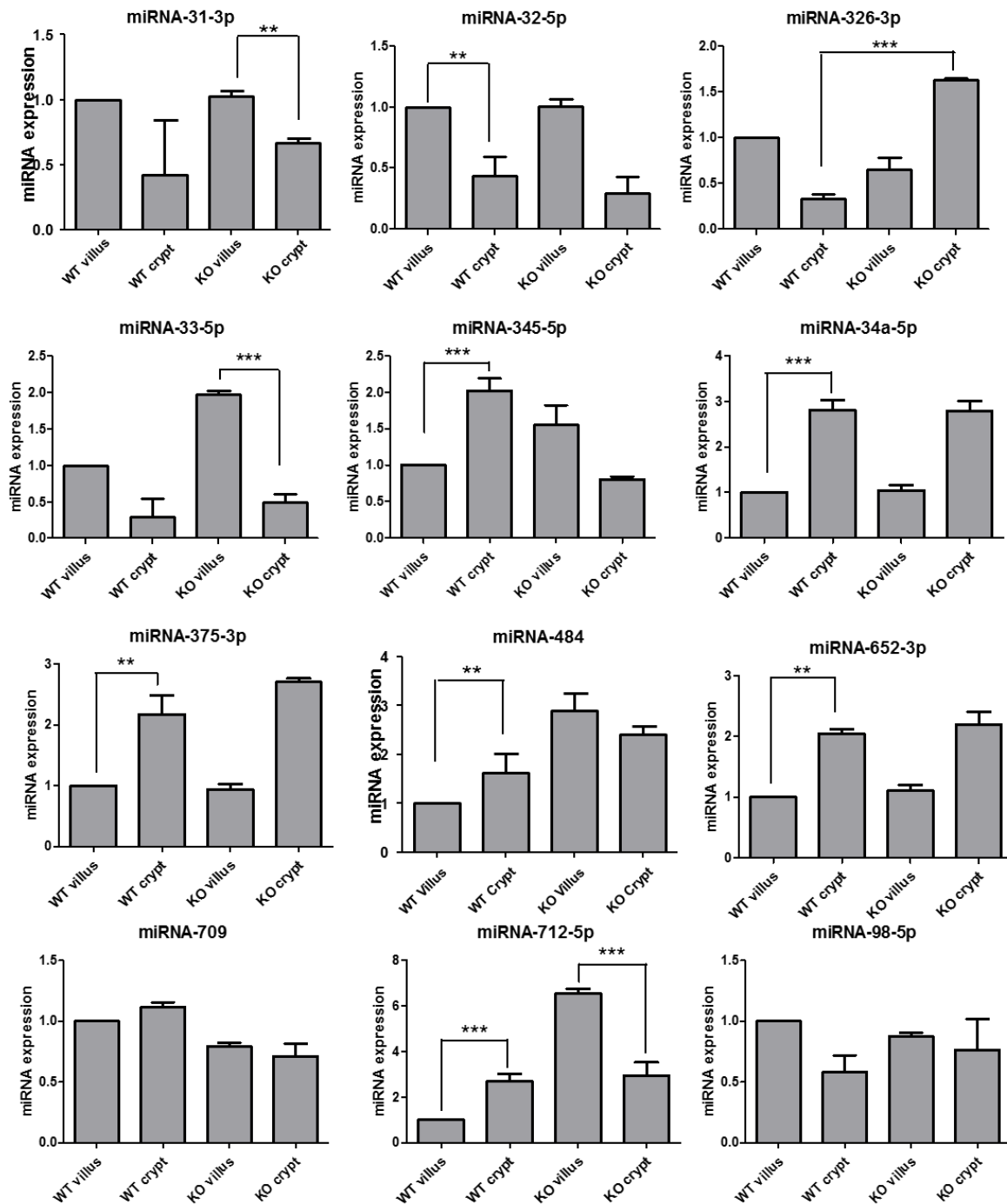
\*  $P < 0.05$ , \*\*  $P < 0.005$ , and \*\*\*  $P < 0.001$ ).



**Supplemental Figure 5.4 Expression levels of selected miRNAs in crypt and villus epithelial cells from BL-6 WT and PepT1 KO mice.**

The expression levels of 36 selected miRNAs were verified by qRT-PCR (n= 5/group;

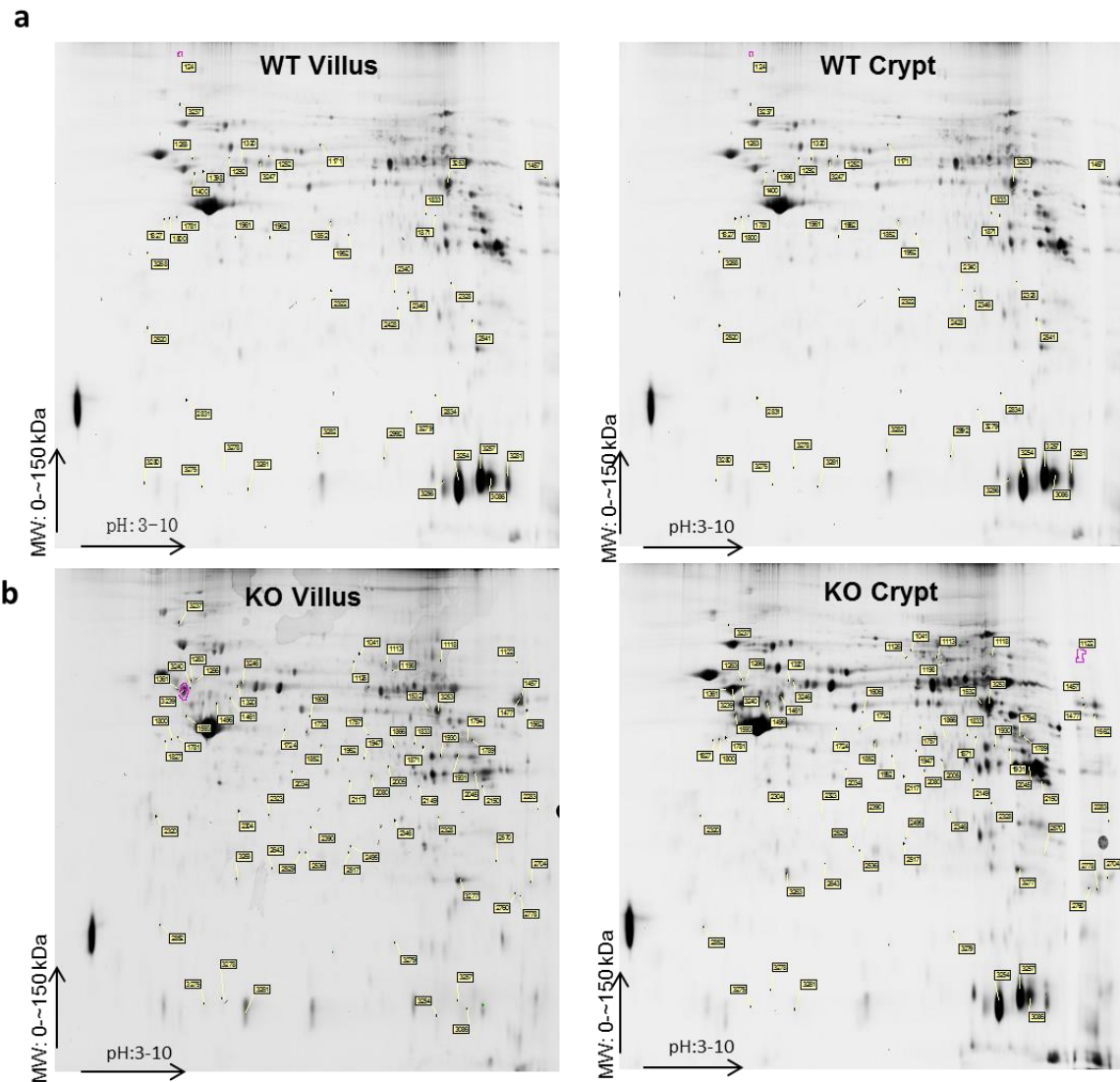
\*  $P < 0.05$ , \*\*  $P < 0.005$ , and \*\*\*  $P < 0.001$ ).



**Supplementary Figure 5.4 Expression levels of selected miRNAs in crypt and villus epithelial cells from BL-6 WT and PepT1 KO mice.**

The expression levels of 36 selected miRNAs were verified by qRT-PCR (n= 5/group;

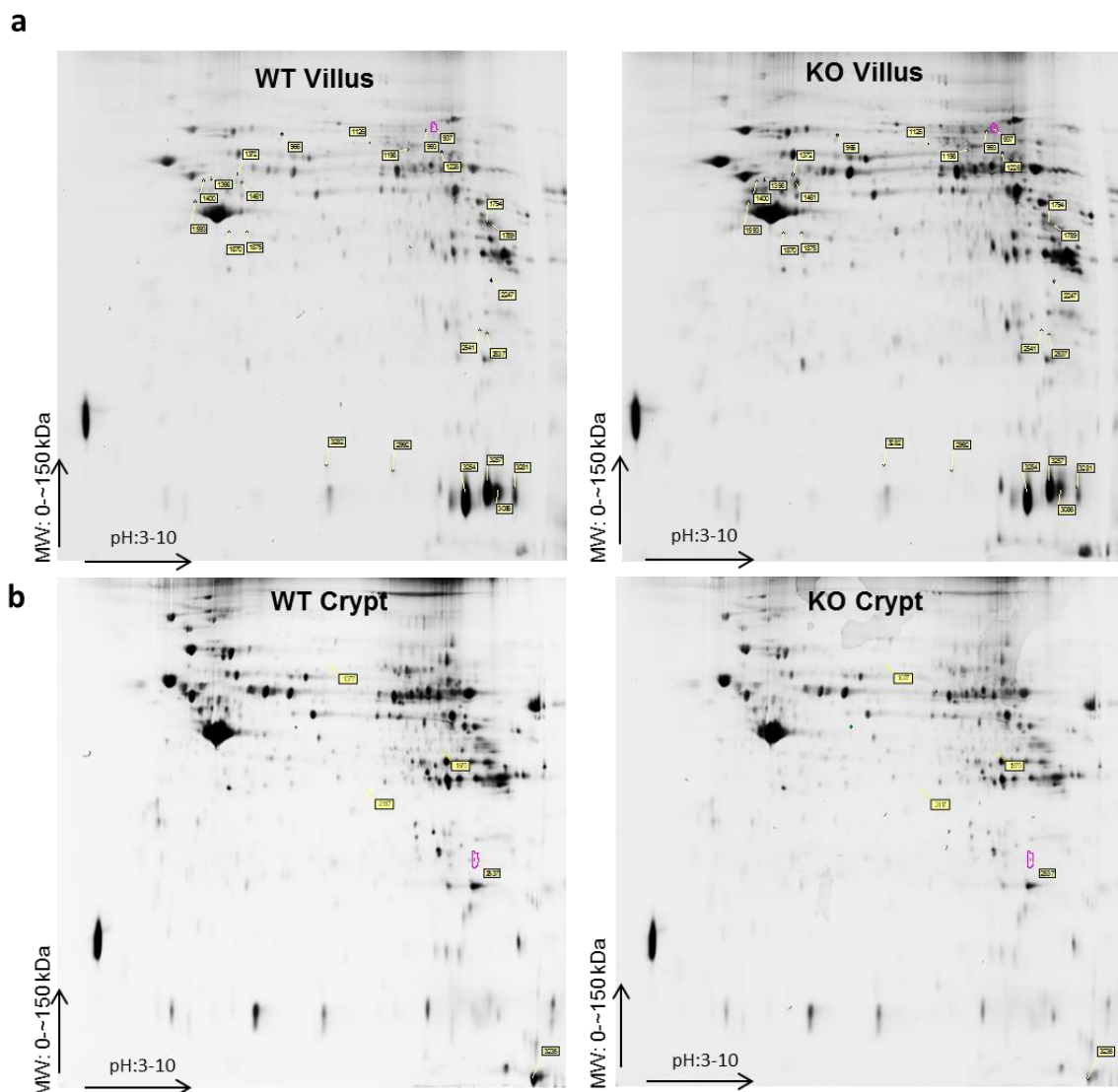
\*  $P < 0.05$ , \*\*  $P < 0.005$ , and \*\*\*  $P < 0.001$ ).



**Supplemental Figure 5.5** PepT1 expression disturbs normal differential protein expression along the crypt-villus axis.

2D-DIGE DeCyder BVA (Biological Variation Analysis) showing a representative gel image with labeled sample of difference. Changes in protein expression were compared between villi and crypts, with a pooled internal standard included. The master gel image shows the locations of the differentially expressed proteins in each comparison. *a.* 43 spots

with > 2.0-fold differences in WT villi vs. WT crypts. *b.* 72 spots with > 2.0-fold differences in KO villi vs. KO crypts.



**Supplemental Figure 5.6 PepT1 expression altered the normal protein profile in villus and crypt, respectively.**

2D-DIGE DeCyder BVA (Biological Variation Analysis) showing a representative gel image with labeled sample of difference. Changes in protein expression were compared between BL-6 WT and PePT1 KO mice, with a pooled internal standard included. The master gel image shows the locations of the differentially expressed proteins in each comparison. *a.*

24 spots with > 2.0-fold differences in WT villi vs. KO villi. *b.* 5 spots with > 2.0-fold differences in WT crypts vs. KO crypts.

## Reference

- Abraham, C., and Cho, J.H. (2009). Inflammatory bowel disease. *N Engl J Med* 361, 2066-2078.
- Abreu, M.T., Fukata, M., and Arditi, M. (2005). TLR signaling in the gut in health and disease. *J Immunol* 174, 4453-4460.
- Adibi, S.A. (2003). Regulation of expression of the intestinal oligopeptide transporter (Pept-1) in health and disease. *Am J Physiol Gastrointest Liver Physiol* 285, G779-788.
- Ambros, V. (2004). The functions of animal microRNAs. *Nature* 431, 350-355.
- Aono, S., and Hirai, Y. (2008). Phosphorylation of claudin-4 is required for tight junction formation in a human keratinocyte cell line. *Experimental cell research* 314, 3326-3339.
- Ayyadurai, S., Charania, M.A., Xiao, B., Viennois, E., and Merlin, D. (2013). PepT1 expressed in immune cells has an important role in promoting the immune response during experimentally induced colitis. *Lab Invest* 93, 888-899.
- Ayyadurai, S., Charania, M.A., Xiao, B., Viennois, E., Zhang, Y., and Merlin, D. (2014). Colonic miRNA expression/secretion, regulated by intestinal epithelial PepT1, plays an important role in cell-to-cell communication during colitis. *PLoS One* 9, e87614.
- Balda, M.S., Whitney, J.A., Flores, C., Gonzalez, S., Cereijido, M., and Matter, K. (1996). Functional dissociation of paracellular permeability and transepithelial electrical resistance and disruption of the apical-basolateral intramembrane diffusion barrier by expression of a mutant tight junction membrane protein. *J Cell Biol* 134, 1031-1049.
- Barker, N., van Es, J.H., Kuipers, J., Kujala, P., van den Born, M., Cozijnsen, M., Haegebarth, A., Korving, J., Begthel, H., Peters, P.J., *et al.* (2007). Identification of stem cells in small intestine and colon by marker gene Lgr5. *Nature* 449, 1003-1007.

Baumgart, D.C., and Carding, S.R. (2007). Inflammatory bowel disease: cause and immunobiology. *Lancet* 369, 1627-1640.

Baumgart, D.C., and Sandborn, W.J. (2007). Inflammatory bowel disease: clinical aspects and established and evolving therapies. *Lancet* 369, 1641-1657.

Berkes, J., Viswanathan, V.K., Savkovic, S.D., and Hecht, G. (2003). Intestinal epithelial responses to enteric pathogens: effects on the tight junction barrier, ion transport, and inflammation. *Gut* 52, 439-451.

Bian, Z., Li, L., Cui, J., Zhang, H., Liu, Y., Zhang, C.Y., and Zen, K. (2011). Role of miR-150-targeting c-Myb in colonic epithelial disruption during dextran sulphate sodium-induced murine experimental colitis and human ulcerative colitis. *J Pathol* 225, 544-553.

Blikslager, A.T., Moeser, A.J., Gookin, J.L., Jones, S.L., and Odle, J. (2007). Restoration of barrier function in injured intestinal mucosa. *Physiol Rev* 87, 545-564.

Bloom, S.M., Bijanki, V.N., Nava, G.M., Sun, L., Malvin, N.P., Donermeyer, D.L., Dunne, W.M., Jr., Allen, P.M., and Stappenbeck, T.S. (2011). Commensal *Bacteroides* species induce colitis in host-genotype-specific fashion in a mouse model of inflammatory bowel disease. *Cell Host Microbe* 9, 390-403.

Bockman, D.E., Ganapathy, V., Oblak, T.G., and Leibach, F.H. (1997). Localization of peptide transporter in nuclei and lysosomes of the pancreas. *Int J Pancreatol* 22, 221-225.

Boggavarapu, R., Jeckelmann, J.M., Harder, D., Ucurum, Z., and Fotiadis, D. (2015). Role of electrostatic interactions for ligand recognition and specificity of peptide transporters. *BMC Biol* 13, 58.

Bretschneider, B., Brandsch, M., and Neubert, R. (1999). Intestinal transport of beta-lactam antibiotics: analysis of the affinity at the H<sup>+</sup>/peptide symporter (PEPT1), the uptake into Caco-2 cell monolayers and the transepithelial flux. *Pharm Res* 16, 55-61.

Brodin, B., Nielsen, C.U., Steffansen, B., and Frokjaer, S. (2002). Transport of peptidomimetic drugs by the intestinal Di/tri-peptide transporter, PepT1. *Pharmacol Toxicol* 90, 285-296.

Buyse, M., Berlioz, F., Guilmeau, S., Tsocas, A., Voisin, T., Peranzi, G., Merlin, D., Laburthe, M., Lewin, M.J., Roze, C., *et al.* (2001). PepT1-mediated epithelial transport of dipeptides and cephalexin is enhanced by luminal leptin in the small intestine. *J Clin Invest* 108, 1483-1494.

Buyse, M., Charrier, L., Sitaraman, S., Gewirtz, A., and Merlin, D. (2003). Interferon-gamma increases hPepT1-mediated uptake of di-tripeptides including the bacterial tripeptide fMLP in polarized intestinal epithelia. *Am J Pathol* 163, 1969-1977.

Cardone, J., Le Friec, G., Vantourout, P., Roberts, A., Fuchs, A., Jackson, I., Suddason, T., Lord, G., Atkinson, J.P., Cope, A., *et al.* (2010). Complement regulator CD46 temporally regulates cytokine production by conventional and unconventional T cells. *Nature immunology* 11, 862-871.

Carroll, S.L., Roth, K.A., and Gordon, J.I. (1990). Liver fatty acid-binding protein: a marker for studying cellular differentiation in gut epithelial neoplasms. *Gastroenterology* 99, 1727-1735.

Cerejido, M., Robbins, E.S., Dolan, W.J., Rotunno, C.A., and Sabatini, D.D. (1978). Polarized monolayers formed by epithelial cells on a permeable and translucent support. *J Cell Biol* 77, 853-880.

Chang, S.K., Dohrman, A.F., Basbaum, C.B., Ho, S.B., Tsuda, T., Toribara, N.W., Gum, J.R., and Kim, Y.S. (1994). Localization of mucin (MUC2 and MUC3) messenger RNA and peptide expression in human normal intestine and colon cancer. *Gastroenterology* 107, 28-36.

Charania, M.A., Ayyadurai, S., Ingersoll, S.A., Xiao, B., Viennois, E., Yan, Y., Laroui, H., Sitaraman, S.V., and Merlin, D. (2012). Intestinal epithelial CD98 synthesis specifically modulates expression of colonic microRNAs during colitis. *Am J Physiol Gastrointest Liver Physiol* 302, G1282-1291.

Charrier, L., Driss, A., Yan, Y., Nduati, V., Klapproth, J.M., Sitaraman, S.V., and Merlin, D. (2006). hPepT1 mediates bacterial tripeptide fMLP uptake in human monocytes. *Lab Invest* 86, 490-503.

Charrier, L., and Merlin, D. (2006). The oligopeptide transporter hPepT1: gateway to the innate immune response. *Lab Invest* 86, 538-546.

Chassaing, B., and Darfeuille-Michaud, A. (2011). The commensal microbiota and enteropathogens in the pathogenesis of inflammatory bowel diseases. *Gastroenterology* 140, 1720-1728.

Chen, B., She, S., Li, D., Liu, Z., Yang, X., Zeng, Z., and Liu, F. (2013). Role of miR-19a targeting TNF-alpha in mediating ulcerative colitis. *Scand J Gastroenterol* 48, 815-824.

Chen, M., Singh, A., Xiao, F., Dringenberg, U., Wang, J., Engelhardt, R., Yeruva, S., Rubio-Aliaga, I., Nassl, A.M., Kottra, G., *et al.* (2010). Gene ablation for PEPT1 in mice abolishes the effects of dipeptides on small intestinal fluid absorption, short-circuit current, and intracellular pH. *Am J Physiol Gastrointest Liver Physiol* 299, G265-274.

Cobb, B.S., Nesterova, T.B., Thompson, E., Hertweck, A., O'Connor, E., Godwin, J., Wilson, C.B., Brockdorff, N., Fisher, A.G., Smale, S.T., *et al.* (2005). T cell lineage choice and differentiation in the absence of the RNase III enzyme Dicer. *J Exp Med* 201, 1367-1373.

Collett, A., Higgs, N.B., Gironella, M., Zeef, L.A., Hayes, A., Salmo, E., Haboubi, N., Iovanna, J.L., Carlson, G.L., and Warhurst, G. (2008). Early molecular and functional changes in colonic epithelium that precede increased gut permeability during colitis development in *mdr1a(-/-)* mice. *Inflamm Bowel Dis* 14, 620-631.

Coyne, C.B., Vanhook, M.K., Gambling, T.M., Carson, J.L., Boucher, R.C., and Johnson, L.G. (2002). Regulation of airway tight junctions by proinflammatory cytokines. *Mol Biol Cell* 13, 3218-3234.

Dai, X., Chen, X., Chen, Q., Shi, L., Liang, H., Zhou, Z., Liu, Q., Pang, W., Hou, D., Wang, C., *et al.* (2015). MicroRNA-193a-3p Reduces Intestinal Inflammation in Response to Microbiota via Down-regulation of Colonic PepT1. *J Biol Chem* 290, 16099-16115.

Dalmaso, G., Charrier-Hisamuddin, L., Nguyen, H.T., Yan, Y., Sitaraman, S., and Merlin, D. (2008). PepT1-mediated tripeptide KPV uptake reduces intestinal inflammation. *Gastroenterology* 134, 166-178.

Dalmaso, G., Nguyen, H.T., Charrier-Hisamuddin, L., Yan, Y., Laroui, H., Demoulin, B., Sitaraman, S.V., and Merlin, D. (2010a). PepT1 mediates transport of the

proinflammatory bacterial tripeptide L-Ala- $\{\gamma\}$ -D-Glu-meso-DAP in intestinal epithelial cells. *Am J Physiol Gastrointest Liver Physiol* 299, G687-696.

Dalmaso, G., Nguyen, H.T., Ingersoll, S.A., Ayyadurai, S., Laroui, H., Charania, M.A., Yan, Y., Sitaraman, S.V., and Merlin, D. (2011). The PepT1-NOD2 signaling pathway aggravates induced colitis in mice. *Gastroenterology* 141, 1334-1345.

Dalmaso, G., Nguyen, H.T., Yan, Y., Laroui, H., Srinivasan, S., Sitaraman, S.V., and Merlin, D. (2010b). MicroRNAs determine human intestinal epithelial cell fate. *Differentiation* 80, 147-154.

de Vrueth, R.L., Smith, P.L., and Lee, C.P. (1998). Transport of L-valine-acyclovir via the oligopeptide transporter in the human intestinal cell line, Caco-2. *J Pharmacol Exp Ther* 286, 1166-1170.

Duchmann, R., Neurath, M.F., and Meyer zum Buschenfelde, K.H. (1997). Responses to self and non-self intestinal microflora in health and inflammatory bowel disease. *Res Immunol* 148, 589-594.

Elson, C.O. (1996a). The basis of current and future therapy for inflammatory bowel disease. *Am J Med* 100, 656-662.

Elson, C.O. (1996b). The basis of current and future therapy for inflammatory bowel disease. *The American journal of medicine* 100, 656-662.

Fanning, A.S., and Anderson, J.M. (2009). Zonula occludens-1 and -2 are cytosolic scaffolds that regulate the assembly of cellular junctions. *Ann N Y Acad Sci* 1165, 113-120.

Fei, Y.J., Kanai, Y., Nussberger, S., Ganapathy, V., Leibach, F.H., Romero, M.F., Singh, S.K., Boron, W.F., and Hediger, M.A. (1994). Expression cloning of a mammalian proton-coupled oligopeptide transporter. *Nature* 368, 563-566.

Filipowicz, W., Jaskiewicz, L., Kolb, F.A., and Pillai, R.S. (2005). Post-transcriptional gene silencing by siRNAs and miRNAs. *Curr Opin Struct Biol* 15, 331-341.

Flint, N., Cove, F.L., and Evans, G.S. (1991). A low-temperature method for the isolation of small-intestinal epithelium along the crypt-villus axis. *Biochem J* 280 ( Pt 2), 331-334.

Ford, D., Howard, A., and Hirst, B.H. (2003). Expression of the peptide transporter hPepT1 in human colon: a potential route for colonic protein nitrogen and drug absorption. *Histochem Cell Biol* 119, 37-43.

Forster, C. (2008). Tight junctions and the modulation of barrier function in disease. *Histochem Cell Biol* 130, 55-70.

Freeman, T.C., Bentsen, B.S., Thwaites, D.T., and Simmons, N.L. (1995). H<sup>+</sup>/di-tripeptide transporter (PepT1) expression in the rabbit intestine. *Pflugers Arch* 430, 394-400.

Friedman, D.I., and Amidon, G.L. (1989). Intestinal absorption mechanism of dipeptide angiotensin converting enzyme inhibitors of the lysyl-proline type: lisinopril and SQ 29,852. *J Pharm Sci* 78, 995-998.

Fukata, M., Michelsen, K.S., Eri, R., Thomas, L.S., Hu, B., Lukasek, K., Nast, C.C., Lechago, J., Xu, R., Naiki, Y., *et al.* (2005). Toll-like receptor-4 is required for intestinal

response to epithelial injury and limiting bacterial translocation in a murine model of acute colitis. *Am J Physiol Gastrointest Liver Physiol* 288, G1055-1065.

Gassler, N., Rohr, C., Schneider, A., Kartenbeck, J., Bach, A., Obermuller, N., Otto, H.F., and Autschbach, F. (2001). Inflammatory bowel disease is associated with changes of enterocytic junctions. *Am J Physiol Gastrointest Liver Physiol* 281, G216-228.

Gaulke, C.A., Porter, M., Han, Y.H., Sankaran-Walters, S., Grishina, I., George, M.D., Dang, A.T., Ding, S.W., Jiang, G., Korf, I., *et al.* (2014). Intestinal epithelial barrier disruption through altered mucosal microRNA expression in human immunodeficiency virus and simian immunodeficiency virus infections. *Journal of virology* 88, 6268-6280.

Gordon, J.I. (1989). Intestinal epithelial differentiation: new insights from chimeric and transgenic mice. *J Cell Biol* 108, 1187-1194.

Gordon, J.I., and Hermiston, M.L. (1994). Differentiation and self-renewal in the mouse gastrointestinal epithelium. *Curr Opin Cell Biol* 6, 795-803.

Griffiths-Jones, S. (2004). The microRNA Registry. *Nucleic Acids Res* 32, D109-111.

Groneberg, D.A., Doring, F., Eynott, P.R., Fischer, A., and Daniel, H. (2001). Intestinal peptide transport: ex vivo uptake studies and localization of peptide carrier PEPT1. *Am J Physiol Gastrointest Liver Physiol* 281, G697-704.

Groschwitz, K.R., and Hogan, S.P. (2009). Intestinal barrier function: molecular regulation and disease pathogenesis. *J Allergy Clin Immunol* 124, 3-20; quiz 21-22.

Halbleib, J.M., and Nelson, W.J. (2006). Cadherins in development: cell adhesion, sorting, and tissue morphogenesis. *Genes Dev* 20, 3199-3214.

Han, X., Ren, X., Jurickova, I., Groschwitz, K., Pasternak, B.A., Xu, H., Wilson, T.A., Hogan, S.P., and Denson, L.A. (2009). Regulation of intestinal barrier function by signal transducer and activator of transcription 5b. *Gut* 58, 49-58.

Hanauer, S.B., and Sandborn, W. (2001). Management of Crohn's disease in adults. *Am J Gastroenterol* 96, 635-643.

He, G., Wang, H.R., Huang, S.K., and Huang, C.L. (2007). Intersectin links WNK kinases to endocytosis of ROMK1. *J Clin Invest* 117, 1078-1087.

Hering, N.A., Fromm, M., and Schulzke, J.D. (2012). Determinants of colonic barrier function in inflammatory bowel disease and potential therapeutics. *The Journal of physiology* 590, 1035-1044.

Hu, Y., Smith, D.E., Ma, K., Jappara, D., Thomas, W., and Hillgren, K.M. (2008). Targeted disruption of peptide transporter Pept1 gene in mice significantly reduces dipeptide absorption in intestine. *Mol Pharm* 5, 1122-1130.

Huang, C.L., Yang, S.S., and Lin, S.H. (2008). Mechanism of regulation of renal ion transport by WNK kinases. *Curr Opin Nephrol Hypertens* 17, 519-525.

Ingersoll, S.A., Ayyadurai, S., Charania, M.A., Laroui, H., Yan, Y., and Merlin, D. (2012). The role and pathophysiological relevance of membrane transporter PepT1 in intestinal inflammation and inflammatory bowel disease. *Am J Physiol Gastrointest Liver Physiol* 302, G484-492.

Inohara, N., Ogura, Y., Fontalba, A., Gutierrez, O., Pons, F., Crespo, J., Fukase, K., Inamura, S., Kusumoto, S., Hashimoto, M., *et al.* (2003). Host recognition of bacterial

muramyl dipeptide mediated through NOD2. Implications for Crohn's disease. *J Biol Chem* 278, 5509-5512.

Ip, Y.T., and Davis, R.J. (1998). Signal transduction by the c-Jun N-terminal kinase (JNK)--from inflammation to development. *Curr Opin Cell Biol* 10, 205-219.

Jankowski, J.A., Bedford, F.K., Boulton, R.A., Cruickshank, N., Hall, C., Elder, J., Allan, R., Forbes, A., Kim, Y.S., Wright, N.A., *et al.* (1998). Alterations in classical cadherins associated with progression in ulcerative and Crohn's colitis. *Lab Invest* 78, 1155-1167.

Johansson, M.E., Phillipson, M., Petersson, J., Velcich, A., Holm, L., and Hansson, G.C. (2008a). The inner of the two Muc2 mucin-dependent mucus layers in colon is devoid of bacteria. *Proc Natl Acad Sci U S A* 105, 15064-15069.

Johansson, M.E., Phillipson, M., Petersson, J., Velcich, A., Holm, L., and Hansson, G.C. (2008b). The inner of the two Muc2 mucin-dependent mucus layers in colon is devoid of bacteria. *Proc Natl Acad Sci U S A* 105, 15064-15069.

John, L.J., Fromm, M., and Schulzke, J.D. (2011). Epithelial barriers in intestinal inflammation. *Antioxid Redox Signal* 15, 1255-1270.

Johnston, A.M., Naselli, G., Gonez, L.J., Martin, R.M., Harrison, L.C., and DeAizpurua, H.J. (2000). SPAK, a STE20/SPS1-related kinase that activates the p38 pathway. *Oncogene* 19, 4290-4297.

Joly, F., Mayeur, C., Messing, B., Lavergne-Slove, A., Cazals-Hatem, D., Noordine, M.L., Cherbuy, C., Duee, P.H., and Thomas, M. (2009). Morphological adaptation with

preserved proliferation/transporter content in the colon of patients with short bowel syndrome. *Am J Physiol Gastrointest Liver Physiol* 297, G116-123.

Kahle, K.T., Gimenez, I., Hassan, H., Wilson, F.H., Wong, R.D., Forbush, B., Aronson, P.S., and Lifton, R.P. (2004). WNK4 regulates apical and basolateral Cl<sup>-</sup> flux in extrarenal epithelia. *Proc Natl Acad Sci U S A* 101, 2064-2069.

Kennedy, R.J., Hoper, M., Deodhar, K., Erwin, P.J., Kirk, S.J., and Gardiner, K.R. (2000). Interleukin 10-deficient colitis: new similarities to human inflammatory bowel disease. *Br J Surg* 87, 1346-1351.

Khatri, R., and Subramanian, S. (2013). MicroRNA-135b and Its Circuitry Networks as Potential Therapeutic Targets in Colon Cancer. *Frontiers in oncology* 3, 268.

Kim, S.H., Kim, K.X., Raveendran, N.N., Wu, T., Pondugula, S.R., and Marcus, D.C. (2009). Regulation of ENaC-mediated sodium transport by glucocorticoids in Reissner's membrane epithelium. *Am J Physiol Cell Physiol* 296, C544-557.

Knutter, I., Rubio-Aliaga, I., Boll, M., Hause, G., Daniel, H., Neubert, K., and Brandsch, M. (2002). H<sup>+</sup>-peptide cotransport in the human bile duct epithelium cell line SK-ChA-1. *Am J Physiol Gastrointest Liver Physiol* 283, G222-229.

Kolodziejczak, D., Spanier, B., Pais, R., Kraiczy, J., Stelzl, T., Gedrich, K., Scherling, C., Zietek, T., and Daniel, H. (2013). Mice lacking the intestinal peptide transporter display reduced energy intake and a subtle maldigestion/malabsorption that protects them from diet-induced obesity. *American journal of physiology Gastrointestinal and liver physiology* 304, G897-907.

Korinek, V., Barker, N., Moerer, P., van Donselaar, E., Huls, G., Peters, P.J., and Clevers, H. (1998). Depletion of epithelial stem-cell compartments in the small intestine of mice lacking Tcf-4. *Nat Genet* 19, 379-383.

Kovacs-Nolan, J., Zhang, H., Ibuki, M., Nakamori, T., Yoshiura, K., Turner, P.V., Matsui, T., and Mine, Y. (2012). The PepT1-transportable soy tripeptide VPY reduces intestinal inflammation. *Biochim Biophys Acta* 1820, 1753-1763.

Kramer, W., Girbig, F., Gutjahr, U., Kleemann, H.W., Leipe, I., Urbach, H., and Wagner, A. (1990). Interaction of renin inhibitors with the intestinal uptake system for oligopeptides and beta-lactam antibiotics. *Biochim Biophys Acta* 1027, 25-30.

Krek, A., Grun, D., Poy, M.N., Wolf, R., Rosenberg, L., Epstein, E.J., MacMenamin, P., da Piedade, I., Gunsalus, K.C., Stoffel, M., *et al.* (2005). Combinatorial microRNA target predictions. *Nat Genet* 37, 495-500.

Kucharzik, T., Walsh, S.V., Chen, J., Parkos, C.A., and Nusrat, A. (2001). Neutrophil transmigration in inflammatory bowel disease is associated with differential expression of epithelial intercellular junction proteins. *Am J Pathol* 159, 2001-2009.

Kurtovic, J., and Segal, I. (2004). Recent advances in biological therapy for inflammatory bowel disease. *Trop Gastroenterol* 25, 9-14.

Kyriakis, J.M. (1999). Signaling by the germinal center kinase family of protein kinases. *J Biol Chem* 274, 5259-5262.

Lagos-Quintana, M., Rauhut, R., Lendeckel, W., and Tuschl, T. (2001). Identification of novel genes coding for small expressed RNAs. *Science* 294, 853-858.

Lathrop, S.K., Bloom, S.M., Rao, S.M., Nutsch, K., Lio, C.W., Santacruz, N., Peterson, D.A., Stappenbeck, T.S., and Hsieh, C.S. (2011). Peripheral education of the immune system by colonic commensal microbiota. *Nature* 478, 250-254.

Leblond, C.P., and Messier, B. (1958). Renewal of chief cells and goblet cells in the small intestine as shown by radioautography after injection of thymidine-H3 into mice. *The Anatomical record* 132, 247-259.

Li, Y., Hu, J., Vita, R., Sun, B., Tabata, H., and Altman, A. (2004). SPAK kinase is a substrate and target of PKC $\theta$  in T-cell receptor-induced AP-1 activation pathway. *The EMBO journal* 23, 1112-1122.

Liang, R., Fei, Y.J., Prasad, P.D., Ramamoorthy, S., Han, H., Yang-Feng, T.L., Hediger, M.A., Ganapathy, V., and Leibach, F.H. (1995). Human intestinal H<sup>+</sup>/peptide cotransporter. Cloning, functional expression, and chromosomal localization. *J Biol Chem* 270, 6456-6463.

Lim, L.P., Lau, N.C., Garrett-Engele, P., Grimson, A., Schelter, J.M., Castle, J., Bartel, D.P., Linsley, P.S., and Johnson, J.M. (2005). Microarray analysis shows that some microRNAs downregulate large numbers of target mRNAs. *Nature* 433, 769-773.

Ma, G., Shi, B., Liu, J., Zhang, H., YinTao, Z., Lou, X., Liang, D., Hou, Y., Wan, S., and Yang, W. (2015). Nod2-Rip2 Signaling Contributes to Intestinal Injury Induced by Muramyl Dipeptide Via Oligopeptide Transporter in Rats. *Dig Dis Sci*.

Mac Donal, O., Chediack, J.G., and Caviedes-Vidal, E. (2008). Isolation of epithelial cells, villi and crypts from small intestine of pigeons (*Columba livia*). *Biocell* 32, 219-227.

Macdonald, T.T., and Monteleone, G. (2005). Immunity, inflammation, and allergy in the gut. *Science* 307, 1920-1925.

Madara, J.L. (1990). Maintenance of the macromolecular barrier at cell extrusion sites in intestinal epithelium: physiological rearrangement of tight junctions. *The Journal of membrane biology* 116, 177-184.

Madsen, K.L., Lewis, S.A., Tavernini, M.M., Hibbard, J., and Fedorak, R.N. (1997). Interleukin 10 prevents cytokine-induced disruption of T84 monolayer barrier integrity and limits chloride secretion. *Gastroenterology* 113, 151-159.

Madsen, K.L., Malfair, D., Gray, D., Doyle, J.S., Jewell, L.D., and Fedorak, R.N. (1999). Interleukin-10 gene-deficient mice develop a primary intestinal permeability defect in response to enteric microflora. *Inflamm Bowel Dis* 5, 262-270.

Manicassamy, S., Reizis, B., Ravindran, R., Nakaya, H., Salazar-Gonzalez, R.M., Wang, Y.C., and Pulendran, B. (2010). Activation of beta-catenin in dendritic cells regulates immunity versus tolerance in the intestine. *Science* 329, 849-853.

Marchiando, A.M., Shen, L., Graham, W.V., Weber, C.R., Schwarz, B.T., Austin, J.R., 2nd, Raleigh, D.R., Guan, Y., Watson, A.J., Montrose, M.H., *et al.* (2010). Caveolin-1-dependent occludin endocytosis is required for TNF-induced tight junction regulation in vivo. *J Cell Biol* 189, 111-126.

Mariadason, J.M., Bordonaro, M., Aslam, F., Shi, L., Kuraguchi, M., Velcich, A., and Augenlicht, L.H. (2001). Down-regulation of beta-catenin TCF signaling is linked to colonic epithelial cell differentiation. *Cancer Res* 61, 3465-3471.

Mariadason, J.M., Nicholas, C., L'Italien, K.E., Zhuang, M., Smartt, H.J., Heerdt, B.G., Yang, W., Corner, G.A., Wilson, A.J., Klampfer, L., *et al.* (2005). Gene expression profiling of intestinal epithelial cell maturation along the crypt-villus axis. *Gastroenterology* 128, 1081-1088.

Mathews, D.M., and Adibi, S.A. (1976). Peptide absorption. *Gastroenterology* 71, 151-161.

McCarroll, S.A., Huett, A., Kuballa, P., Chilewski, S.D., Landry, A., Goyette, P., Zody, M.C., Hall, J.L., Brant, S.R., Cho, J.H., *et al.* (2008). Deletion polymorphism upstream of IRGM associated with altered IRGM expression and Crohn's disease. *Nat Genet* 40, 1107-1112.

McCarthy, K.M., Skare, I.B., Stankewich, M.C., Furuse, M., Tsukita, S., Rogers, R.A., Lynch, R.D., and Schneeberger, E.E. (1996). Occludin is a functional component of the tight junction. *J Cell Sci* 109 ( Pt 9), 2287-2298.

McKenna, L.B., Schug, J., Vourekas, A., McKenna, J.B., Bramswig, N.C., Friedman, J.R., and Kaestner, K.H. (2010). MicroRNAs control intestinal epithelial differentiation, architecture, and barrier function. *Gastroenterology* 139, 1654-1664, 1664 e1651.

Medzhitov, R., and Janeway, C., Jr. (2000). Innate immunity. *N Engl J Med* 343, 338-344.

Merlin, D., Si-Tahar, M., Sitaraman, S.V., Eastburn, K., Williams, I., Liu, X., Hediger, M.A., and Madara, J.L. (2001). Colonic epithelial hPepT1 expression occurs in inflammatory bowel disease: transport of bacterial peptides influences expression of MHC class 1 molecules. *Gastroenterology* 120, 1666-1679.

Merlin, D., Steel, A., Gewirtz, A.T., Si-Tahar, M., Hediger, M.A., and Madara, J.L. (1998). hPepT1-mediated epithelial transport of bacteria-derived chemotactic peptides enhances neutrophil-epithelial interactions. *J Clin Invest* 102, 2011-2018.

Mirnezami, A.H., Pickard, K., Zhang, L., Primrose, J.N., and Packham, G. (2009). MicroRNAs: key players in carcinogenesis and novel therapeutic targets. *Eur J Surg Oncol* 35, 339-347.

Momboisse, F., Ory, S., Calco, V., Malacombe, M., Bader, M.F., and Gasman, S. (2009). Calcium-regulated exocytosis in neuroendocrine cells: intersectin-1L stimulates actin polymerization and exocytosis by activating Cdc42. *Ann N Y Acad Sci* 1152, 209-214.

Monteleone, G., Boirivant, M., Pallone, F., and MacDonald, T.T. (2008). TGF-beta1 and Smad7 in the regulation of IBD. *Mucosal Immunol* 1 Suppl 1, S50-53.

Muise, A.M., Walters, T.D., Glowacka, W.K., Griffiths, A.M., Ngan, B.Y., Lan, H., Xu, W., Silverberg, M.S., and Rotin, D. (2009). Polymorphisms in E-cadherin (CDH1) result in a mis-localised cytoplasmic protein that is associated with Crohn's disease. *Gut* 58, 1121-1127.

Mutoh, H., Satoh, K., Kita, H., Sakamoto, H., Hayakawa, H., Yamamoto, H., Isoda, N., Tamada, K., Ido, K., and Sugano, K. (2005). Cdx2 specifies the differentiation of morphological as well as functional absorptive enterocytes of the small intestine. *Int J Dev Biol* 49, 867-871.

Nata, T., Fujiya, M., Ueno, N., Moriichi, K., Konishi, H., Tanabe, H., Ohtake, T., Ikuta, K., and Kohgo, Y. (2013). MicroRNA-146b improves intestinal injury in mouse colitis by

activating nuclear factor-kappaB and improving epithelial barrier function. *J Gene Med* 15, 249-260.

Nava, P., Koch, S., Laukoetter, M.G., Lee, W.Y., Kolegraff, K., Capaldo, C.T., Beeman, N., Addis, C., Gerner-Smidt, K., Neumaier, I., *et al.* (2010). Interferon-gamma regulates intestinal epithelial homeostasis through converging beta-catenin signaling pathways. *Immunity* 32, 392-402.

Nduati, V., Yan, Y., Dalmasso, G., Driss, A., Sitaraman, S., and Merlin, D. (2007). Leptin transcriptionally enhances peptide transporter (hPepT1) expression and activity via the cAMP-response element-binding protein and Cdx2 transcription factors. *J Biol Chem* 282, 1359-1373.

Nguyen, H.T., Charrier-Hisamuddin, L., Dalmasso, G., Hiol, A., Sitaraman, S., and Merlin, D. (2007). Association of PepT1 with lipid rafts differently modulates its transport activity in polarized and nonpolarized cells. *Am J Physiol Gastrointest Liver Physiol* 293, G1155-1165.

O'Connell, R.M., Taganov, K.D., Boldin, M.P., Cheng, G., and Baltimore, D. (2007). MicroRNA-155 is induced during the macrophage inflammatory response. *Proc Natl Acad Sci U S A* 104, 1604-1609.

Ogihara, H., Saito, H., Shin, B.C., Terado, T., Takenoshita, S., Nagamachi, Y., Inui, K., and Takata, K. (1996a). Immuno-localization of H<sup>+</sup>/peptide cotransporter in rat digestive tract. *Biochem Biophys Res Commun* 220, 848-852.

Ogihara, H., Saito, H., Shin, B.C., Terado, T., Takenoshita, S., Nagamachi, Y., Inui, K., and Takata, K. (1996b). Immuno-localization of H<sup>+</sup>/peptide cotransporter in rat digestive tract. *Biochem Biophys Res Commun* 220, 848-852.

Ogihara, H., Suzuki, T., Nagamachi, Y., Inui, K., and Takata, K. (1999). Peptide transporter in the rat small intestine: ultrastructural localization and the effect of starvation and administration of amino acids. *The Histochemical journal* 31, 169-174.

Opdam, F.J., Kamps, G., Croes, H., van Bokhoven, H., Ginsel, L.A., and Fransen, J.A. (2000). Expression of Rab small GTPases in epithelial Caco-2 cells: Rab21 is an apically located GTP-binding protein in polarised intestinal epithelial cells. *Eur J Cell Biol* 79, 308-316.

Panwala, C.M., Jones, J.C., and Viney, J.L. (1998). A novel model of inflammatory bowel disease: mice deficient for the multiple drug resistance gene, *mdr1a*, spontaneously develop colitis. *J Immunol* 161, 5733-5744.

Paradela, A., Bravo, S.B., Henriquez, M., Riquelme, G., Gavilanes, F., Gonzalez-Ros, J.M., and Albar, J.P. (2005). Proteomic analysis of apical microvillous membranes of syncytiotrophoblast cells reveals a high degree of similarity with lipid rafts. *Journal of proteome research* 4, 2435-2441.

Piechotta, K., Lu, J., and Delpire, E. (2002). Cation chloride cotransporters interact with the stress-related kinases Ste20-related proline-alanine-rich kinase (SPAK) and oxidative stress response 1 (OSR1). *J Biol Chem* 277, 50812-50819.

Pinto, D., Robine, S., Jaisser, F., El Marjou, F.E., and Louvard, D. (1999). Regulatory sequences of the mouse villin gene that efficiently drive transgenic expression in immature

and differentiated epithelial cells of small and large intestines. *The Journal of biological chemistry* 274, 6476-6482.

Plevy, S.E., Landers, C.J., Prehn, J., Carramanzana, N.M., Deem, R.L., Shealy, D., and Targan, S.R. (1997a). A role for TNF-alpha and mucosal T helper-1 cytokines in the pathogenesis of Crohn's disease. *J Immunol* 159, 6276-6282.

Plevy, S.E., Landers, C.J., Prehn, J., Carramanzana, N.M., Deem, R.L., Shealy, D., and Targan, S.R. (1997b). A role for TNF-alpha and mucosal T helper-1 cytokines in the pathogenesis of Crohn's disease. *J Immunol* 159, 6276-6282.

Polek, T.C., Talpaz, M., and Spivak-Kroizman, T. (2006). The TNF receptor, RELT, binds SPAK and uses it to mediate p38 and JNK activation. *Biochem Biophys Res Commun* 343, 125-134.

Resta-Lenert, S., Smitham, J., and Barrett, K.E. (2005). Epithelial dysfunction associated with the development of colitis in conventionally housed *mdr1a*<sup>-/-</sup> mice. *Am J Physiol Gastrointest Liver Physiol* 289, G153-162.

Rioux, J.D., Xavier, R.J., Taylor, K.D., Silverberg, M.S., Goyette, P., Huett, A., Green, T., Kuballa, P., Barmada, M.M., Datta, L.W., *et al.* (2007). Genome-wide association study identifies new susceptibility loci for Crohn disease and implicates autophagy in disease pathogenesis. *Nat Genet* 39, 596-604.

Ruan, K., Fang, X., and Ouyang, G. (2009). MicroRNAs: novel regulators in the hallmarks of human cancer. *Cancer Lett* 285, 116-126.

San Roman, A.K., Aronson, B.E., Krasinski, S.D., Shivdasani, R.A., and Verzi, M.P. (2015). Transcription factors GATA4 and HNF4A control distinct aspects of intestinal

homeostasis in conjunction with transcription factor CDX2. *The Journal of biological chemistry* *290*, 1850-1860.

Sartor, R.B. (1994). Cytokines in intestinal inflammation: pathophysiological and clinical considerations. *Gastroenterology* *106*, 533-539.

Sartor, R.B. (2008). Therapeutic correction of bacterial dysbiosis discovered by molecular techniques. *Proc Natl Acad Sci U S A* *105*, 16413-16414.

Schmitz, H., Barmeyer, C., Gitter, A.H., Wullstein, F., Bentzel, C.J., Fromm, M., Riecken, E.O., and Schulzke, J.D. (2000). Epithelial barrier and transport function of the colon in ulcerative colitis. *Ann N Y Acad Sci* *915*, 312-326.

Sepehri, S., Kotlowski, R., Bernstein, C.N., and Krause, D.O. (2007). Microbial diversity of inflamed and noninflamed gut biopsy tissues in inflammatory bowel disease. *Inflammatory bowel diseases* *13*, 675-683.

Shen, H., Smith, D.E., and Brosius, F.C., 3rd (2001). Developmental expression of PEPT1 and PEPT2 in rat small intestine, colon, and kidney. *Pediatr Res* *49*, 789-795.

Shen, H., Smith, D.E., Yang, T., Huang, Y.G., Schnermann, J.B., and Brosius, F.C., 3rd (1999). Localization of PEPT1 and PEPT2 proton-coupled oligopeptide transporter mRNA and protein in rat kidney. *Am J Physiol* *276*, F658-665.

Smythies, L.E., Sellers, M., Clements, R.H., Mosteller-Barnum, M., Meng, G., Benjamin, W.H., Orenstein, J.M., and Smith, P.D. (2005). Human intestinal macrophages display profound inflammatory anergy despite avid phagocytic and bacteriocidal activity. *J Clin Invest* *115*, 66-75.

Sood, P., Krek, A., Zavolan, M., Macino, G., and Rajewsky, N. (2006). Cell-type-specific signatures of microRNAs on target mRNA expression. *Proceedings of the National Academy of Sciences of the United States of America* *103*, 2746-2751.

Stockton, R., Reutershan, J., Scott, D., Sanders, J., Ley, K., and Schwartz, M.A. (2007). Induction of vascular permeability: beta PIX and GIT1 scaffold the activation of extracellular signal-regulated kinase by PAK. *Mol Biol Cell* *18*, 2346-2355.

Stockton, R.A., Schaefer, E., and Schwartz, M.A. (2004). p21-activated kinase regulates endothelial permeability through modulation of contractility. *J Biol Chem* *279*, 46621-46630.

Suenaert, P., Bulteel, V., Lemmens, L., Noman, M., Geypens, B., Van Assche, G., Geboes, K., Ceuppens, J.L., and Rutgeerts, P. (2002). Anti-tumor necrosis factor treatment restores the gut barrier in Crohn's disease. *Am J Gastroenterol* *97*, 2000-2004.

Sun, L., Nava, G.M., and Stappenbeck, T.S. (2011). Host genetic susceptibility, dysbiosis, and viral triggers in inflammatory bowel disease. *Curr Opin Gastroenterol* *27*, 321-327.

Sydora, B.C., Macfarlane, S.M., Walker, J.W., Dmytrash, A.L., Churchill, T.A., Doyle, J., and Fedorak, R.N. (2007). Epithelial barrier disruption allows nondisease-causing bacteria to initiate and sustain IBD in the IL-10 gene-deficient mouse. *Inflamm Bowel Dis* *13*, 947-954.

Taddei, A., Giampietro, C., Conti, A., Orsenigo, F., Breviario, F., Pirazzoli, V., Potente, M., Daly, C., Dimmeler, S., and Dejana, E. (2008). Endothelial adherens junctions

control tight junctions by VE-cadherin-mediated upregulation of claudin-5. *Nat Cell Biol* 10, 923-934.

Van Itallie, C.M., and Anderson, J.M. (2004). The role of claudins in determining paracellular charge selectivity. *Proceedings of the American Thoracic Society* 1, 38-41.

Vavricka, S.R., Musch, M.W., Chang, J.E., Nakagawa, Y., Phanvijhitsiri, K., Waypa, T.S., Merlin, D., Schneewind, O., and Chang, E.B. (2004). hPepT1 transports muramyl dipeptide, activating NF-kappaB and stimulating IL-8 secretion in human colonic Caco2/bbe cells. *Gastroenterology* 127, 1401-1409.

Vavricka, S.R., Musch, M.W., Fujiya, M., Kles, K., Chang, L., Eloranta, J.J., Kullak-Ublick, G.A., Drabik, K., Merlin, D., and Chang, E.B. (2006). Tumor necrosis factor-alpha and interferon-gamma increase PepT1 expression and activity in the human colon carcinoma cell line Caco-2/bbe and in mouse intestine. *Pflugers Arch* 452, 71-80.

Vijay-Kumar, M., Sanders, C.J., Taylor, R.T., Kumar, A., Aitken, J.D., Sitaraman, S.V., Neish, A.S., Uematsu, S., Akira, S., Williams, I.R., *et al.* (2007). Deletion of TLR5 results in spontaneous colitis in mice. *J Clin Invest* 117, 3909-3921.

Vitari, A.C., Deak, M., Morrice, N.A., and Alessi, D.R. (2005). The WNK1 and WNK4 protein kinases that are mutated in Gordon's hypertension syndrome phosphorylate and activate SPAK and OSR1 protein kinases. *Biochem J* 391, 17-24.

Wang, W., Wang, W.H., Azadzo, K.M., Su, N., Dai, P., Sun, J., Wang, Q., Liang, P., Zhang, W., Lei, X., *et al.* (2016). Activation of innate antiviral immune response via double-stranded RNA-dependent RLR receptor-mediated necroptosis. *Sci Rep* 6, 22550.

Weber, C.R., and Turner, J.R. (2007). Inflammatory bowel disease: is it really just another break in the wall? *Gut* 56, 6-8.

Weiser, M.M. (1973). Intestinal epithelial cell surface membrane glycoprotein synthesis. II. Glycosyltransferases and endogenous acceptors of the undifferentiated cell surface membrane. *J Biol Chem* 248, 2542-2548.

Widmann, C., Gibson, S., Jarpe, M.B., and Johnson, G.L. (1999). Mitogen-activated protein kinase: conservation of a three-kinase module from yeast to human. *Physiol Rev* 79, 143-180.

Wirtz, S., and Neurath, M.F. (2007). Mouse models of inflammatory bowel disease. *Adv Drug Deliv Rev* 59, 1073-1083.

Wojtal, K.A., Eloranta, J.J., Hruz, P., Gutmann, H., Drewe, J., Staumann, A., Beglinger, C., Fried, M., Kullak-Ublick, G.A., and Vavricka, S.R. (2009). Changes in mRNA expression levels of solute carrier transporters in inflammatory bowel disease patients. *Drug Metab Dispos* 37, 1871-1877.

Wong, V., and Gumbiner, B.M. (1997). A synthetic peptide corresponding to the extracellular domain of occludin perturbs the tight junction permeability barrier. *J Cell Biol* 136, 399-409.

Wyatt, J., Vogelsang, H., Hubl, W., Waldhoer, T., and Lochs, H. (1993). Intestinal permeability and the prediction of relapse in Crohn's disease. *Lancet* 341, 1437-1439.

Xavier, R.J., and Podolsky, D.K. (2007). Unravelling the pathogenesis of inflammatory bowel disease. *Nature* 448, 427-434.

Xiao, L., and Wang, J.Y. (2014). RNA-binding proteins and microRNAs in gastrointestinal epithelial homeostasis and diseases. *Current opinion in pharmacology* *19*, 46-53.

Xu, B.E., Stippec, S., Chu, P.Y., Lazrak, A., Li, X.J., Lee, B.H., English, J.M., Ortega, B., Huang, C.L., and Cobb, M.H. (2005). WNK1 activates SGK1 to regulate the epithelial sodium channel. *Proc Natl Acad Sci U S A* *102*, 10315-10320.

Yan, F., and Polk, D.B. (2002). Probiotic bacterium prevents cytokine-induced apoptosis in intestinal epithelial cells. *J Biol Chem* *277*, 50959-50965.

Yan, Y., Dalmaso, G., Nguyen, H.T., Obertone, T.S., Charrier-Hisamuddin, L., Sitaraman, S.V., and Merlin, D. (2008). Nuclear factor-kappaB is a critical mediator of Ste20-like proline-/alanine-rich kinase regulation in intestinal inflammation. *Am J Pathol* *173*, 1013-1028.

Yan, Y., Dalmaso, G., Nguyen, H.T., Obertone, T.S., Sitaraman, S.V., and Merlin, D. (2009). Ste20-related proline/alanine-rich kinase (SPAK) regulated transcriptionally by hyperosmolarity is involved in intestinal barrier function. *PLoS One* *4*, e5049.

Yan, Y., Laroui, H., Ingersoll, S.A., Ayyadurai, S., Charania, M., Yang, S., Dalmaso, G., Obertone, T.S., Nguyen, H., Sitaraman, S.V., *et al.* (2011). Overexpression of Ste20-related proline/alanine-rich kinase exacerbates experimental colitis in mice. *J Immunol* *187*, 1496-1505.

Yan, Y., and Merlin, D. (2008). Ste20-related proline/alanine-rich kinase: a novel regulator of intestinal inflammation. *World J Gastroenterol* *14*, 6115-6121.

Yan, Y., Nguyen, H., Dalmasso, G., Sitaraman, S.V., and Merlin, D. (2007). Cloning and characterization of a new intestinal inflammation-associated colonic epithelial Ste20-related protein kinase isoform. *Biochim Biophys Acta* 1769, 106-116.

Yang, Q., Bermingham, N.A., Finegold, M.J., and Zoghbi, H.Y. (2001). Requirement of Math1 for secretory cell lineage commitment in the mouse intestine. *Science* 294, 2155-2158.

Yasuoka, T., Sasaki, M., Fukunaga, T., Tsujikawa, T., Fujiyama, Y., Kushima, R., and Goodlad, R.A. (2003). The effects of lectins on indomethacin-induced small intestinal ulceration. *Int J Exp Pathol* 84, 231-237.

Ye, D., Guo, S., Al-Sadi, R., and Ma, T.Y. (2011). MicroRNA regulation of intestinal epithelial tight junction permeability. *Gastroenterology* 141, 1323-1333.

Yu, A.S., Enck, A.H., Lencer, W.I., and Schneeberger, E.E. (2003). Claudin-8 expression in Madin-Darby canine kidney cells augments the paracellular barrier to cation permeation. *J Biol Chem* 278, 17350-17359.

Zhang, Y.Z., and Li, Y.Y. (2014). Inflammatory bowel disease: pathogenesis. *World J Gastroenterol* 20, 91-99.

Ziegler, T.R., Fernandez-Estivariz, C., Gu, L.H., Bazargan, N., Umeakunne, K., Wallace, T.M., Diaz, E.E., Rosado, K.E., Pascal, R.R., Galloway, J.R., *et al.* (2002). Distribution of the H<sup>+</sup>/peptide transporter PepT1 in human intestine: up-regulated expression in the colonic mucosa of patients with short-bowel syndrome. *Am J Clin Nutr* 75, 922-930.

**APPENDICES: PUBLICATIONS**

1. Zhang, Y., Viennois, E., Zhang, M., Xiao, B., Han, M., Walter, L., Garg, P., Merlin, D., PepT1 Expression Helps Maintain Intestinal Homeostasis by Mediating the Differential Expression of miRNAs along the Crypt-Villus Axis, *Sci Rep.* 2016 Jun 1;6:27119.

2. Zhang, Y., Viennois, E., Xiao, B., Yan, Y., Knockout of Ste20-like proline/alanine-rich kinase (SPAK) attenuates intestinal inflammation in mice. *The American journal of pathology*, 2013 May; 182 (5): 1617-28

3. Xiao, B., Zhang, M., Viennois, E., Zhang, Y., Wei, N., Baker, M.T., Jung, Y., Merlin, D., Inhibition of MDR1 gene expression and enhancing cellular uptake for effective colon cancer treatment using dual-surface-functionalized nanoparticles. *Biomaterials*, 2015 Apr

4. Xiao, B., Viennois, E., Zhang, Y., Ayyadurai, S., Laroui, H., Merlin, D., Sa1970 CD98 as a ligand for colitis-targeted delivery of nanoparticle. *gastroenterology*, 2014 Feb

5. Ayyadurai, S., Charania, M., Xiao, B., Viennois, E., Zhang, Y., Merlin, D., Colonic miRNA Expression/Secretion, Regulated by Intestinal Epithelial PepT1, Plays an Important Role in Cell-to-Cell Communication during Colitis. *PLOS ONE*, 2014 Feb

6. Xiao, B., Laroui, H., Viennois, E., Ayyadurai, S., Charania, M., Zhang, Y., Zhang, Z., Baker, M., Zhang, B., Gewirtz, A., Merlin, D., Nanoparticles with Surface Antibody Against CD98 and Carrying CD98 Small Interfering RNA Reduce Colitis in Mice. *Gastroenterology*, 2014 Feb

7. Xiao, B., Yang, Y., Viennois, E., Zhang, Y., Ayyadurai, S., Baker, M., Laroui, H., Merlin, D., Glycoprotein CD98 as a receptor for colitis-targeted delivery of nanoparticle. *Journal of materials chemistry B*, 2014 Feb
8. Xiao, B., Laroui, H., Ayyadurai, S., Viennois, E., Charania, M., Zhang, Y., Merlin D., Mannosylated bioreducible nanoparticle-mediated macrophage-specific TNF- $\alpha$  RNA interference for IBD therapy. *Biomaterials*, 2013 Oct; 34 (30):7471-82
9. Nguyen, H.T., Dalmaso, G., Yan, Y., Laroui, H., Charania, M., Ingersoll, S., Zhang, Y., Merlin, D., Intestinal epithelial cell-specific CD98 expression regulates tumorigenesis in *Apc (Min/+)* mice. *Lab Invest*, 2012. 92(8): p. 1203-12